SMRT | A WORLD OF KNOWLEDGE
FOR MR TECHNOLOGISTS & RADIOGRAPHERS

SECTION FOR MAGNETIC RESONANCE TECHNOLOGISTS
OF THE INTERNATIONAL SOCIETY FOR MAGNETIC RESONANCE IN MEDICINE

SMRT Home Study *Educational Seminars*

VOLUME 18 • NUMBER 2

MR-PET (Positron Emission Tomography)

Expert Reviewer:
Julia Lowe, B.S.,R.T.(R)(MR) FSMRT

SMRT Educational Seminars Editor:
Anne Marie Sawyer, B.S., R.T.(R)(MR), FSMRT

Chair, SMRT Publications Committee:
Vanessa Orchard, DCR(D), PGDip.(NucMed), M.Sc.(MRI)

Editor, SMRT Educational Seminars, Home Study Program

Anne Marie Sawyer, B.S., R.T.(R)(MR), FSMRT
Home Study Program
Lucas Center for Imaging
Stanford University, Stanford, California, USA
T: +1 650 725 9697
E: amsawyer@stanford.edu

Chair, SMRT Publications Committee

Vanessa Orchard, DCR(D), PGDip.(Nuc Med), M.Sc.(MRI)
Lead Radiographer
Cardiac Imaging Centre
Golden Jubilee National Hospital
Dunbartonshire, Glasgow, Scotland, UK
T: +0141 951 5187
E: vanessa.orchard@gjnh.scot.nhs.uk

MR-PET (Positron Emission Tomography)

March 2015

We are pleased to present the SMRT Home Study *Educational Seminar*, Volume 18, Number 2: *MR-PET (Positron Emission Tomography)*. This is the 68th accredited Home Study developed by the SMRT, exclusively for SMRT members. The accreditation is conducted by the SMRT acting as a RCEEM (Recognized Continuing Education Evaluation Mechanism) for the ARRT. Category A credits are assigned to each home study, which can be used to maintain one's ARRT advanced registry. SMRT Home Studies *Educational Seminars* are also approved for AIR (Australian Institute of Radiography), NZIMRT (New Zealand Institute of Radiation Technology) and CPD Now (The College of Radiographers, United Kingdom) continuing professional development (CPD) activities.

Three peer-reviewed articles have been chosen for this Home Study issue. As introduced in the first article by the authors, "Initiated by the success story of hybrid imaging by combining positron emission tomography (PET) and computed tomography (CT) in PET/CT, researchers have pursued the technically challenging but diagnostically attractive idea of integrating PET and MR imaging in one single system. Such PET/MR hybrid imaging modality has potential diagnostic advantages in cases where MR outperforms CT (i.e., increased soft tissue contrast and reduced radiation dose) with clinical potential in oncology, neurology, cardiology and monitoring of early therapeutic success." What follows is an intriguing and detailed description of this recently introduced hybrid-imaging modality.

"Such PET/MR hybrid imaging modality has potential diagnostic advantages in cases where MR outperforms CT (i.e., increased soft tissue contrast and reduced radiation dose) with clinical potential in oncology, neurology, cardiology and monitoring of early therapeutic success."

The authors of the second article continue to expand on the technology of MR-PET but with more specific information regarding the adaptation and optimization of imaging software given the challenges of hardware modifications required to merge these two complex imaging systems. They support this endeavor by saying "As the newest hybrid imaging technology, simultaneous PET/MR combines these exciting areas of growth for radiology and nuclear medicine and further bridges the divide between anatomic and molecular imaging. PET/MR can noninvasively provide molecular, functional, and anatomic information in a single imaging session using FDG and other PET tracers in conjunction with state-of-the-art MRI."

In the third and final article that discusses the initial experience at a clinical cancer center with MR/PET, the authors begin by reminding us: "Staging, re-staging and therapy monitoring are important steps in the management of oncologic patients. All of these imaging management categories consist of a determination of the local tumor extent, detection of adenopathy, and secondary spread to their organs. MR/PET leverages the inherent strengths of both technologies and thereby opens new horizons in functional and molecular imaging."

A special thank you to Julia Lowe, B.S., R.T.(R)(MR) from Columbus, Indiana, USA, for acting as the Expert Reviewer. Thanks also to Heidi Berns, M.S., R.T.(R)(MR), FSMRT, Chair of the SMRT RCEEM Ad-hoc committee from Coralville, Iowa, USA, and all those who participate on this committee by reviewing the Home Studies *Educational Seminars* for accreditation. Finally, many thanks to Kerry Crockett, Associate Executive Director, ISMRM/SMRT, Mary Keydash, Publications Director, Linda O-Brown, SMRT Coordinator, Sally Moran, Director of Electronic Communications and the entire staff in the Berkeley, California, USA, office of the ISMRM and SMRT, for their insight and long hours spent supporting these educational symposia.

MR-PET (Positron Emission Tomography)

ISMRM SECTION FOR MAGNETIC RESONANCE TECHNOLOGISTS

Home Study *Educational Seminars* VOLUME 18 • NUMBER 2

Educational Objectives

Integrated PET/MR

- Discuss the history behind the development of PET/MR;
- Review the technical considerations of an integrated PET/MR system;
- Describe the attenuation correction (AC) and motion correction (MC) software;
- Review the clinical applications including oncology, neurology, pediatric and cardiovascular;
- Explain the workflow of the hybrid imaging modality, artifacts, quantification and standardization; and
- Show imaging examples including MRI, PET and merged data acquired simultaneously.

Whole-Body Simultaneous Positron Emission Tomography (PET)-MR: Optimization and Adaptation of MRI Sequences

- Discuss the technologic challenges involved in integrating PET and MR;
- Review the attenuation correction (AC) and its importance for generation of accurate PET data;
- Describe optimization of MR sequences for whole body PET/MR including body imaging at 3T; (continued next column)

Continued from *Whole-Body Simultaneous Positron Emission Tomography (PET)-MR: Optimization and Adaptation of MRI Sequences*

- Review the development of PET/MR scan protocols and selection of scan parameters;
- List whole body anatomically focused protocol trees; and
- Show imaging examples including MRI, PET and merged data acquired simultaneously.

Initial Experience of MR/PET in a Clinical Cancer Center

- Review the pre-MR Conditional cardiac device era;
- Describe the technology and workflow considerations in a sequential MR/PET system;
- Review the opportunities and challenges of MR/PET;
- Describe the clinical oncologic applications including head and neck cancer, lung cancer, genitourinary cancer, and rectal cancer;
- Explain the importance of low-dose oncologic imaging in the pediatric population; and
- Show imaging examples including MRI, PET and merged data acquired sequentially.

Expert Reviewer

Julia Lowe, B.S.,R.T.(R)(MR) FSMRT
South Central Indiana Local SMRT Chapter
Columbus, IN USA

NZIMRT APPROVED CPD ACTIVITY
SMRT Home Studies, Online Electronic Studies & Online Video Studies
Credits: 6.25 points per module
Valid: 2015

Accreditation by cpd now the College of Radiographers

ENDORSED BY THE COLLEGE OF RADIOGRAPHERS - UNITED KINGDOM
Credit levels according to SMRT certificate - Valid 2015
CoR Assessment: A combined programme covering a wide range of clinical applications and current issues in MR imaging.
May support outcomes 1-13, 18 and 19 of CPD Now

Integrated PET/MR

Harald H. Quick, Ph.D.*

Reprinted with permission from the ISMRM Journal of Magnetic Resonance Imaging: Volume 39: 243–258, © 2014 with permission from 2014 Wiley Periodicals, Inc.

Integrated whole-body PET/MR hybrid imaging combines excellent soft tissue contrast and various functional imaging parameters provided by MR with high sensitivity and quantification of radiotracer metabolism provided by positron emission tomography (PET). While clinical evaluation now is under way, integrated PET/MR demands for new technologies and innovative solutions, currently subject to interdisciplinary research. Attenuation correction of human soft tissues and of hardware components has to be MR-based to maintain quantification of PET imaging because computed tomography (CT) attenuation information is missing. This brings up the question of how to provide bone information with MR imaging. The limited field-of-view in MR imaging leads to truncations in body imaging and MR-based attenuation correction. Another research field is the implementation of motion correction technologies to correct for breathing and cardiac motion in view of the relatively long PET data acquisition times. Initial clinical applications of integrated PET/MR in oncology, neurology, pediatric oncology, and cardiovascular disease are highlighted. The hybrid imaging workflow here has to be tailored to the clinical indication to maximize diagnostic information while minimizing acquisition time. PET/MR introduces new artifacts that need special observation and innovative solutions for correction. Finally, the rising need for appropriate phantoms and standardization efforts in PET/MR hybrid imaging is discussed.

Key Words: integrated PET/MR; PET/MR hybrid imaging; whole-body PET/MR; attenuation correction (AC); motion correction (MC); simultaneous data acquisition
J. Magn. Reson. Imaging 2014;39:243–258.
© **2013 Wiley Periodicals, Inc.**

INITIATED BY THE success story of hybrid imaging by combining positron emission tomography (PET) and computed tomography (CT) in PET/CT, researchers have pursued the technically challenging but diagnostically attractive idea of integrating PET and MR imaging in one single system (1–3). Such PET/MR hybrid imaging modality has potential diagnostic advantages in cases where MR outperforms CT (i.e., increased soft tissue contrast and reduced radiation dose) with clinical potential in oncology, neurology, cardiology and monitoring of early therapeutic success (4, 5). Integration of MR and PET, however, is technically demanding; standard PET detectors could not be placed in the isocenter of an MRI scanner because of their scintillation crystal blocks read out by photomultiplier tubes (PMT), which are highly susceptible to magnetic fields (2, 3). MR compatible detectors had to be developed, substituting PMT with, e.g., Avalanche Photo Diodes (APD). These detectors are able to detect gamma quanta even inside of strong magnetic fields up to 9.4 Tesla (T) (6) and convert the detected events from scintillation light to electrical signals. To retain space for the patient inside the bore, the detector system needs to have a low geometric profile, which is solved by implementing APD technology (1). Recent developments also consider the use of silicon photomultipliers (SiPM) as MR compatible PET detectors that due to their timing resolution qualify for time-of-flight PET detection mode (7). This technology, however, is not yet available for clinical use.

In 2006, prototype hybrid systems featuring a PET head insert based on Lutetium Oxyorthosilicate (LSO)/APD detector rings in a 3T whole-body MR system were introduced for clinical research applications. These prototype systems offered simultaneous PET and MR data acquisition in humans for the first time (8–10). In 2010, the first commercially available whole-body systems for PET/MR hybrid imaging entered the market, based on two separate MR and PET imagers in one room (Philips Ingenuity TF PET-MRI, Best, The Netherlands) (11), followed by a fully integrated whole-body PET/MR hybrid imaging system (Biograph mMR, Siemens AG, Healthcare Sector, Erlangen, Germany) that enables simultaneous PET/MR data acquisition (12). Since then the number of worldwide installations of PET/MR systems has steadily increased and as of today (May 2013) has reached approximately 40 installations worldwide considering only the fully integrated whole-body PET/

Institute of Medical Physics (IMP), Friedrich Alexander-University Erlangen-Nürnberg, Erlangen, Germany.

*Address reprint requests to: H.H.Q., Institute of Medical Physics (IMP), Friedrich Alexander-University Erlangen-Nürnberg, Henkestr. 91, D-91052 Erlangen, Germany. E-mail: harald.quick@imp.uni-erlangen.de

Received June 13, 2013; Accepted August 27, 2013.

DOI 10.1002/jmri.24523
View this article online at wileyonlinelibrary.com.

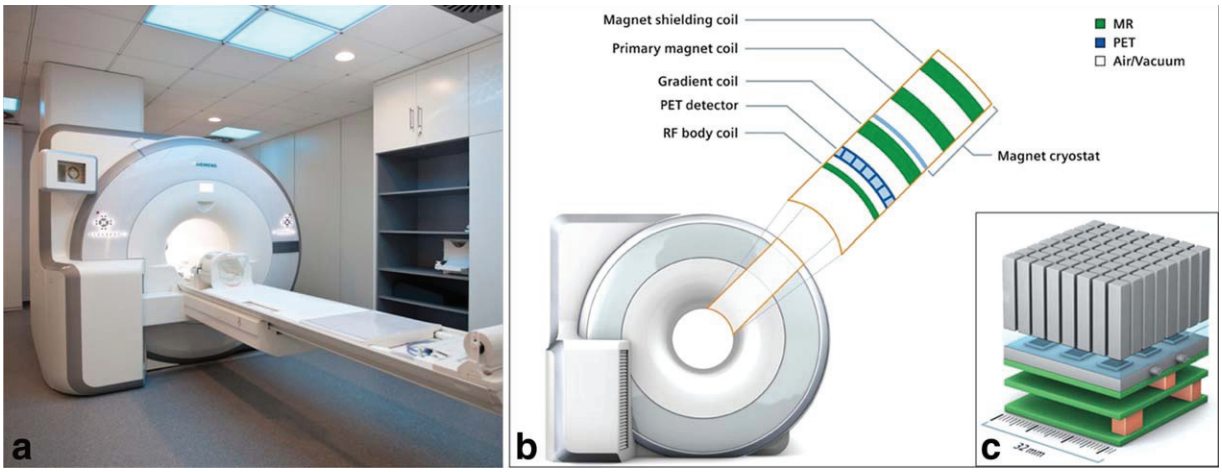

Figure 1. A: Integrated PET/MR System (Biograph mMR, Siemens AG, Healthcare Sector) installed at the Institute of Medical Physics, University of Erlangen, Germany. **B:** Schematic drawing showing the integration of the PET detectors in the MR hardware structure of the Biograph mMR. From the inside to the outside: RF body coil, PET detector, gradient coil assembly, primary magnet coil, and magnet shielding coil. The latter two magnet coil assemblies are contained in the helium filled magnet cryostat. The PET/MR integration as shown requires that the PET detector works within strong static and dynamic magnetic fields, and does not disturb any of the associated electromagnetic MR fields. The PET detector must not disturb the static B_0-field, the gradient fields nor the RF transmission and reception. Additionally, in this configuration the RF body coil needs to be designed "PET transparent" with little attenuation of gamma quanta. **C:** PET detector assembly: 64 Lutetium Oxyorthosilicate (LSO) crystals form one block that transforms 511 keV gamma quanta into light flashes. Light events in the LSO crystals are detected by a 3 × 3 array of avalanche photo diodes (ADP). [Color figure can be viewed in the online issue, which is available at wileyonlinelibrary.com.]

MR systems. This trend is ongoing and expected to gain further pace once initial clinical evidence has been established, new diagnostic applications have been successfully introduced and further technical refinements and products find their way into the clinical arena.

While the first clinical evaluation is under way (13–15), integrated PET/MR demands for new technologies and also for innovative solutions, currently subject to interdisciplinary research. Attenuation correction (AC) of human soft tissues and of hardware components in integrated PET/MR has to be based on MR imaging to maintain quantification of PET imaging because CT attenuation information is missing. This brings up the question of how to provide bone information with MR imaging. Furthermore, the limited field-of-view (FOV) in MR imaging may lead to truncation of, e.g., the patient's arms in body imaging. Attenuation correction in PET/MR, however, mandates the arms to be considered in the AC to provide quantitative results. Another field of active research is the implementation of motion correction (MC) technologies to correct for gross patient motion as well as breathing and cardiac motion in view of the relatively long PET data acquisition times. This holds promise for quantification of lesions and tissue viability in moving organs. Furthermore, hybrid imaging workflow has to be tailored to the clinical indication to provide a maximum of diagnostic information in a minimum of acquisition time for both PET and for MR data acquisition. Finally, each new imaging modality introduces the potential for new artifacts that need special observation and innovative solutions for correction.

TECHNICAL CONSIDERATIONS

Integrated PET/MR System Technology

To achieve a full integration of an MR and PET imaging modality in one whole-body system, numerous physical and technical preconditions and challenges had to be overcome. The potential physical interactions of both modalities in both directions—PET on MRI and MRI on PET—are manifold. Full integration of a PET system into an MRI environment required technical solutions for three groups of potential electromagnetic interaction: (i) the strong static magnetic B_0-field for spin alignment, (ii) the electromagnetic changing fields of the gradient system (G_{xyz}) for spatial signal encoding, and (iii) the radiofrequency (RF) B_1-field for MR signal excitation and MR signal readout. PET hardware and PET signals must not be disturbed by any of these fields. Equally, for full and unlimited MRI system performance, PET must not disturb any of these electromagnetic MR fields and signals (12).

One current example of an integrated whole-body PET/MR system is the Biograph mMR (Siemens Healthcare Sector, Erlangen, Germany) (Fig. 1A,B) (12, 15). This hybrid system comprises a 3.0T whole-body MR system with a length of 199 cm (magnet length 163 cm) that hosts a fully integrated PET detector in its magnet isocenter providing a 60 cm diameter patient bore. Maximum gradient strength is 45 mT/m in all three axes and maximum slew rate is 200 mT/m/ms. The FOV of the MR system is specified to 50 × 50 × 45 cm^3. The hybrid system is equipped with a set of phased-array RF receiver coils connected to 32 independent RF receiver channels.

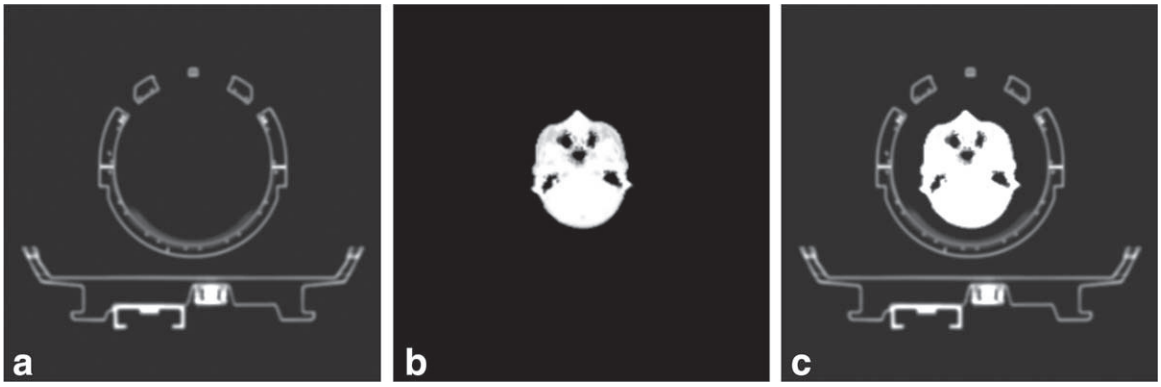

Figure 2. Attenuation maps for attenuation correction (AC) of PET data in PET/MR hybrid imaging. Image (**A**) shows a transversal view through the CT-based hardware attenuation map of a PET/MR system patient table with a radiofrequency head coil in place. Image (**B**) adds the MR-based human soft tissue attenuation map of the patient's head. Image (**C**) shows the completed attenuation map that represents the geometric distribution of attenuating hardware and soft tissue structures in the PET field-of-view. The attenuation map from (C) is then used for AC of PET data in PET/MR hybrid imaging.

The RF coil system provides coverage of the patient's body from head to the upper legs featuring a rigid 16-channel head/neck coil, a rigid 24-channel spine array coil, and up to five flexible 6-channel body matrix RF coils.

A total of 56 LSO-APD detector blocks, each consisting of 64 crystal elements with a block area of 32 × 32 mm^2, are aligned circumferentially to form one PET detector block ring (Fig. 1C). Eight detector block rings form the full PET detector unit, spanning a field of view of 25.8 cm in z-direction (12, 15).

Attenuation Correction (AC)

PET data need to be attenuation corrected in the reconstruction process to provide a valid quantification of tracer activity distribution in the human body. Scanner hardware components (e.g., table top, positioning aids, RF coils, etc.) as well as patient tissues within the FOV of the PET detector during data acquisition attenuate the number of true annihilation events and consequently lead to false results without AC. Depending on the relative position of an active lesion in the patient's body, the associated gamma quanta experience different attenuation on their way through different body tissues to the PET detector. Non-AC PET data generally show underestimation of the tracer activity deep in the patient's body. In conventional PET/CT hybrid systems, AC is obtained by performing a CT scan of the patient's body that provides geometric representations of the tissue distribution and associated 80–140 keV attenuation values as Hounsfield units (HU). These data are then converted to linear attenuation coefficients (LAC) at the 511 keV energy level of the PET annihilation photons and used for AC of PET data (16, 17). Because the PET/MR hybrid system cannot measure linear attenuation, AC here needs to be performed differently (Fig. 2).

Hardware Component AC

Radiofrequency surface receiver coils are a technical precondition for high resolution MR imaging and are well established in clinical MRI. In integrated PET/MR imaging, the RF surface coils cover the patient's body during simultaneous MR and PET data acquisition. Thus, all RF surface coils have to be optimized for PET-transparency, i.e., such coils should attenuate gamma quanta only minimally (18–21).

The PET signal attenuation of rigid and stationary equipment such as the RF spine array and the RF head/neck coil can be compensated for by straightforward AC methods. After scanning this equipment by using CT, a three-dimensional (3D) map of attenuation values can be generated (Fig. 3A, B). These data can then be converted into a 3D representation of the 511 keV attenuation values, the so-called "μ-map" (Fig. 3C). The CT-based measurement of 3D attenuation values is only necessary once for each rigid hardware component to integrate the adapted μ-map into the PET image reconstruction algorithm. This procedure is usually performed by the systems manufacturer for all associated hardware components and the user does not have to interact with the system to perform hardware component AC. By linking the RF spine—or RF head coils position to the patient's table position, the corresponding AC μ-map for each table position is automatically selected by the system for PET image reconstruction (Fig. 3C). Another recent example of hardware component AC is the integration of a four-channel RF breast coil into the concept of PET/MR breast imaging (Fig. 4A,B) (22). The RF breast coil in that study has been selected regarding its PET transparency and is used in conjunction with CT-based 3D attenuation maps (Fig. 4C,D) that are completed with MR-based patient soft tissue AC for overall AC of PET data (Fig. 4E). Another aspect of hardware component AC is, that the use of patient positioning aids might have an influence on PET quantification in PET/MR (23).

Human Tissue AC

Attenuation correction of human soft tissue is necessary to correct for the individual patient anatomy. Because no linear attenuation coefficient-based CT information is available in integrated PET/MR hybrid imaging, tissue-specific AC has to be based on MR

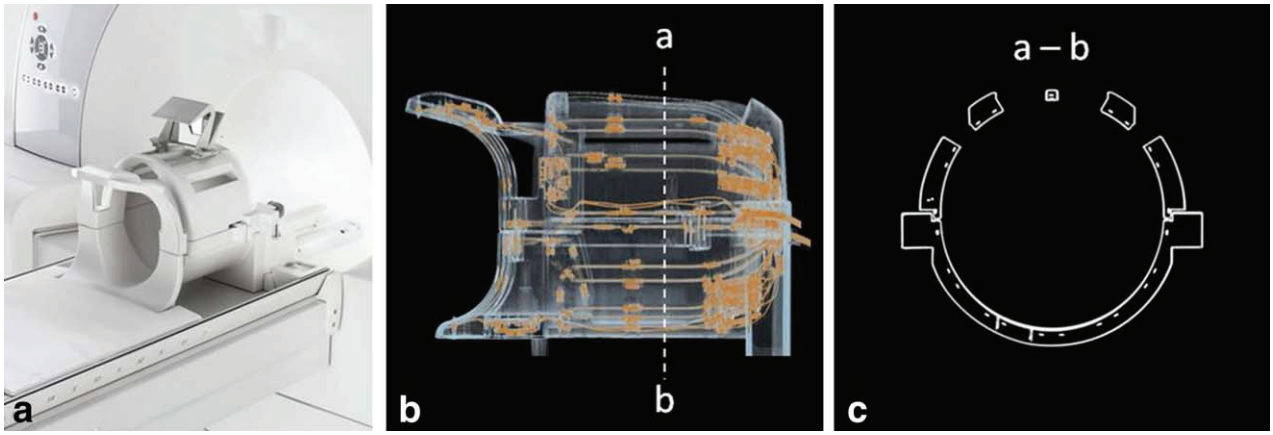

Figure 3. Photograph (**A**) shows a head/neck radiofrequency (RF) coil that was designed and optimized for PET-transparency for use in an integrated PET/MR hybrid system. This RF coil serves as an example for a rigid hardware component that is stationary at its known position with regard to the patient table. Image (**B**) shows a 3D CT-scan of this rigid RF coil. Such CT-template provides hardware attenuation values that can be transformed from the CTs 140 keV energy level with appropriate conversion factors to the 511 keV energy level of PET to derive a PET-equivalent attenuation map (μ-map), shown in image (**C**). The μ-map in (C) has been acquired at level a–b shown in image (B). [Color figure can be viewed in the online issue, which is available at wileyonlinelibrary.com.]

information which is based on proton density and relaxation properties (e.g., T1 and T2 relaxation times), rather than on the attenuation of X-rays in tissue. Both air and solid bone lack signal in MRI, thus these fundamentally different tissue classes are difficult to separate. Different methods have been proposed recently for MR-based tissue AC (24–31). In the current implementation of integrated PET/MR systems, tissue attenuation and scatter correction is performed using a 3D Dixon-VIBE (volume interpolated breath hold examination) technique, providing two sets of images where water and fat are "in phase" and "out-of phase" (Fig. 5) (26). This allows reconstruction of fat-only, water-only, and fat–water images and results in tissue segmentation of air, fat, muscle, and lungs in the reconstructed and displayed μ-maps (Fig. 5) (26). Studies have been initiated to evaluate the impact of segmentation-based AC methods on PET quantification in PET/MR hybrid imaging (32–34). Cortical bone is currently not being accounted for in the Dixon-based MR-AC approach. Bone is here classified as soft tissue and thus the exact magnitude of PET signal attenuation of bone might be underestimated (35, 36).

Bone in AC (UTE)

Because bone and air both do not provide signal in conventional MRI sequences, bone is currently not considered in MR-based AC. In current Dixon-based methods, bone is assigned the LAC of soft tissues during tissue segmentation (26). This leads to a systematic underestimation of the attenuating effects of bone during MR-based AC (35, 36). Samarin et al (35) have evaluated and quantified the amount of underestimation when bone is assigned the LAC of soft tissue. This evaluation was performed on PET/CT patient datasets in which bone has been assigned with soft tissue attenuation values as it is the case in MR-based AC. The result is that an overall underestimation of up to

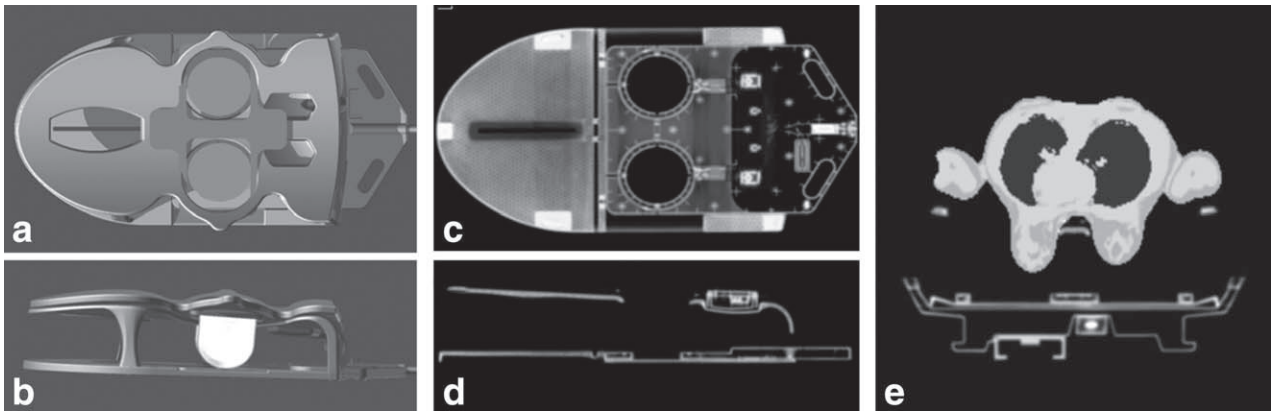

Figure 4. Computer rendering of a four-channel radiofrequency (RF) breast coil with breast phantoms for integrated PET/MR breast imaging in coronal (**A**) and sagittal (**B**) orientation. Corresponding CT-based hardware attenuation map of the RF breast coil in coronal (**C**) and sagittal (**D**) orientation. Image (**E**) shows the combined CT-based hardware (patient table and RF breast coil) and MR-based soft tissue attenuation map of a female patient in transversal orientation. Note that only the middle part of the RF breast coil with the region around the two circular openings is placed in the PET field-of-view during simultaneous PET and MR data acquisition.

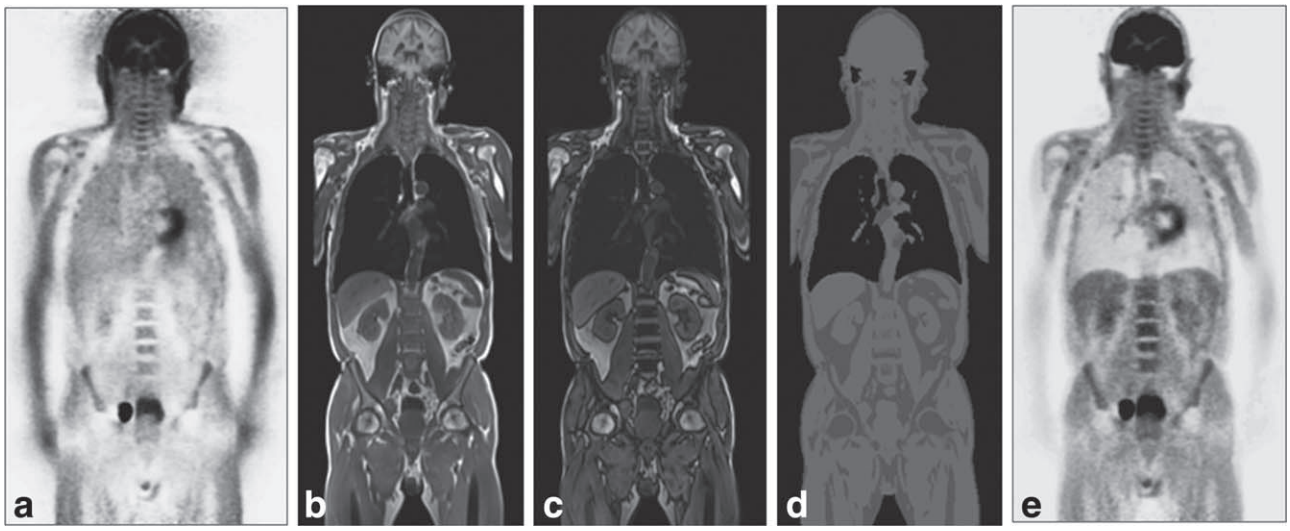

Figure 5. Soft-tissue attenuation correction (AC) based on MR imaging. **A:** Uncorrected whole-body PET scan showing relative activity enhancement in the lungs and along the outer contours of the patient. **B,C:** Dixon-VIBE MR sequence providing separate water/fat "in-phase" and "opposed phase" images that serve as basis for soft-tissue segmentation. **D:** Segmented soft tissue groups (air, fat, muscle, lungs) that can be assigned to a PET attenuation map. **E:** Resulting attenuation corrected whole-body PET scan of the initial dataset (A). Note: Bone signal is assigned as soft tissue values in this MR-based approach for AC.

4% for soft tissue lesions close to bone has been found when compared with PET/CT data where bone has been assigned with the correct LAC values from CT (35). However, when quantifying osseous lesions this value might increase to substantial quantification errors of up to 31% (35).

Atlas-based methods have been proposed (27) to retrospectively add bone information to MR-based attenuation maps. As was demonstrated, atlas-based AC methods have the potential to work robustly and deliver reliable AC results (27). However, such methods require previous knowledge, correct assignment and registration of the atlas data to the actual patient data. This method may thus be limited whenever the current patient anatomy deviates significantly from the average patient cases stored in the atlas due to pathological variations or implants. An AC method that derives bone and tissue information from current MR-based patient data is therefore required.

Current methods for MR-based AC include ultrashort echo time (UTE) sequences able to also display tissues with very short T2* (e.g., bone) (37–39). This is to render information about trabecular and cortical bone that then will be assigned LAC of bone during image segmentation (Fig. 6A,B). Further refinements use the combination with Dixon-based sequences to provide soft tissue information within the FOV and to generate pseudo-CT like AC maps (40–42) leading to further improved quantification results. Further refinements of the method have been pursued to include pattern recognition knowledge (support vector regression, SVR) (43). This method recently succeeded in assigning continuous LAC instead of only 3–4 discrete LAC for limited number of tissue classes (Fig. 6C,D) (43). While UTE-based protocols and combinations of UTE with Dixon sequences have been validated in the head region in numerous initial studies (38–43), the application to other body regions is still at the beginning (43) (Fig. 6E,F). This is reasoned to the fact that UTE sequences are limited to rather small FOVs, supporting bone imaging only in head-like volumes. Exceeding the limited FOV, however, as would be required for body imaging is often associated with progressively increasing artifacts that hamper bone visualization in larger FOVs. The relatively long acquisition time, in the range of several minutes per bed position, is another obstacle. In body imaging, this might be associated with motion artifacts that impede accurate tissue and bone segmentation for AC purposes. Limited FOV, overall image quality, and long acquisition times are the current limitations to be handled before a broad implementation of UTE sequences can be expected in MR-based bone detection in whole-body applications. New ultrashort echo time imaging strategies with improved features are currently under development (44, 45).

Truncation of field-of-view (FOV)

The field-of-view in MR imaging is inherently limited and often specified to a spherical volume of 45–50 cm diameter. This limitation is mainly substantiated by two factors: (i) homogeneity of the static magnetic field B_0, and (ii) linearity of the gradient fields associated with spatial signal encoding in all three dimensions. Both effects lead to geometric distortions, image truncations, and even signal voids of body portions that exceed the dimensions of a conventional FOV in MR imaging. This is consequently also associated with limitations in MR-based AC generation. If the patient body is not completely and correctly assessed in its overall dimensions and current shape, the human tissue AC based on truncated images will not consider the exact amount and position of tissues that contribute to PET signal attenuation and thus provide wrong values for PET quantification following AC (46). This

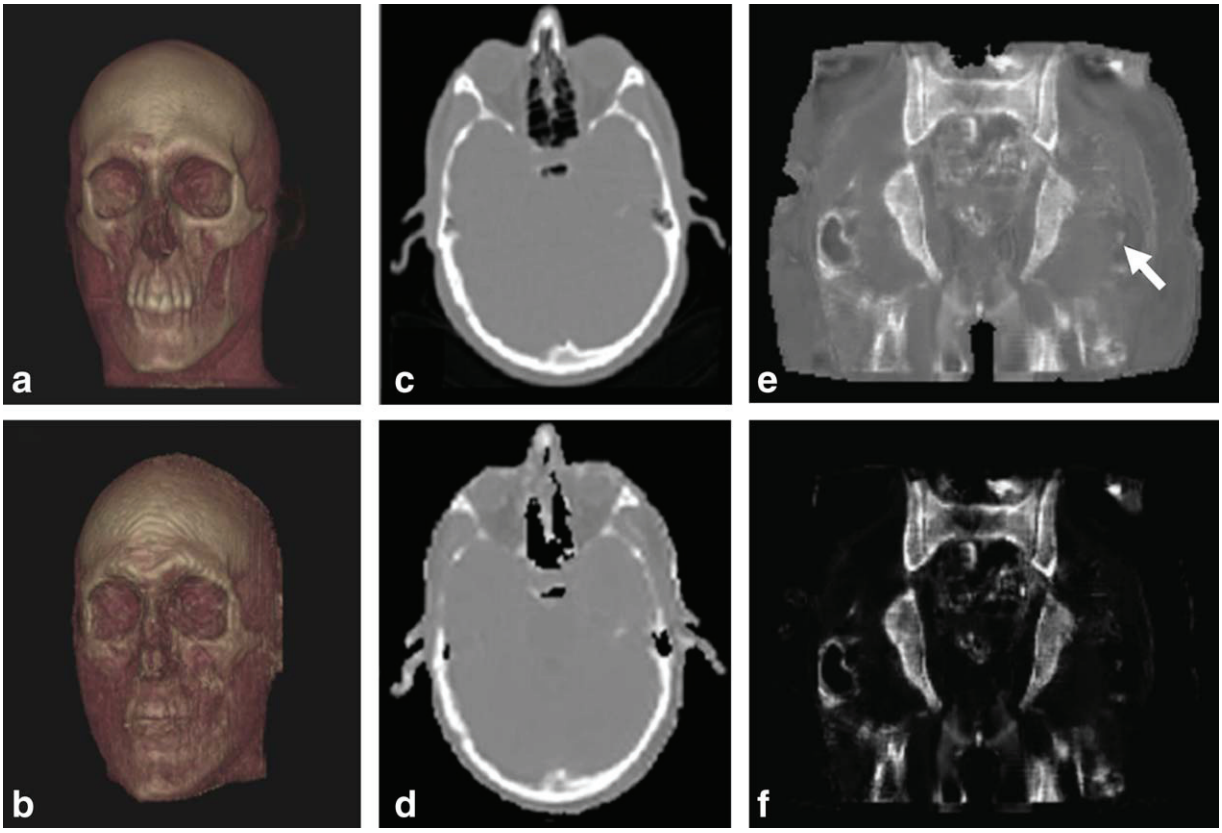

Figure 6. Adding bone to MR-based attenuation correction (AC) with UTE sequences. Three-dimensional renderings (**A,B**) of a CT-scan (A) and of MR-based bone information (B) of the same patient. Attenuation maps (**C,D**) for attenuation correction of PET data. The CT-based attenuation map (C) correlates well with the corresponding MR-based "pseudo-CT" attenuation map (D) that was acquired using a Dixon-VIBE and UTE sequence and pattern recognition information. Coronal views (**E,F**) of MR-predicted "pseudo-CT" data acquired in the pelvis of a volunteer using the Dixon-VIBE and UTE acquisition model from (D). The window/level in (F) was adjusted to display bone only. The field-of-view of the UTE sequence was limited to 300 × 300 mm. Accordingly the model predicts cortical bone in this pelvic study where both UTE and Dixon-VIBE information is available or simply water/fat in the absence of UTE intensities (white arrow in E). [Color figure can be viewed in the online issue, which is available at wileyonlinelibrary.com.]

frequently has an impact on correction of the patient's arms because they in most cases exceed the lateral dimensions of conventional FOVs and it especially applies to larger patients with high body mass indices (BMI). Truncation also might appear when imaging patients are in noncentered imaging positions as, e.g., during a PET/MR breast examination when the patient is positioned on top of a radiofrequency (RF) breast coil (22).

Several methods have been explored to complement the truncated MR-based information in AC. One method that is currently implemented in integrated PET/MR systems is to iteratively extract the contours of the arms in 3D from PET data (Maximum Likelihood reconstruction of Attenuation and Activity, MLAA) and use this information to complete the MR-based AC map of the body trunk (47, 48). This is a robust method that may, however, show limitations when radiotracers other than FDG are associated that do not render the body contours as well. The iterative nature of this approach also requires increased data processing times because PET and MR data that are not necessarily acquired simultaneously need to be combined for completion of the AC map.

A novel approach for the extension of the MR-based FOV has been proposed by Blumhagen et al (49). This method (Homogenization Using Gradient Enhancement, HUGE) (49) is based on a measurement and quantification of the B_0 and gradient nonlinearities of a specific MRI system followed by patient-specific optimization of the readout gradient used for imaging such that MR signal truncations and deformations outside of the regular specified FOV are compensated to a large extent. Applying the HUGE method thus provides an extension of the lateral FOV from the conventional 50 cm to a lateral FOV of 60 cm (49) (Fig. 7A–C). Because this method of FOV extension with according gradient adaption works best in the immediate isocenter of the magnet (axial z-position = 0 mm), a combination with moving table imaging strategies (50–52) seems attractive and straightforward in the context of MR-based AC acquisition. With such a continuously moving table strategy, MR data are acquired only in the isocenter of the MR system while the patient is slowly moved through the isocenter using fast 2D imaging in combination with compensating gradients (HUGE). This leads to seamless FOVs in longitudinal direction (up to 200 cm) in

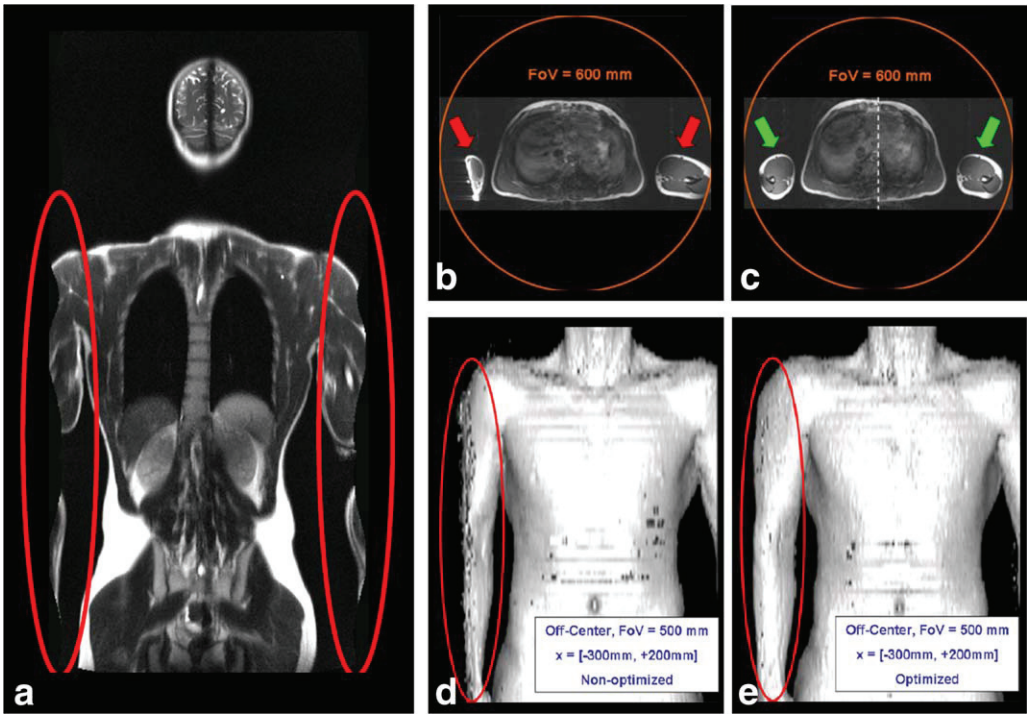

Figure 7. Truncation of structures exceeding the conventional MR field-of-view (here the arms in coronal localizer, **A)** also affects MR-based attenuation correction of the truncated tissues. Transversal slice with a field-of-view of 600 mm. Typical distortions of the patient's arms lying at offcenter positions (red arrows in **B)** were reduced using an optimal readout gradient during MR data acquisition for the patient's left and right arms (green arrows in **B)** using the HUGE method (HUGE, B_0 Homogenization Using Gradient Enhancement). **D,E:** The 3D shaded surface display of a volunteer measured with a transaxial oriented HASTE sequence in conjunction with using continuous table movement (CTM). Distortions and signal voids at off-center positions (D) could successfully be reduced using the HUGE method and CTM (E). Courtesy of JO Blumhagen and K Scheffler, University of Basel, Switzerland. [Color figure can be viewed in the online issue, which is available at wileyonlinelibrary.com.]

combination with extended lateral FOV (up to 60 cm) also including the arms of the patient (Fig. 7D,E) (52).

Motion Correction (MC)

Integrated PET/MR systems provide the inherent advantage of simultaneous PET and MR data acquisition. In view of motion correction (MC), this is an inherent advantage over PET/CT that is currently being explored (53). While in PET/CT, the CT data are static and for dose considerations are acquired only once at the beginning at a typical hybrid examination, the MR data in PET/MR are acquired simultaneously to PET data acquisition and this applies to data acquisition in each bed position. This inherently leads to less deviation and gross motion between both imaging modalities when compared with PET/CT imaging (54). Furthermore, real-time MRI data and 4D MR data can be used to retrospectively motion correct PET data to provide improved fusion of PET and MR data sets (55, 56). Another aspect of MC is that the MR-based AC, e.g., in the thorax can be acquired in different positions of the breathing cycle (57) and PET data acquired during free breathing over several minutes can retrospectively be matched to the individually best corresponding breathing phases of the preacquired AC map (58). This may potentially lead to improved lesion visibility in the lungs, upper abdomen, and liver and may also result in better lesion quantification because lesions are better depicted and less smeared over a larger volume which otherwise leads to reduced standardized uptake values (SUV) of lesions subject to motion (55–62).

CLINICAL APPLICATIONS

Hybrid imaging with PET/MR is generally characterized with providing excellent soft tissue contrast paired with the high inherent sensitivity of PET regarding the detection of metabolism of specific radiotracers. At the same time, PET/MR provides these diagnostic features while reducing overall radiation dose when compared with PET/CT examinations. It is thus to be expected that PET/MR will outperform PET/CT in diagnostic value in selected applications where MR is superior to CT. Beyond the scope of initial clinical PET/CT versus PET/MR comparison studies (13–15, 63) integrated PET/MR hybrid imaging is now under evaluation to define its diagnostic value in various clinical applications in oncology, neurology, pediatric imaging, cardiovascular disease, and therapy planning and response monitoring.

Oncologic Disease

Among the first studies evaluating the diagnostic potential of PET/MR are intraindividual PET/CT versus PET/MR comparison studies on oncologic

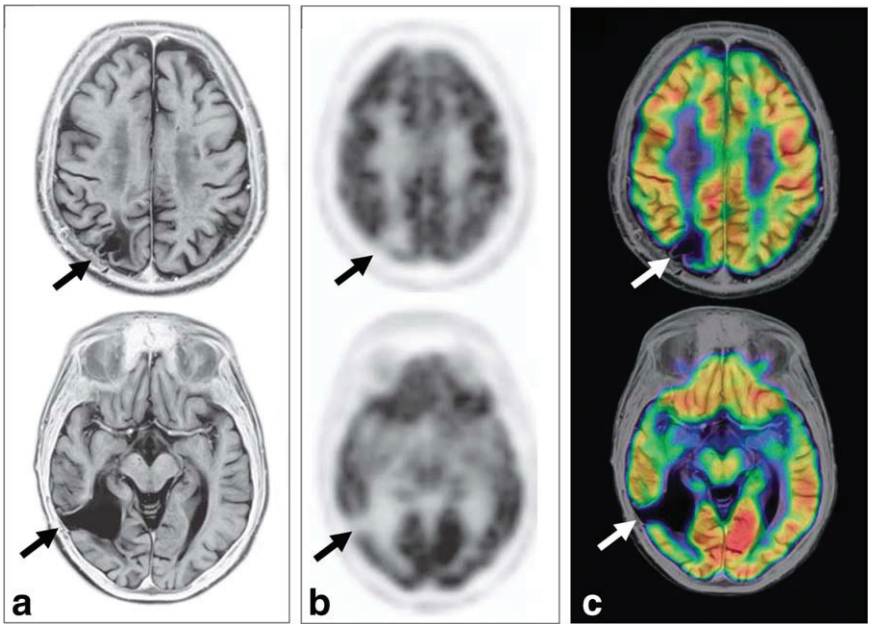

Figure 8. Patient with successfully treated lung carcinoma and with two resected brain metastasis. Axial slices in (**A**) show T2-weighted and inverted MR images acquired at each position of the resected brain metastasis (both right side, black arrows in A). Simultaneously acquired corresponding PET data in (**B**) do not show any signs of recurrence (black arrows in B). The PET/MR hybrid data (**C**) show exact spatial overlap of anatomical and functional information.

patients encompassing a broad spectrum of tumor entities (13–15, 63, 64) (Fig. 8). PET/MR imaging in this oncologic patient population is applied to cover single organ region to whole-body tumor staging and metastasis screening (65–67) (Figs. 9, 10). Lesion detection rates in these studies showed high correlation values (>90%) for detection of congruent lesions in PET/CT as well as PET/MR (13–15, 63). Quantification of lesion activity with PET/CT compared with PET/MR, however, indicated somewhat lower SUV for PET/MR compared with identical lesions measured with PET/CT. Potential reasons for these differences are inherent to the study design: In all comparison studies PET/CT has been performed first, then followed by PET/MR. Starting time of the PET/MR exam thus was delayed by several hours when compared with PET/CT (13–15, 63). Consequently, the advanced tracer metabolism and biodistribution over time might have had an influence on lesion quantification (68–70). Another potential source of error is the MR-based attenuation correction with the above listed shortcomings (segmentation into discrete tissue classes, missing bone information, FOV truncation, etc). These aspects should not be overrated because first clinical studies overall show very good, robust, and reproducible results, however, deserve further investigation in carefully designed studies systematically separating physiological effects of tracer dynamics from technical and methodological effects.

Neurologic Disease

In diagnosis of neurologic disease integrated PET/MR unveils its full morphologic and functional potential. The diagnostic power of MR in neuro imaging here is multiplied with the capabilities of PET using various specific tracers. Because PET and MR data are acquired simultaneously at one bed position only, the overall acquisition time can be invested in multiple contrast weightings, spectroscopic information (71), and also in adding dynamic information in PET and/or MR. Contrast agent dynamics (in MR) as well as tracer metabolism (in PET) can be monitored over time (72). Motion correction algorithms have been developed (53) to further improve the image quality also when imaging uncooperative patients of patients with tremor (e.g., Parkinson's disease). First results applying amyloid-specific PET tracers in PET/MR have shown to support the diagnosis of Alzheimer's disease using PET and MR information (73–75) (Fig. 11).

Pediatric Oncology

In pediatric oncology, MR can provide valuable diagnostic information complementary to PET or PET/CT (76–78) (Fig. 12). Moreover, considering dose aspects, PET/MR can be seen as a valuable alternative to PET/CT imaging for longitudinal follow-up studies monitoring the therapeutic response to chemotherapy. Especially in a pediatric patient population, dose considerations are of high importance. The substitution of PET/CT by PET/MR in these patients reduces the overall dose by the fraction of the CT scan multiplied by the individually necessary number of follow-up imaging sessions per patient. Although this is a rather new application and data are still sparse, first studies have demonstrated impressive diagnostic results (79). Potential dose savings of up to 80% have been postulated when using PET/MR instead of PET/CT in pediatric oncologic imaging (79), however, this has to be validated in larger studies.

Cardiovascular Disease

Integrated PET/MR appears an attractive diagnostic tool in cardiovascular disease because it combines the strength of MR imaging in providing anatomic, functional, flow, and perfusion information and the strength of PET imaging in quantifying physiologic

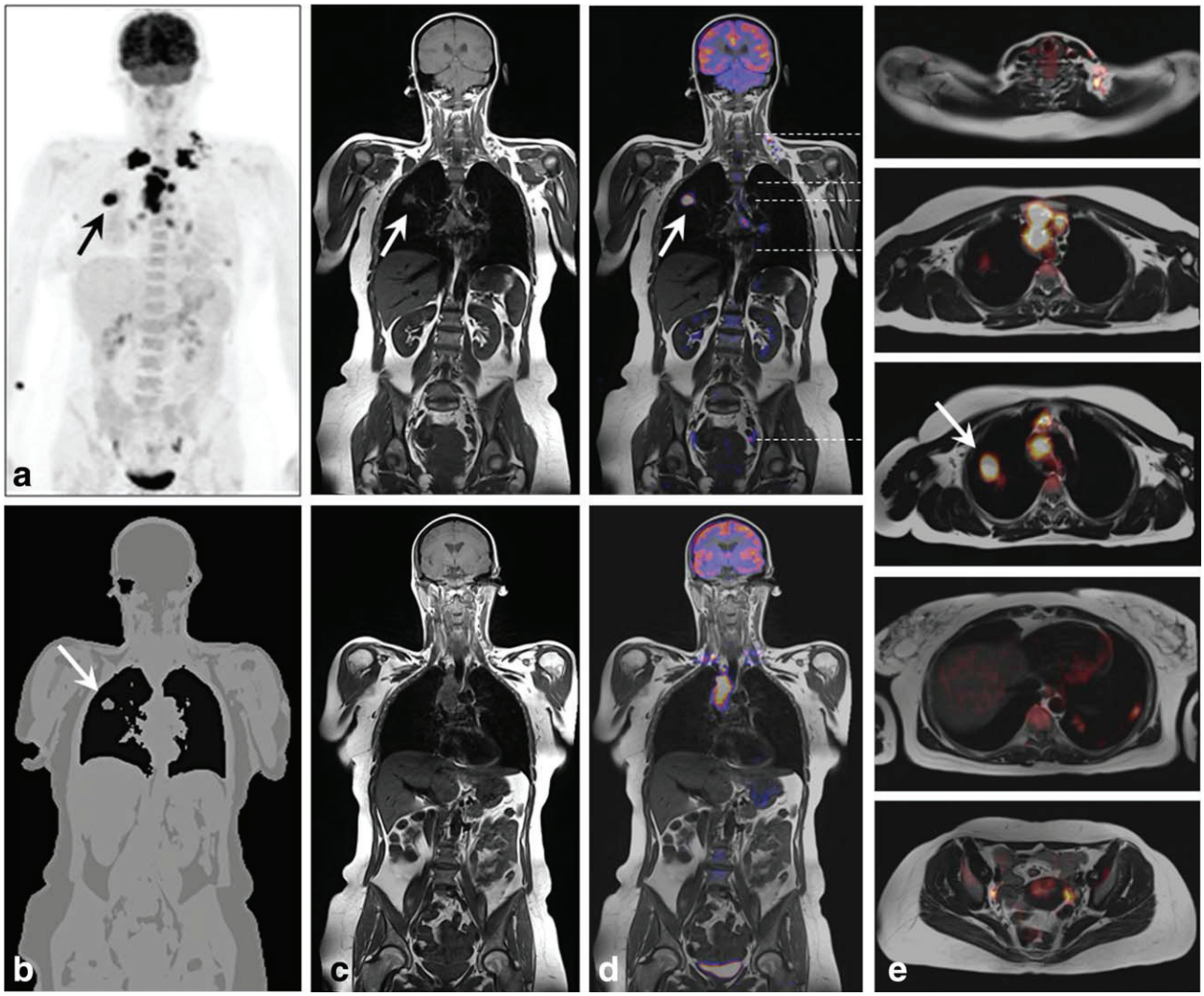

Figure 9. A 44-year-old female with bronchial carcinoma (NSCLC, stage IV). PET data (**A**; 236 MBq F18 FDG) and MR-based attenuation map (**B**) for the attenuation correction (AC) of human soft-tissue. The AC map (B) is based on a multi-station 3D Dixon-VIBE sequence and segments into air, fat, soft tissue and lung tissue. **C:** T1-weighted coronal views of two planes. **D:** PET/MR data fusion of the two planes shown in (C). **E:** Axial PET/MR views at different body levels show FDG-positive lesions in the left supraclavicular groove, ipsi- and contralateral mediastinum, and contralateral lung. There are additional FDG-positive lymph nodes in bilateral iliac lymph nodes. The five image levels of (E) are indicated with white lines in the upper panel of (D). Arrows point to an identical lesion in different views. Note that in the AC map (B) this lesion has been correctly identified as soft tissue in the surrounding lung tissue.

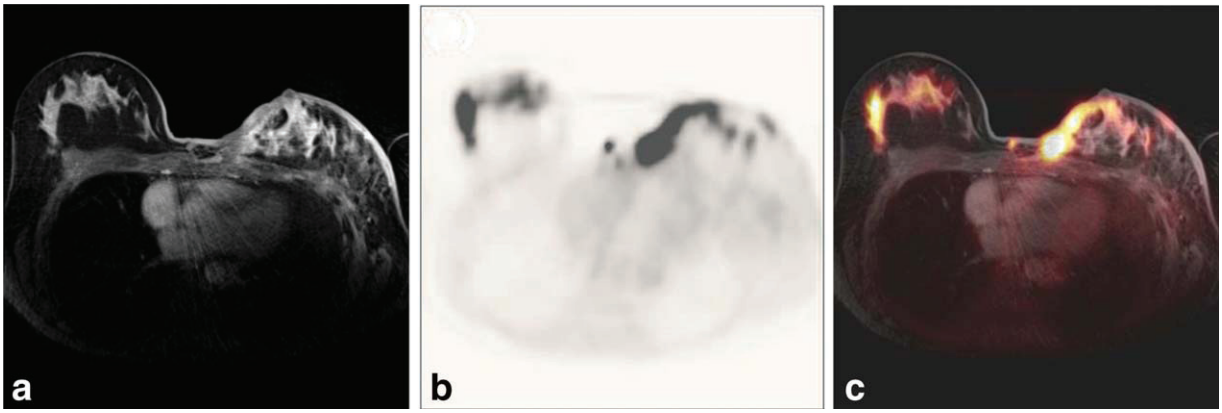

Figure 10. Breast cancer patient with invasive breast cancer and ductal carcinoma in situ (DCIS) in the right breast and postradiation cellulitis, inflammation, and residual tumor in the left breast. **A:** Contrast-enhanced fat-suppressed T1-weighted MRI shows bilateral contrast enhancement. **B:** Corresponding PET images show bilateral 18F-FDG-enhancement. **C:** PET/MR datasets show excellent spatial and geometric overlap of the breast lesions.

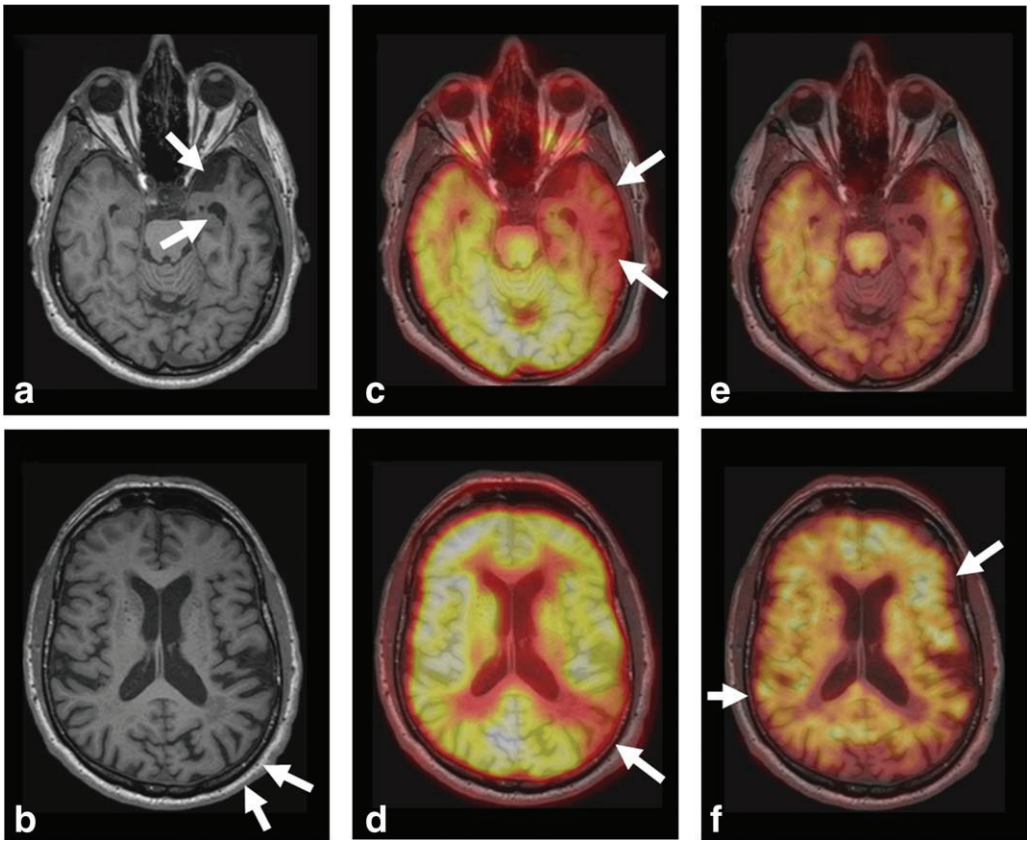

Figure 11. A 77-year-old male patient with suspected dementia disorder due to change of personality, impaired long and short term memory, and productive aphasia. MR imaging (**A,B**; T1-FLAIR) in a simultaneous PET/MR examination reveals hippocampal and temporal atrophy (arrows in (A,B)) while 18F-FDG-PET imaging (**C,D**) in this hybrid examination shows severe unilateral glucose hypometabolism (arrows in (C,D)). An additional 11C-PIB-PET examination (**E,F**) shows cortical β-amyloid deposition (arrows in (F)). The patient was diagnosed with unilateral Alzheimer's disease. Courtesy of Department of Nuclear Medicine (Director: Prof. Dr. O. Sabri), University of Leipzig, Germany.

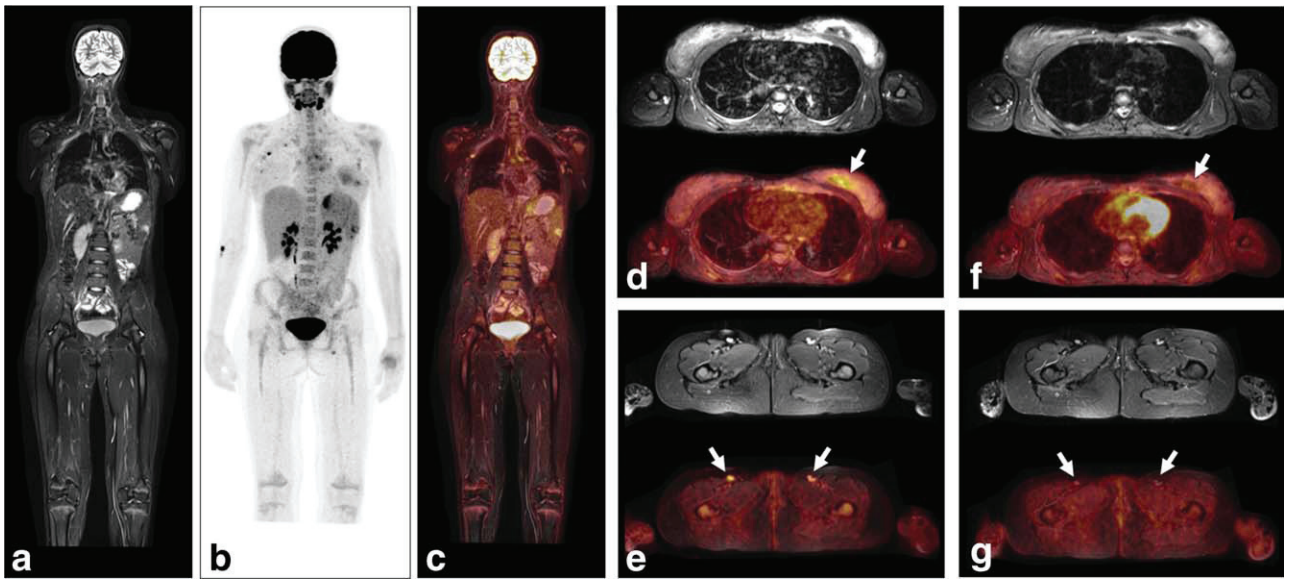

Figure 12. A 14-year-old female patient that was diagnosed with acute myeloid leukemia (AML). Primary staging with integrated PET/MR (**A–C**) revealed renal, pancreatic, mammary, splenic, and lymph node involvement. Chemotherapy was thus commenced. PET/MR imaging at 1 months follow-up after start of chemotherapy (**D,E**) revealed residual tumor in left mammary formation ($SUV_{max} = 3.6$) (arrow in D) and residual tumor in inguinal lymph nodes ($SUV_{max} = 3.1$) (arrows in E). PET/MR imaging at 2 months follow-up after start of chemotherapy (**F,G**) shows a complete response to chemotherapy and no sign of increased tracer activity in the same regions (arrows in F,G). Courtesy of Department of Nuclear Medicine (Director: Prof. Dr. O. Sabri), University of Leipzig, Germany.

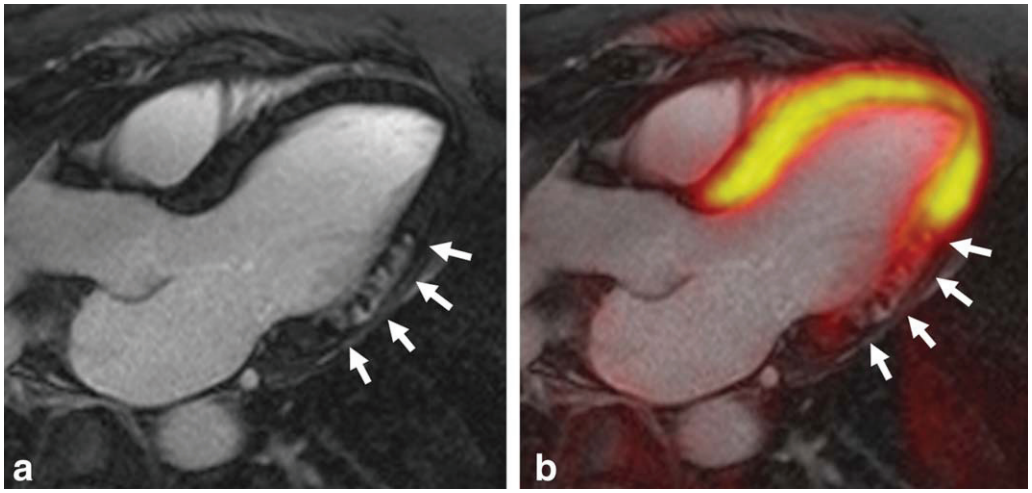

Figure 13. Simultaneous cardiac PET/MR with 18F-FDG after oral glucose loading in a patient with STEMI because of an acute occlusion of the left circumflex artery (CX). Imaging was performed 5 days after the event and subsequent interventional revascularization. The MR data (**A**) show late gadolinium-enhancement (LGE) with transmural extend (bright area in the lateral wall, white arrows in A) and areas of microvascular obstruction (dark spots within bright area). Image (**B**) shows a fusion of the MR image (A) and corresponding PET image. The fusion shows almost perfect agreement between LGE and reduced glucose uptake (white arrows in B). Courtesy of F. Nensa and T. Schlosser, University Hospital Essen, Germany.

and metabolic processes in vivo (80). Potential clinical applications in cardiac imaging have been identified, such as the detection of myocardial viability (80) where the unique strengths of each modality could potentially be combined to complement each other (81). In a recent simultaneous PET/MR feasibility study, Nensa et al investigated 20 patients with myocardial infarction. The results of the study demonstrated high correlation of ischemic myocardial segments in MR late gadolinium enhancement (LGE) and 18F-FDG (PET) (82) (Fig. 13).

Hybrid imaging with PET/MR may also find a role in atherosclerotic imaging. Initial experimental studies on atherosclerotic rabbits with PET/MR using ultra small particles of iron oxide (USPIO) for contrast enhancement in MR and 18F-FDG as PET tracer allowed for assessment of changes in the inflammation of atherosclerotic plaques (83). The authors concluded that 18F-FDG PET seemed more sensitive than USPIO MR to detect early changes in plaque inflammation (83).

With the heart being subject to cardiac and breathing motion during PET and MR data acquisition, it is expected that the development and application of advanced triggering, nonrigid motion correction, and attenuation correction methods will have a substantial impact on PET/MR cardiac imaging in general and more specific in myocardial tissue quantification (62).

WORKFLOW AND STANDARDIZATION

Hybrid Imaging Workflow

Because integrated PET/MR systems allow for the simultaneous data acquisition of PET and MR data, the imaging workflow should be designed to maximize diagnostic information in the shortest possible acquisition time without sacrificing image quality. This strategy also maximizes patient comfort and patient throughput. However, PET and MR are rather slow imaging modalities that acquire data in the range of several minutes for each bed position which has to be multiplied by the number of typically 5–7 bed positions (each with approximately 26 cm coverage along z-axis in current integrated PET/MR systems) for whole-body coverage. In contrast to MR-only imaging, additional acquisition time has to be assigned to the MR-based attenuation correction sequences that typically amounts to one breath hold acquisition (18–19 s) per bed position for a 3D Dixon-VIBE sequence (13–15, 26) (Fig. 14).

Two basic whole-body imaging workflow strategies are currently being pursued in integrated PET/MR: (i) Fast whole-body screening with 2–3 min acquisition time for simultaneous PET and MR data acquisition featuring only a Dixon sequence on the MR side to provide MR-based AC and some anatomic reference (84). This allows for fast whole-body coverage and if necessary for dedicated local protocols at defined body regions (e.g., liver) then featuring other MR sequences (e.g., contrast agent). (ii) Imaging with a comprehensive MR protocol featuring standard T1, T2 anatomic sequences supplemented by functional imaging with, e.g., diffusion weighted imaging (DWI) (67, 85), followed by contrast agent administration and multi-phase perfusion studies, if necessary. In such protocols, the MR data acquisition time determines the overall bed position time and thus is the limiting factor. Bed position times here amount to approximately 6–10 min and accordingly comprehensive whole-body imaging protocols last in the range of 40–60 min (13, 15).

First studies now investigate the aspect of imaging workflow optimization with the motivation to tailor MR imaging protocols but also PET imaging times according to the clinical indication while supporting diagnostic image quality (86–88). New whole-body

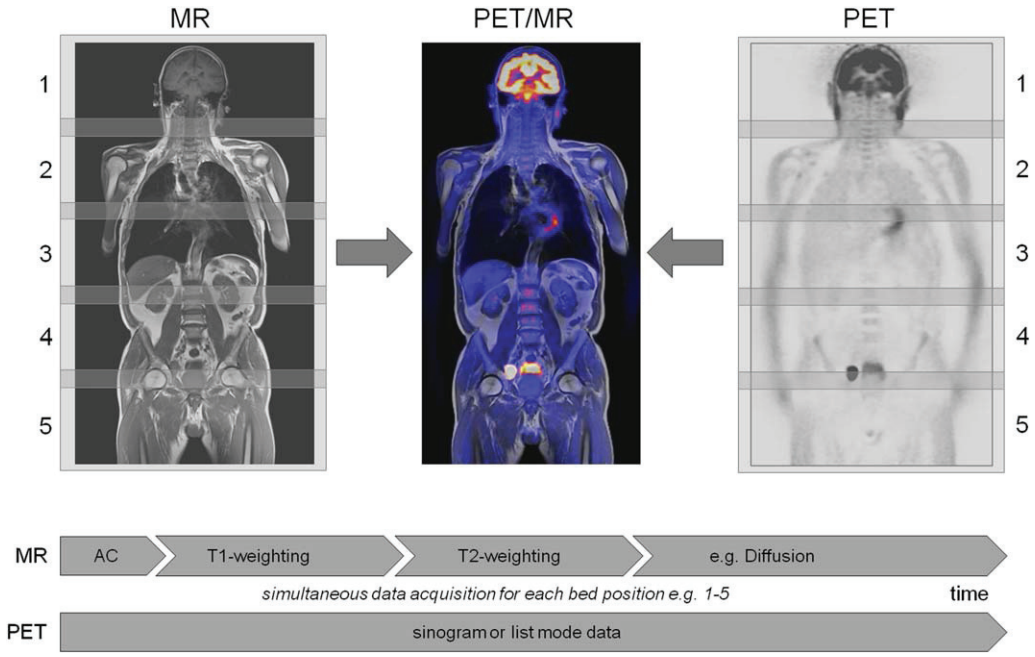

Figure 14. PET/MR simultaneous imaging workflow. MR (left) and PET (right) data acquisition is performed simultaneously during a multi-step examination with typically 4–7 bed positions (here 5 positions) for whole-body coverage. The standard MR examination encompasses sequences for attenuation correction (AC), and T1 and T2-weighted imaging for each individual station (time bars). Depending on the clinical indication other or additional sequences (e.g., diffusion weighted imaging, DWI) are acquired during simultaneous PET data acquisition. [Color figure can be viewed in the online issue, which is available at wileyonlinelibrary.com.]

data acquisition strategies are also being explored revisiting the concept of data acquisition during continuous movement of the patient table (51). Such a strategy allows for more flexibility in whole-body data acquisition and holds potential for further improvements in the PET/MR hybrid imaging workflow.

Artifacts

Each new imaging modality and technical system introduces new types of artifacts and in new hybrid imaging concepts the potential for new artifacts is even higher than just considering two independent systems. Artifacts in PET/MR might not only affect the visual impression of either MR or PET data but may also have an effect on quantification in MR and even stronger on PET being a quantitative method. Artifacts in integrated PET/MR may result from technical crosstalk between the MR and the PET components of the hybrid system. Both imaging centers might not be co-aligned correctly. Differences in the data acquisition speed between MR and PET might lead to local misalignments. MR-based AC is still a new concept that is supposed to support PET data quantification in the best possible way. All deviations from the real physical gamma quanta attenuation will ultimately lead to false values in PET quantification following attenuation correction (89, 90). Administration of contrast agents before application of MR-based AC due to changes in contrast potentially may lead to errors in tissue segmentation (91). Patient implants made from metal in this context introduce new associated artifacts. Metal implants might introduce signal voids or local image distortions in the MR-based AC sequence (e.g., Dixon), that exceed the physical implant volume. Such signal voids might then be assigned with the low linear attenuation coefficients of air in the image segmentation process. This will then lead to undercorrection of the real attenuation values in the region of and around the implant. While the first clinical studies evaluate the impact of implants on MR-based AC (92), current methods for artifact reduction suggest, e.g., to assign the implant induced signal voids with the LAC of soft tissue by inpainting (92). This, in consequence, reduces the quantification error but does not completely eliminate the problem of undercorrection.

Artifact reduction in MR imaging of patients with implants is currently an active topic of research. New methods such as MAVRIC (multi-acquisition variable-resonance image combination) (93), VAT (view-angle tilting) (94), SEMAC (slice encoding for metal artifact correction) (95) are currently under development with the overall goal of reducing the amount of image distortion and signal voids often exceeding the physical size of the implant by multitudes (93–95). The use of such artifact reducing sequences also appears potentially attractive in the context of MR-based AC in PET/MR. Knowing the real extent of an implant can help reducing the amount of wrong LAC assignments and basically allows for substitution of the implant induced signal voids with high attenuation values.

The CT-based attenuation correction in PET/CT hybrid imaging is also confronted with quantification errors when imaging patients with metal implants, e.g., dental implants (96, 97) and hip prosthesis. Here, however, local streak artifacts from CT beam hardening around metal structures can lead to an

Table 1
Challenges and current correction methods for attenuation correction (AC) in integrated PET/MR hybrid imaging

Challenge	Correction method	Reference #
• Attenuation correction (AC) of hardware components	• CT-based and energy converted templates of hardware components (e.g. Patient table, RF coils, etc.)	(15–24)
• Attenuation correction (AC) of human tissues	• MR-based tissue segmentation into tissue classes (e.g. background air, soft tissues, fat, lung) with Dixon-sequences	(24–34)
• Adding bone information to MR-based attenuation correction	• MR-based bone segmentation with ultrashort echo time sequences (e.g. UTE, PETRA)	(35–42, 44, 45)
	• Training data using pattern recognition methods (e.g. support vector regression, SVR) and UTE sequences	(43)
	• Atlas-based registration of pre-acquired bone information (CT-data) to individual patient cases	(24, 27)
• Truncation of body structures exceeding the field-of-view in MR-based attenuation correction	• PET-based detection of outer patient contours and subsequent image segmentation (e.g. MLAA algorithm)	(46–48)
	• MR-based extension of the field-of-view with optimized read out gradients (e.g. HUGE algorithm)	(49, 52)
• Motion during MR and/or PET data acquisition	• MR-derived motion fields applied to PET reconstruction	(53–62)
• Motion between MR-based attenuation map and PET data acquisition	• Acquisition of multi-phase MR-based AC maps during breathing and co-reconstruction of list-mode PET-data to matching AC phase	(57, 58)
• Implants causing artifacts in MR-based attenuation correction	• Artifact reducing MR sequences (e.g. MAVRIC, VAT, SEMAC, UTE, etc.). Inpainting to assign artifacts to soft-tissue	(89, 90, 92–95)

assignment of higher LAC in the tissue volume surrounding implants and this consequently leads to an overcorrection and associated higher PET activity values around implants (96, 97). Also, in PET/CT imaging artifact reducing algorithms have been proposed to optimize CT-based AC in regions around implants (97) (Table 1).

Quantification and Standardization

In PET, CT, and combined PET/CT imaging quantification and standardization mechanisms as well as according phantom tests have been developed and routinely implemented because these imaging modalities methods are associated with ionizing radiation (98). Furthermore, PET is a quantitative method and in standardized calibration measurements it must be assured that each PET system provides correct values for tracer activity and quantification as well as constant image quality (68, 69, 98). Because MR imaging is not associated with ionizing radiation, such calibrations and image quality testing is not mandatory on a regular basis to date. This might change in the future with the current introduction of PET/MR hybrid imaging systems. At least the PET component of PET/MR systems for aforementioned reasons requires routine calibration and image quality testing along established standards (98) which is currently performed with according phantoms. Because AC of PET data is an important aspect for quantification with hybrid

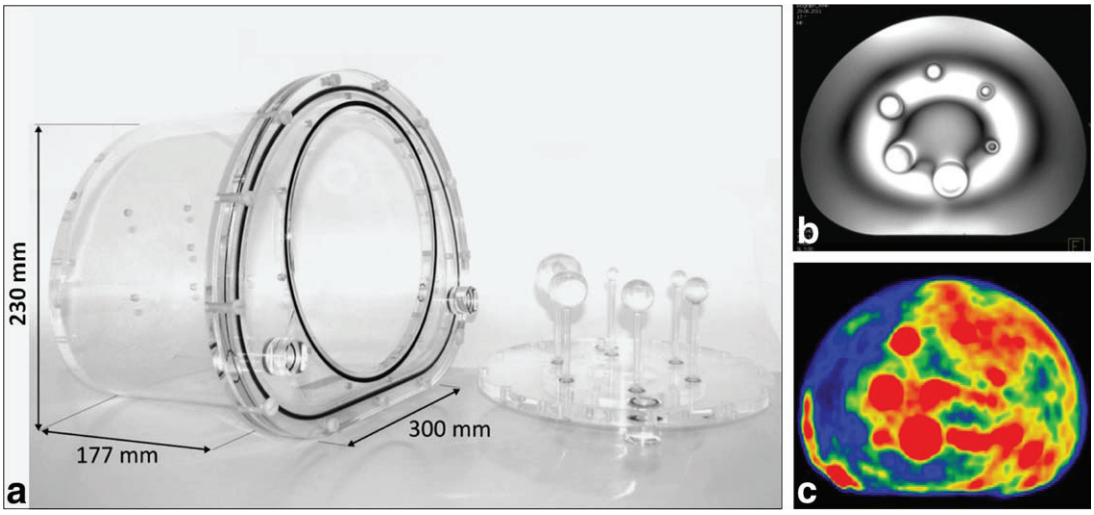

Figure 15. The IEC 61675-1 standard PET body-phantom for image quality testing in PET imaging (**A**) (14). The images on the right show examples of inhomogeneous MR excitation (at 3.0T) in water (**B**) and inhomogeneous PET-tracer distribution (18F-FDG) in oil-based substances (**C**) in the described phantom. [Color figure can be viewed in the online issue, which is available at wileyonlinelibrary.com.]

systems, standardization will long-term also have an impact on the methods of overall AC-map generation and, more specific, on MR-based AC. An important first step in this direction is the development of phantoms that are visible and quantifiable in MR imaging as well as in PET (99). This is demanding because water-filled large body phantoms (e.g., NEMA standard image quality phantom, 10 Liters volume) (Fig. 15A) show artifacts and B_1-signal inhomogeneities and MR signal voids when imaged at 3.0T field strength as with the current 3T PET/MR systems (99) (Fig. 15B). This is attributed to the high dielectric constant epsilon r (ε_r) of water reducing the RF excitation wavelength resulting in standing RF waves in phantoms (100–102) and central brightening effects (103). Phantom oil fillings thus are an established alternative in highfield MR imaging and due to their low ε_r show improved B_1-signal homogeneity. The most common PET tracer, FDG, however, does not dissolve well in oily substances (Fig. 15C) (99). Phantom fluids that provide favorable image quality features in PET, MR, and PET/MR hybrid imaging are currently under development and can be considered a first step toward standardization in PET/MR hybrid imaging (99, 104). As in PET/CT hybrid imaging before, the development of appropriate phantoms and standards for PET/MR is driven by the motivation to standardize aspects of PET activity quantification and attenuation correction. A success in this regard potentially will allow for standardized on-site quality control, multicenter trials, and inter-modality comparisons in PET/MR hybrid imaging.

CONCLUSIONS

Integrated whole-body MR/PET imaging has entered the clinical arena. On the physics and hardware development level, this opens up completely new options for medical imaging research. Hardware component and tissue attenuation correction, MR-based motion correction for PET imaging, development of dedicated RF coils and hardware components designed toward PET-transparency, and standardization efforts are only few examples of this exciting hybrid imaging field. Beyond the scope of initial clinical PET/CT versus PET/MR comparison studies, integrated PET/MR hybrid imaging is now under evaluation to define its diagnostic value in various clinical applications in oncology, neurology, cardiology, pediatric imaging, and therapy planning and monitoring. Already today neurologic diagnostic imaging and therapy monitoring in pediatric oncology emerge as potential key applications of integrated PET/MR. The use of various radiotracers, administration of MR contrast agent, and dedicated MR sequences for specific indications will unveil the full diagnostic potential of this new hybrid imaging modality.

EDUCATIONAL OBJECTIVES

Upon completion of this educational activity, participants will be better able to describe the basic principles of integrated PET/MR, methods for attenuation correction, hybrid imaging workflow, artifact characterization, and the clinical application of integrated PET/MR in various diseases.

ACTIVITY DISCLOSURES

The Biograph mMR integrated PET/MR system at the Institute of Medical Physics (IMP), Erlangen, Germany, is funded by a research agreement between the University of Erlangen and Siemens AG Healthcare Sector, Erlangen, Germany.

REFERENCES

1. Pichler BJ Judenhofer MS, Catana C, et al. Performance test of an LSO-APD detector in a 7-T MRI scanner for simultaneous PET/MRI. J Nucl Med 2006;47:639–647.
2. Pichler BJ, Wehrl HF, Kolb A, Judenhofer MS. Positron emission tomography/magnetic resonance imaging: the next generation of multimodality imaging? Semin Nucl Med 2008;38:199–208.
3. Pichler BJ, Judenhofer MS, Wehrl HF. PET/MRI hybrid imaging: devices and initial results. Eur Radiol 2008;18:1077–1086.
4. Antoch G, Bockisch A. Combined PET/MRI: a new dimension in whole-body oncology imaging? Eur J Nucl Med Mol Imaging 2009;36(Suppl 1):S113–S120.
5. Schiepers C, Dahlbom M. Molecular imaging in oncology: the acceptance of PET/CT and the emergence of MR/PET imaging. Eur Radiol 2011;21:548–554.
6. Maramraju SH, Smith SD, Junnarkar SS, et al. Small animal simultaneous PET/MRI: initial experiences in a 9.4 T microMRI. Phys Med Biol 2011;56:2459–2480.
7. Levin C, Glover G, Deller T, McDaniel D, Peterson W, Maramraju SH. Prototype time-of-flight PET ring integrated with a 3T MRI system for simultaneous whole-body PET/MR imaging. J Nucl Med 2013;(Suppl 2):148.
8. Schlemmer H-PW, Pichler BJ, Schmand M, et al. Simultaneous MR/PET imaging of the human brain: feasibility study. Radiology 2008;248:1028–1035.
9. Boss A, Stegger L, Bisdas S, et al. Feasibility of simultaneous PET/MR imaging in the head and upper neck area. Eur Radiol 2011;21:1439–1446.
10. Schwenzer NF, Stegger L, Bisdas S, et al. Simultaneous PET/MR imaging in a human brain PET/MR system in 50 patients–current state of image quality. Eur J Radiol 2012;81:3472–3478.
11. Zaidi H, Ojha N, Morich M, et al. Design and performance evaluation of a whole-body Ingenuity TF PET-MRI system. Phys Med Biol 2011;21:3091–3106.
12. Delso G, Fürst S, Jakoby B, et al. Performance measurements of the Siemens mMR integrated whole-body PET/MR scanner. J Nucl Med 2011;52:1914–1922.
13. Drzezga A, Souvatzoglou M, Eiber M, et al. First clinical experience with integrated whole-body PET/MR: comparison to PET/CT in patients with oncologic diagnoses. J Nucl Med 2012;53:845–855.
14. Schwenzer NF, Schraml C, Müller M, et al. Pulmonary lesion assessment: comparison of whole-body hybrid MR/PET and PET/CT imaging–pilot study. Radiology 2012;264:551–558.
15. Quick HH, von Gall C, Zeilinger M, et al. Integrated whole-body PET/MR hybrid imaging: clinical experience. Invest Radiol 2013;48:280–289.
16. Kinahan PE, Hasegawa BH, Beyer T. X-ray-based attenuation correction for positron emission tomography/computed tomography scanners. Semin Nucl Med 2003;33:166–179.
17. Carney JPJ, Townsend DW, Rappoport V, Bendriem B. Method for transforming CT images for attenuation correction in PET/CT imaging. Med Phys 2006;33:976–983.
18. Delso G, Martinez-Moller A, Bundschuh RA, et al. Evaluation of the attenuation properties of MR equipment for its use in a whole-body PET/MR scanner. Phys Med Biol 2010;55:4361–4374.
19. Tellmann L, Quick HH, Bockisch A, Herzog H, Beyer T. The effect of MR surface coils on PET quantification in whole-body PET/MR: results from a pseudo-PET/MR phantom study. Med Phys 2011;38:2795–2805.

20. MacDonald LR, Kohlmyer S, Liu C, Lewellen TK, Kinahan PE. Effects of MR surface coils on PET quantification. Med Phys 2011;38:2948–2956.
21. Paulus D, Braun H, Aklan B, Quick HH. Simultaneous PET/MR imaging: MR-based attenuation correction of local radiofrequency surface coils. Med Phys 2012;39:4306–4315.
22. Aklan B, Paulus DH, Wenkel E, et al. Toward simultaneous PET/MR breast imaging: systematic evaluation and integration of a radiofrequency breast coil. Med Phys 2013;40:024301.
23. Mantlik F, Hofmann M, Werner MK, et al. The effect of patient positioning aids on PET quantification in PET/MR imaging. Eur J Nucl Med Mol Imaging 2011;38:920–929.
24. Hofmann M, Pichler B, Scholkopf B, Beyer T, Towards quantitative PET/MRI: a review of MR-based attenuation correction techniques. Eur J Nucl Med Mol Imaging 2009;36(Suppl 1):S93–S104.
25. Beyer T, Weigert M, Quick HH, et al. MR-based attenuation correction for torso-PET/MR imaging: pitfalls in mapping MR to CT data. Eur J Nucl Med Mol Imaging 2008;35:1142–1146.
26. Martinez-Moller A, Souvatzoglou M, Delso G, et al. Tissue classification as a potential approach for attenuation correction in whole-body PET/MRI: evaluation with PET/CT data. J Nucl Med 2009;50:520–526.
27. Hofmann M, Bezrukov I, Mantlik F, et al. MRI-based attenuation correction for whole-body PET/MRI: quantitative evaluation of segmentation- and atlas-based methods. J Nucl Med 2011;52: 1392–1399.
28. Schulz V, Torres-Espallardo I, Renisch S, et al. Automatic, three-segment, MR-based attenuation correction for whole-body PET/MR data. Eur J Nucl Med Mol Imaging 2011;38:138–152.
29. Berker Y, Franke J, Salomon A, et al. MRI-based attenuation correction for hybrid PET/MRI systems: a 4-class tissue segmentation technique using a combined ultrashort-echo-time/ Dixon MRI sequence. J Nucl Med 2012;53:796–804.
30. Bezrukov I, Mantlik F, Schmidt H, Scholkopf B, Pichler BJ. MR-based PET attenuation correction for PET/MR imaging. Semin Nucl Med 2013;43:45–59.
31. Schramm G, Langner J, Hofheinz F, et al. Quantitative accuracy of attenuation correction in the Philips Ingenuity TF whole-body PET/MR system: a direct comparison with transmission-based attenuation correction. MAGMA 2013;26:115–126.
32. Keereman V, Holen RV, Mollet P, Vandenberghe S. The effect of errors in segmented attenuation maps on PET quantification. Med Phys 2011;38:6010–6019.
33. Kim JH, Lee JS, Song IC, Lee DS. Comparison of segmentation-based attenuation correction methods for PET/MRI: evaluation of bone and liver standardized uptake value with oncologic PET/ CT data. J Nucl Med 2012;53:1878–1882.
34. Marshall HR, Prato FS, Deans L, Theberge J, Thompson RT, Stodilka RZ. Variable lung density consideration in attenuation correction of whole-body PET/MRI. J Nucl Med 2012;53:977–984.
35. Samarin A, Burger C, Wollenweber SD, et al. PET/MR imaging of bone lesions - implications for PET quantification from imperfect attenuation correction. Eur J Nucl Med Mol Imaging 2012; 39:1154–1160.
36. Akbarzadeh A, Ay MR, Ahmadian A, Alam NR, Zaidi H. MRI-guided attenuation correction in whole-body PET/MR: assessment of the effect of bone attenuation. Ann Nucl Med 2013;27: 152–162.
37. Waldman A, Rees JH, Brock CS, Robson MD, Gatehouse PD, Bydder GM. MRI of the brain with ultra-short echo-time pulse sequences. Neuroradiology 2003;45:887–892.
38. Catana C, van der Kouwe A, Benner T, et al. Toward implementing an MRI-based PET attenuation-correction method for neurologic studies on the MR-PET brain prototype. J Nucl Med 2010; 51:1431–1438.
39. Keereman V, Fierens Y, Broux T, De Deene Y, Lonneux M, Vandenberghe S. MRI-based attenuation correction for PET/MRI using ultrashort echo time sequences. J Nucl Med 2010;51:812–818.
40. Johansson A, Karlsson M, Nyholm T. CT substitute derived from MRI sequences with ultrashort echo time. Med Phys 2011;38: 2708–2714.
41. Berker Y, Franke J, Salomon A, et al. MRI-based attenuation correction for hybrid PET/MRI systems: a 4-class tissue segmentation technique using a combined ultrashort-echo-time/ Dixon MRI sequence. J Nucl Med 2012;53:796–804.
42. Larsson A, Johansson A, Axelsson J, et al. Evaluation of an attenuation correction method for PET/MR imaging of the head based on substitute CT images. MAGMA 2013;26:127–136.
43. Navalpakkam BK, Braun H, Kuwert T, Quick HH. Magnetic resonance-based attenuation correction for PET/MR hybrid imaging using continuous valued attenuation maps. Invest Radiol 2013;48:323–332.
44. Li C, Magland JF, Rad HS, Song HK, Wehrli FW. Comparison of optimized soft-tissue suppression schemes for ultrashort echo time MRI. Magn Reson Med 2012;68:680–689.
45. Grodzki DM, Jakob PM, Heismann B. Ultrashort echo time imaging using pointwise encoding time reduction with radial acquisition (PETRA). Magn Reson Med 2012;67:510–518.
46. Delso G, Martinez-Moller A, Bundschuh RA, Nekolla SG, Ziegler SI. The effect of limited MR field of view in MR/PET attenuation correction. Med Phys 2010;37:2804–2812.
47. Nuyts J, Dupont P, Stroobants S, Benninck R, Mortelmans L, Suetens P. Simultaneous maximum a posteriori reconstruction of attenuation and activity distributions from emission sinograms. IEEE Trans Med Imaging 1999;18:393–403.
48. Nuyts J, Bal G, Kehren F, Fenchel M, Michel C, Watson C. Completion of a truncated attenuation image from the attenuated PET emission data. IEEE Trans Med Imaging 2013;32:237–246.
49. Blumhagen JO, Ladebeck R, Fenchel M, Scheffler K. MR-based field-of-view extension in MR/PET: B(0) homogenization using gradient enhancement (HUGE). Magn Reson Med 2012. doi: 10.1002/mrm.24555. [Epub ahead of print].
50. Zenge MO, Ladd ME, Quick HH. Novel reconstruction method for three-dimensional axial continuously moving table whole-body magnetic resonance imaging featuring autocalibrated parallel imaging GRAPPA. Magn Reson Med 2009;61:867–873.
51. Braun H, Ziegler S, Paulus DH, et al. Hybrid PET/MRI imaging with continuous table motion. Med Phys 2012;39:2735–2745.
52. Blumhagen JO, Ladebeck R, Fenchel M, Scheffler K, Quick HH. MR-based FOV extension in whole-body MR/PET using continuous table move. In: Proceedings of the 20th Annual Meeting of ISMRM, Melbourne, 2012. (abstract 2720).
53. Catana C, Benner T, van der Kouwe A, et al. MRI-assisted PET motion correction for neurologic studies in an integrated MR-PET scanner. J Nucl Med 2011;52:154–161.
54. Brendle CB, Schmidt H, Fleischer S, Braeuning UH, Pfannenberg CA, Schwenzer NF. Simultaneously acquired MR/ PET images compared with sequential MR/PET and PET/CT: alignment quality. Radiology 2013;268:190–199.
55. Tsoumpas C, Mackewn JE, Halsted P, et al. Simultaneous PET-MR acquisition and MR-derived motion fields for correction of non-rigid motion in PET. Ann Nucl Med 2010;24:745–750.
56. Tsoumpas C, Buerger C, King AP, et al. Fast generation of 4D PET-MR data from real dynamic MR acquisitions. Phys Med Biol 2011;56:6597–6613.
57. Würslin C, Schmidt H, Martirosian P, et al. Respiratory motion correction in oncologic PET using T1-weighted MR imaging on a simultaneous whole-body PET/MR system. J Nucl Med 2013;54: 464–471.
58. Grimm R, Fürst S, Dregely I, et al. MR-PET Respiration compensation using self-gated motion modeling. In: Proceedings of the 21st Annual Meeting of ISMRM, Salt Lake City, 2013. (abstract 829).
59. Guerin B, Cho S, Chun SY, et al. Nonrigid PET motion compensation in the lower abdomen using simultaneous tagged-MRI and PET imaging. Med Phys 2011;38:3025–3038.
60. Chun SY, Reese TG, Ouyang J, et al. MRI-based nonrigid motion correction in simultaneous PET/MRI. J Nucl Med 2012;53: 1284–1291.
61. Dikaios N, Izquierdo-Garcia D, Graves MJ, Mani V, Fayad ZA, Fryer TD. MRI-based motion correction of thoracic PET: initial comparison of acquisition protocols and correction strategies suitable for simultaneous PET/MRI systems. Eur Radiol 2012; 22:439–446.
62. Fieseler M, Kugel H, Gigengack F, et al. A dynamic thorax phantom for the assessment of cardiac and respiratory motion correction in PET/MRI: a preliminary evaluation. Nuc Instr Meth Physics Res A 2013;702:59–63.
63. Wiesmüller M, Quick HH, Lell M, et al. Comparison of lesion detection between PET from a simultaneously acquiring whole-

body PET/MR hybrid scanner and PET from PET/CT. Eur J Nucl Med Mol Imaging 2013;40:12–21.
64. Gaertner FC, Beer AJ, Souvatzoglou M, et al. Evaluation of feasibility and image quality of 68Ga-DOTATOC positron emission tomography/magnetic resonance in comparison with positron emission tomography/computed tomography in patients with neuroendocrine tumors. Invest Radiol 2013;48:263–272.
65. Eiber M, Souvatzoglou M, Pickhard A, et al. AJ. Simulation of a MR-PET protocol for staging of head-and-neck cancer including Dixon MR for attenuation correction. Eur J Radiol 2012;81: 2658–2665.
66. Wetter A, Lipponer C, Nensa F, et al. Simultaneous 18F choline positron emission tomography/magnetic resonance imaging of the prostate: initial results. Invest Radiol 2013;48:256–262.
67. Buchbender C, Hartung-Knemeyer V, Beiderwellen K, et al. Diffusion-weighted imaging as part of hybrid PET/MRI protocols for whole-body cancer staging: does it benefit lesion detection? Eur J Radiol 2013;82:877–882.
68. Adams MC, Turkington TG, Wilson JM, et al. A systematic review of the factors affecting accuracy of SUV measurements. AJR Am J Roentgenol 2010;195:310–320.
69. Boellaard R, O'Doherty MJ, Weber WA, et al. FDG PET and PET/CT: EANM procedure guidelines for tumor PET imaging: version 1.0. Eur J Nucl Med Mol Imaging 2010;37:181–200.
70. Heusch P, Buchbender C, Beiderwellen K, et al. Standardized uptake values for [^{18}F] FDG in normal organ tissues: comparison of whole-body PET/CT and PET/MRI. Eur J Radiol 2013;82: 870–876.
71. Bisdas S, Ritz R, Bender B, et al. Metabolic mapping of gliomas using hybrid MR-PET imaging: feasibility of the method and spatial distribution of metabolic changes. Invest Radiol 2013;48: 295–301.
72. Stegger L, Martirosian P, Schwenzer N, et al. Simultaneous PET/MR imaging of the brain: feasibility of cerebral blood flow measurements with FAIR-TrueFISP arterial spin labeling MRI. Acta Radiol 2012;53:1066–1072.
73. Barthel H, Gertz HJ, Dresel S, et al. Florbetaben Study Group. Cerebral amyloid-β PET with florbetaben (18F) in patients with Alzheimer's disease and healthy controls: a multicentre phase 2 diagnostic study. Lancet Neurol 2011;10:424–435.
74. Dukart J, Mueller K, Barthel H, Villringer A, Sabri O, Schroeter ML; Alzheimer's Disease Neuroimaging Initiative. Meta-analysis based SVM classification enables accurate detection of Alzheimer's disease across different clinical centers using FDG-PET and MRI. Psychiatry Res 2013;212:230–236.
75. Becker GA, Ichise M, Barthel H, et al. PET Quantification of 18F-florbetaben binding to β-amyloid deposits in human brains. J Nucl Med 2013;54:723–731.
76. Chavhan GB, Babyn PS. Whole-body MR imaging in children: principles, technique, current applications, and future directions. Radiographics 2011;31:1757–1772.
77. Goo HW, Choi SH, Ghim T, Moon HN, Seo JJ. Whole-body MR of paediatric malignant tumours: comparison with conventional oncological imaging methods. Pediatr Radiol 2005;35:766–773.
78. Kwee TC, Takahara T, Vermoolen MA, Bierings MB, Mali WP, Nievelstein RA. Whole-body diffusion-weighted imaging for staging malignant lymphoma in children. Pediatr Radiol 2010;40: 1592–1602.
79. Hirsch FW, Sattler B, Sorge I, et al. PET/MR in children. Initial clinical experience in paediatric oncology using an integrated PET/MR scanner. Pediatr Radiol 2013;43:860–875.
80. Klein C, Nekolla SG, Bengel FM, et al. Assessment of myocardial viability with contrast-enhanced magnetic resonance imaging: comparison with positron emission tomography. Circulation 2002;105:162–167.
81. Rischpler C, Nekolla SG, Dregely I, Schwaiger M. Hybrid PET/MR imaging of the heart: potential, initial experiences, and future prospects. J Nucl Med 2013;54:402–415.
82. Nensa F, Poeppel TD, Beiderwellen K, et al. Hybrid PET/MR imaging of the heart: feasibility and initial results. Radiology 2013;268:366–373.
83. Millon A, Dickson SD, Klink A, et al. Monitoring plaque inflammation in atherosclerotic rabbits with an iron oxide (P904) and (18)F-FDG using a combined PET/MR scanner. Atherosclerosis 2013;228:339–345.
84. Eiber M, Martinez-Möller A, Souvatzoglou M, et al. Value of a Dixon-based MR/PET attenuation correction sequence for the localization and evaluation of PET-positive lesions. Eur J Nucl Med Mol Imaging 2011;38:1691–1701.
85. Schmidt H, Brendle C, Schraml C, et al. Correlation of simultaneously acquired diffusion-weighted imaging and 2-Deoxy-[18F] fluoro-2-D-glucose positron emission tomography of pulmonary lesions in a dedicated whole-body magnetic resonance/positron emission tomography system. Invest Radiol 2013;48:247–255.
86. Martinez-Moller A, Eiber M, Nekolla SG, et al. Workflow and scan protocol considerations for integrated whole-body PET/MRI in oncology. J Nucl Med 2012;53:1415–1426.
87. Hartung-Knemeyer V, Beiderwellen KJ, Buchbender C, et al. Optimizing positron emission tomography image acquisition protocols in integrated positron emission tomography/magnetic resonance imaging. Invest Radiol 2013;48:290–294.
88. Vargas MI, Becker M, Garibotto V, et al. Approaches for the optimization of MR protocols in clinical hybrid PET/MRI studies. MAGMA 2013;26:57–69.
89. Keller SH, Holm S, Hansen AE, et al. Image artifacts from MR-based attenuation correction in clinical, whole-body PET/MRI. MAGMA 2013;26:173–181.
90. Buchbender C, Hartung-Knemeyer V, Forsting M, Antoch G, Heusner TA. Positron emission tomography (PET) attenuation correction artefacts in PET/CT and PET/MRI. Br J Radiol 2013; 86:20120570.
91. Lois C, Bezrukov I, Schmidt H, et al. Effect of MR contrast agents on quantitative accuracy of PET in combined whole-body PET/MR imaging. Eur J Nucl Med Mol Imaging 2012;39:1756–1766.
92. Ladefoged CN, Andersen FL, Keller SH, et al. PET/MR imaging of the pelvis in the presence of endoprostheses: reducing image artifacts and increasing accuracy through inpainting. Eur J Nucl Med Mol Imaging 2013;40:594–601.
93. Koch KM, Lorbiecki JE, Hinks RS, King KF. A multispectral three-dimensional acquisition technique for imaging near metal implants. Magn Reson Med 2009;61:381–390.
94. Sutter R, Ulbrich EJ, Jellus V, Nittka M, Pfirrmann CW. Reduction of metal artifacts in patients with total hip arthroplasty with slice-encoding metal artifact correction and view-angle tilting MR imaging. Radiology 2012;265:204–214.
95. Lee YH, Lim D, Kim E, Kim S, Song HT, Suh JS. Usefulness of slice encoding for metal artifact correction (SEMAC) for reducing metallic artifacts in 3-T MRI. Magn Reson Imaging 2013;31:703–706.
96. Nahmias C, Lemmens C, Faul D, et al. Does reducing CT artifacts from dental implants influence the PET interpretation in PET/CT studies of oral cancer and head and neck cancer? J Nucl Med 2008;49:1047–1052.
97. Delso G, Wollenweber S, Lonn A, Wiesinger F, Veit-Haibach P. MR-driven metal artifact reduction in PET/CT. Phys Med Biol 2013;58:2267–2280.
98. National Electrical Manufacturers Association. NEMA Standards Publication NU 2-2007, Performance measurements of positron emission tomographs. Rosslyn, VA; NEMA; 2007. p 26–33.
99. Ziegler S, Braun H, Ritt P, Hocke C, Kuwert T, Quick HH. Systematic evaluation of phantom fluids for simultaneous PET/MR hybrid imaging. J Nucl Med 2013;54:1464–1471.
100. Tofts PS. Standing waves in uniform water phantoms. JMR Series B 1994;104:143–147.
101. Tofts PS, Barker GJ, Dean TL, Gallagher H, Gregory AP, Clarke RN. A low dielectric constant customized phantom design to measure RF coil nonuniformity. Magn Reson Imaging 1997;15: 69–75.
102. Sled JG, Pike GB. Standing-wave and RF penetration artifacts caused by elliptic geometry: an electrodynamic analysis of MRI. IEEE Trans Med Imaging 1998;17:653–662.
103. Tropp J. Image brightening in samples of high dielectric constant. J Magn Reson 2004;167:12–24.
104. Hattori K, Ikemoto Y, Takao W, et al. Development of MRI phantom equivalent to human tissues for 3.0-T MRI. Med Phys 2013; 40:032303.

Whole-Body Simultaneous Positron Emission Tomography (PET)-MR: Optimization and Adaptation of MRI Sequences

Kathryn J. Fowler, M.D.,* Jon McConathy, M.D., Ph.D., and Vamsi R. Narra, M.D.

Reprinted with permission from the ISMRM Journal of Magnetic Resonance Imaging: Volume 39: 259–268 © with permission from 2013 Wiley Periodicals, Inc.

The purpose of this article is to introduce the underlying challenges associated with the incorporation of magnetic resonance imaging (MRI) into the new hybrid imaging modality simultaneous positron emission tomography (PET)/MR and their impact on attenuation correction, sequence optimization, and protocol development. Many adjustments to MR sequences are necessary for optimal whole-body and fused image results.

Key Words: PET/MR; MRI; oncology; mMR; whole-body imaging
J. Magn. Reson. Imaging 2014;39:259–268.
© **2013 Wiley Periodicals, Inc.**

RADIOLOGY AND NUCLEAR MEDICINE are evolving fields, expanding beyond the traditional boundaries of anatomic and molecular imaging. As one of the fastest-growing modalities in radiology, magnetic resonance imaging (MRI) gives both anatomic and functional information. Positron emission tomography (PET) / computed tomography (CT) with the glucose analog 2-[^{18}F]fluoro-2-deoxy-D-glucose (FDG) has been a main area of growth for nuclear medicine in recent years. One of the main strengths of FDG-PET/CT is the clinically relevant metabolic information obtained with FDG that complements the anatomic and morphologic information provided by CT. As the newest hybrid imaging technology, simultaneous PET/MR combines these exciting areas of growth for radiology and nuclear medicine and further bridges the divide between anatomic and molecular imaging. PET/MR can noninvasively provide molecular, functional, and anatomic information in a single imaging session using FDG and other PET tracers in conjunction with state-of-the-art MRI.

Department of Radiology, Washington University, St. Louis, Missouri, USA.
*Address reprint requests to: K.J.F., Department of Radiology, Washington University, Mail stop: 8131, 510 S. Kingshighway Blvd., St. Louis, MO 63110. E-mail: fowlerk@mir.wustl.edu
Received October 30, 2012; Accepted June 18, 2013.
DOI 10.1002/jmri.24308
View this article online at wileyonlinelibrary.com.

Technological challenges of incorporating the photomultiplier tubes used in traditional PET acquisition within the magnetic field prompted the first PET/MR systems to be developed as sequential imaging units. In the sequential approach, the whole-body MR images and PET data are acquired separately with a common table to shuttle the patient between scanners and postacquisition fusion of the images. This approach, while avoiding the issue of crosstalk between PET and MRI hardware, led to long examination times and potentially poor patient compliance. The first simultaneous system was a head-only prototype consisting of an MR-compatible PET-insert in 2007 (1). Shortly thereafter, the first simultaneous integrated whole-body PET/MR system was introduced in 2010 (Siemens Biograph mMR, Erlangen, Germany). This review focuses primarily on simultaneous PET/MR, although many of the same challenges are also faced by sequential PET/MR systems.

While representing a true technological advancement, the clinical role and impact of PET/MR has yet to be fully defined. Several potential benefits of PET/MR over PET/CT are clear. These include improved coregistration of PET and anatomic MR images through simultaneous acquisition, improved soft-tissue contrast compared to CT for anatomic imaging, and reduction in overall radiation exposure. While these benefits are evident, the translation into improved clinical care for patients has yet to be shown. Early studies demonstrate the feasibility and noninferiority of PET/MR compared to PET/CT with comparable standard uptake values (SUV) and anatomic localization (2–4). However, there remain many challenges and obstacles to overcome prior to widespread adoption into clinical use.

This article focuses on outlining and addressing some of the clinical challenges of PET/MR, with specific emphasis on optimization of MR sequences for oncologic imaging within the context of simultaneous imaging. Topics to be covered include MR-based attenuation correction, optimization of sequences on 3T for whole-body imaging, adapting MR sequences to PET/MR, and development of clinical protocols for whole-body imaging.

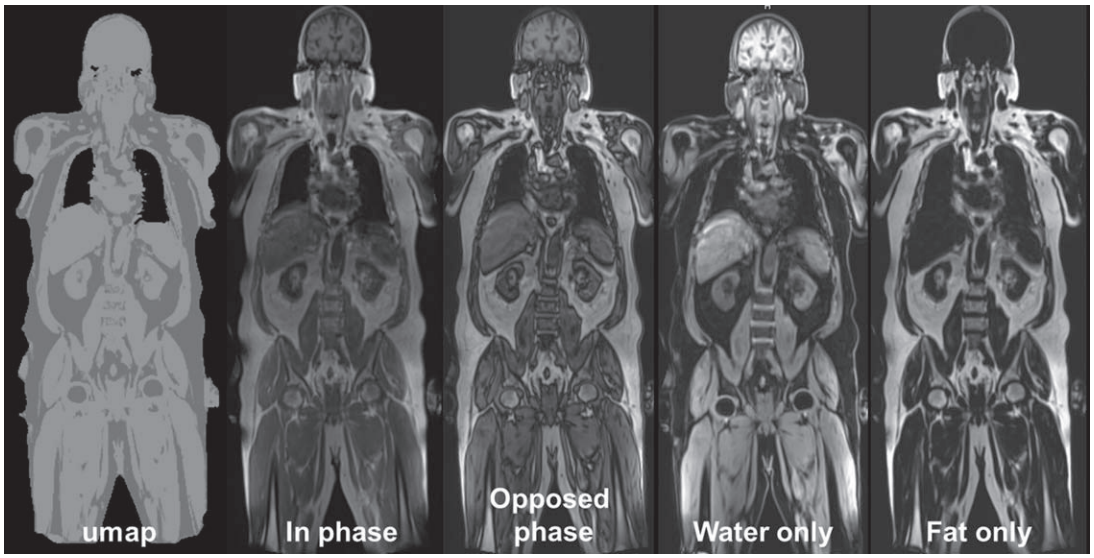

Figure 1. uMap and four Dixon sequences from attenuation correction sequences. The umap segments tissues in soft tissue, fat, lung, and air for attenuation correction of the PET data.

ATTENUATION CORRECTION

Attenuation correction in PET/CT is achieved through electron density information provided directly from CT transmission images, where Hounsfield units are used to create linear attenuation coefficients for the 511-keV photons. A common source of error in CT-based attenuation correction is the lack of simultaneous acquisition and subsequent misregistration of the PET and CT data. While modern postprocessing and reconstruction can correct for a majority of this misregistration, potential errors of up to 10% in SUV measurements have been reported (5,6). In contradistinction to CT Hounsfield units, MRI signal intensity reflects a combination of proton density and tissue relaxation properties, yielding no direct information about electron density and hence no inherent attenuation correction factor for the PET data. An additional source of error in attenuation correction that applies to both CT and MR methods is that of artifact related to metallic implanted devices.

Current MR-based attenuation correction methods can be divided into two types: segmentation-based and template-based. The US Food and Drug Administration (FDA)-approved Dixon segmentation method divides the body into four distinct tissue types based directly on the MR image intensity: soft tissue (muscle and solid organs), lungs, air, and fat (3,7–9) (Fig. 1). These tissues are then assigned a corresponding linear attenuation coefficient based on known densities. While soft tissues can be readily segmented using MRI sequences, cortical bone and air pose more challenges, as they contain virtually no proton signal when imaged with Dixon techniques. Hofmann et al (9,10) proposed an atlas registration and pattern recognition approach as an alternative method for whole-body attenuation correction. This template-based method uses multiple MR image sets averaged to form high signal-to-noise ratio (SNR) templates that are coregistered to the patient's images. Spatial transformations are then applied to a corresponding CT atlas dataset producing a pseudo-CT from which weighted intensities are generated for each voxel. While the segmentation method is likely sufficient for most clinical instances, this template-based approach may be useful where segmentation fails, such as artifact related to implanted prostheses, and may potentially improve PET quantification in bone marrow and brain, where segmentation may underestimate uptake (9,10).

Attenuation correction for osseous structures and adjacent soft tissues has proven particularly challenging using MR-based segmentation methods. Mineralized bone has a higher linear attenuation coefficient for 511 keV photons than soft tissues but is not represented in Dixon-based MR attenuation methods. Cortical bone has a much faster transverse relaxation rate than soft tissues, and hence any signal produced within traditional MR sequences disappears prior to sampling. As a result, the Dixon-based attenuation correction method does not take cortical bone into consideration and is less robust for osseous lesions and for the brain due to attenuation from the calvarium. For example, a study comparing standardized uptake values (SUVs) of FDG with attenuation maps that included and did not include cortical bone demonstrated underestimation of SUVs by ~10%–20% when cortical bone was not included in the attenuation map with a maximum error of 30.8% (11). It is possible to image with an ultrashort echo time (UTE) sequence, using TE less than 100 μsec, and visualize signal from cortical bone allowing for segmentation and hence attenuation correction (12,13). While the UTE approach to MRAC is promising, this approach currently is not suitable for routine clinical use and can introduce segmentation artifacts in the attenuation map. Overall, there are several approaches to MR-based attenuation correction that are particularly relevant to the brain and bones, and this issue remains an active area of research and development (8–13).

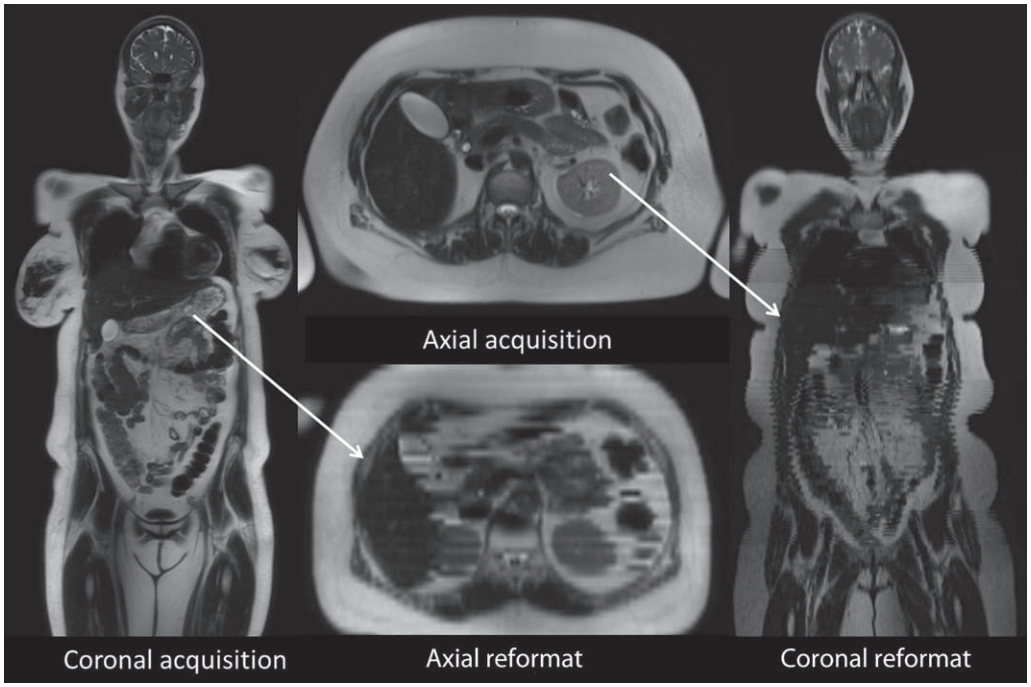

Figure 2. Single-shot fast spin echo images acquired with traditional parameters show respiratory motion and misregistration artifact which degrades image quality when reconstructed in different planes.

The initial research and clinical experience with FDG-PET/MR for oncologic imaging suggests that MR-based attenuation correction using the Dixon sequence provides PET data that is qualitatively very similar to data obtained from PET/CT (4,8). Because much of the interpretation of clinical FDG-PET is based on qualitative assessment of FDG uptake compared to adjacent tissues, relatively small differences in measured SUVs between PET/MR and PET/CT may not have substantial effect on lesion detection or characterization. The amount of variability in SUVs measured with MR-based attenuation correction is similar to or less than the ~20% test–retest variability seen with FDG-PET/CT studies (14). However, further studies are needed to prove this fundamental concept for clinical and research applications.

OPTIMIZATION OF MR SEQUENCES FOR WHOLE-BODY PET/MRI

Body Imaging at 3T

Given that the first simultaneous system for PET/MR was a 3T magnet, issues related to body imaging at 3T are relevant to the discussion of PET/MR development. Inherent benefits of imaging at 3T relate primarily to increased SNR, which can be traded for increased speed and/or spatial resolution; however, several challenges prevent full realization of these benefits for body imagers (15). These revolve mostly around more pronounced MR artifacts and specific absorption rate (SAR) issues. Image quality may be impacted by bands of signal loss, susceptibility artifact, poor fat suppression, and pronounced edge of field of view artifacts. Spin echo and turbo spin echo sequences may provide better image quality over gradient echo as the 180° refocusing pulse reduces susceptibility artifact. Other traditional options to decrease artifact such as obtaining images in isocenter mode (such that the center of the MR field of view is optimally positioned in the center of the magnetic field with regard to the z axis) and limiting the MR z-axis field of view are not ideal for simultaneous PET/MR. During simultaneous acquisition, the field of view and table translation are determined by the PET acquisition, which is maximized for coverage and must be acquired in a stationary fashion, which precludes continuous table movement or multiple small sequential stack/slab acquisitions that have traditionally been used in whole-body MR protocols. As a result, some gradient echo sequences which would otherwise be ideal in terms of speed of acquisition, such as balanced gradient echo sequences (true fast imaging with steady-state precession, True FISP), may not be the best option for whole-body coverage due to accentuated artifacts. Other challenges of body imaging at 3T are not unique to PET/MR and have for the most part been overcome. Issues related to image contrast as a result of increased T1 relaxation times and T2* effects at greater field strength may be overcome by optimally adjusting the time to repetition (TR), bandwidth, and flip angle and most sequences provide default parameters allowing for reasonable image quality (16). Additionally, chemical shift in- and opposed-phase imaging may be acquired with ultrashort TE allowing for acquisition of the first sequence during opposed phase (1.1 msec), which is ideal for identification of steatosis in the liver and characterization of adrenal and renal lesions.

SAR remains a challenge for 3T body imagers, and while not specific to PET/MR, deserves discussion as it may lead to unpredictable acquisition times not

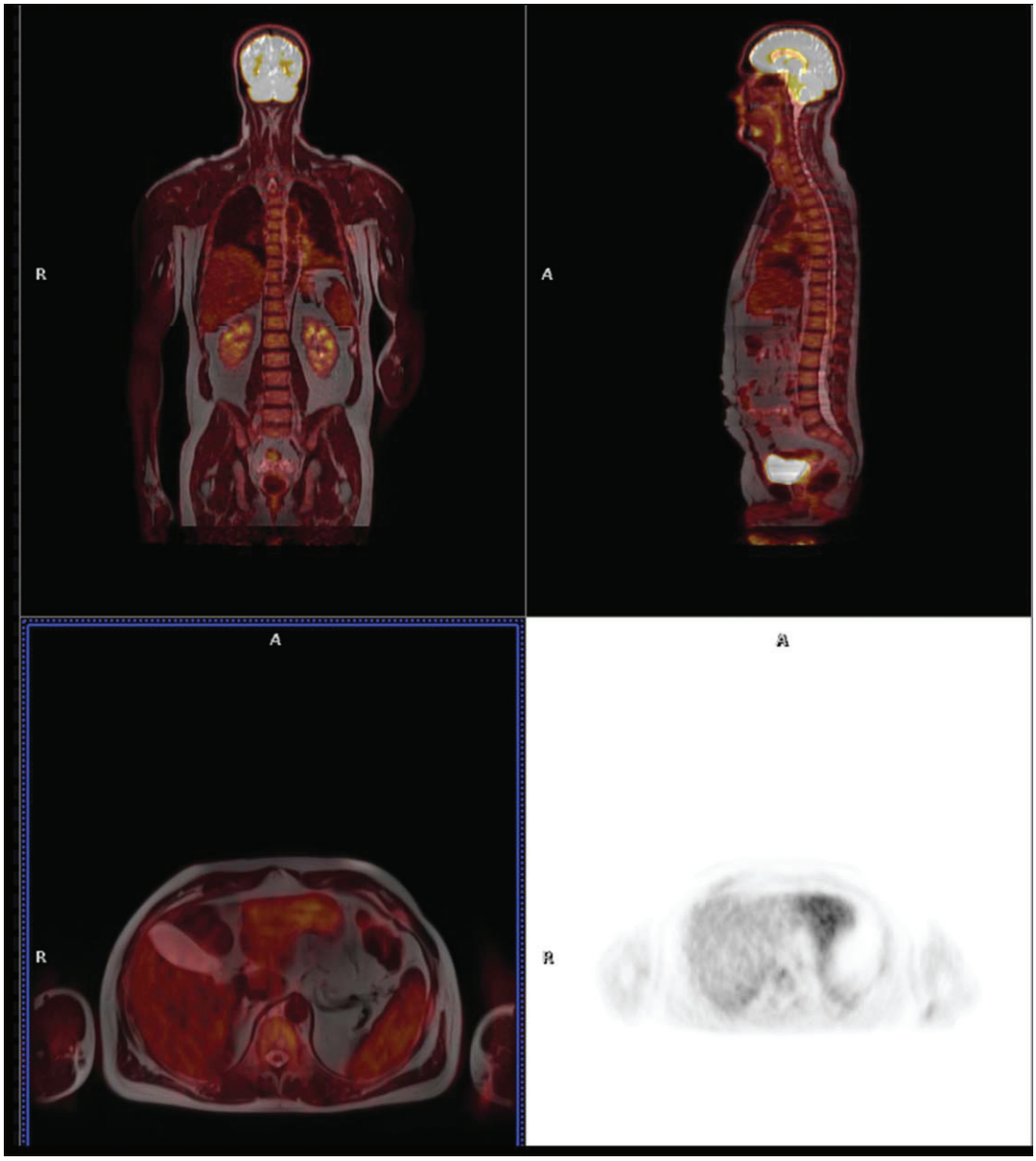

Figure 3. T2 single-shot fast spin echo sequence obtained at free-breathing with adjusted parameters (Table 2) demonstrate very little artifact when reformatted and register well with the PET data acquired simultaneously.

encountered with PET/CT that can negatively impact the workflow. SAR is a measure of the radiofrequency (RF) power absorbed per unit mass of the object being imaged (watts/kg). As magnetic field strength increases, SAR increases (from 1.5T to 3T, SAR quadruples). Other factors that increase SAR include increased flip angles, increased number of RF pulses, and reduced spacing of RF pulses. Hence, single-shot sequences or sequences with long echo trains are notorious for triggering SAR warnings on the console. Modifiers that affect SAR and potential solutions are shown in Table 1. These solutions are not without cost. Balancing sequence acquisition time, image quality, and SAR are a constant battle for the body imager. Manufacturer solutions may provide the best balance of image quality and safety. These include hyperecho-turbo spin echo sequences and low SAR RF options. Hyperecho is a variable flip angle sequence, with highest flip angle determining contrast in the center of *k*-space and lower flip angles applied to the periphery. This results in 60%–80% reduction in SAR and has been shown to have no significant impact on image quality when used for brain imaging (17). In our experience, this option results in reasonable image contrast and SNR for body imaging as well.

OPTIMIZATION OF MR SEQUENCES FOR PET/MR

Several factors must be taken into account when designing PET/MR protocols. These include issues related to free-breathing acquisition and multiplanar viewing of the composed fused datasets, as is the traditional approach to PET/CT viewing. In addition, specific challenges related to simultaneous acquisition warrant discussion.

Table 1
Specific Absorption Rate (SAR) Variables and Solutions

Parameters	Effect on SAR	Possible solutions
Flip angle (FA)	Increases as FA increases	Hyperecho option allows up to 60–80% decrease in SAR
Echo train length (ETL)	Increases with length of ETL	Reduce length of ETL
RF pulse	Increases as RF pulses increase in number and get closer together	Low SAR RF option
Magnetic field strength	Quadruples from 1.5T→3T	Opt for 1.5T (not currently an option for mMR)
Time to repetition (TR)	Increases as TR decreases	Increase TR if possible

Free-breathing FDG-PET data acquisition is the standard approach for whole-body staging examinations on PET/CT and PET/MR due to the need for at least 90–120 seconds of data acquisition at each bed position to obtain sufficient counting statistics. Unfortunately, respiratory motion results in blurring and distortion that can reduce the maximal achievable resolution of PET from the intrinsic spatial resolution of ~4 mm to closer to 11 mm (18–20). Prospective or retrospective gating of the PET data to the respiratory cycle may theoretically achieve optimal resolution. However, this form of motion correction generates a final image that is reconstructed from only a portion of the total useful counts. The end result is an image that either suffers from reduced SNR or requires a very long acquisition to recoup counts and image quality, making this option temporally inefficient for whole-body imaging. While a full discussion of motion correction is beyond the scope of this article, it should be noted that the simultaneous acquisition of PET and MR images affords the opportunity for more sophisticated motion correction. In particular, tagged MRI shows promise in animal and phantom models for nonrigid motion correction (21–24). Using this methodology, it may be possible to obtain motion-corrected PET data without increasing the imaging time for PET acquisition.

With regard to free-breathing acquisition, this approach is not ideal for MR sequences, which are sensitive to motion artifact and are often broken into multiple breath-holds or are acquired using respiratory navigation. While free-breathing sequences might offer the best coregistration for whole-body PET data, few MRI sequences are optimized for this type of acquisition. Pairing free-breathing PET data with end-expiration MR sequences might be the best option, allowing for minor misregistration, and this is often done with PET/CT examinations. A few MR sequences provide reasonable image quality when obtained during free-breathing. These include, single-shot ultrafast sequences such as half-Fourier acquisition single shot turbo spin echo (HASTE), short-tau inversion recovery T2 weighted sequences (STIR), and echo-planar diffusion-weighted imaging (DWI). Additional sequences show promise with regard to whole-body imaging, but are optimally acquired as breath-held sequences, such as 3D volumetric interpolated breath-held examination (VIBE) or turbo spin echo T1-weighted images. Further discussion of the merits of each sequence is presented under the protocol development section.

While free-breathing sequences may provide the best registration for PET data, respiratory motion is often apparent as one scrolls through MR slices, and this presents a challenge to multiplanar viewing of the composed datasets (Fig. 2). MR sequences are traditionally optimized for in-plane resolution at the expense of slice thickness and historically without any consideration for how the image may appear as a multiplanar reconstructed dataset. In contradistinction, PET data are isotropic in nature and often viewed in three dimensions (sagittal, coronal, and transverse) without loss of resolution, both with and without fusion to anatomic images. Acquisition of true

Table 2
T2 HASTE Whole Body Sequence Parameters

MR sequence parameters	Possible utility of sequence	Tips/pearls
FOV-500 mm TR/TE-3000/116 ms Ave-1 ST-5 mm Res-320 x 240 mm FS-no BH-no FA-150 degrees TA-approximately 90 seconds per station IPAT GRAPPA-2	Anatomic localization. T2 contrast allows visualization of fluid structures like bile ducts, bowel, ureters, CSF.	nonoverlapping MR FOV if acquired in transverse plane, acquire in main viewing plane, ascending order of acquisition

FOV, field of view; TR, time to repetition; TE, time to echo; Ave, number of averages; ST, slice thickness; Res, resolution; BW, bandwidth; FS, fat suppression; BH, breath hold; TA, acquisition time.

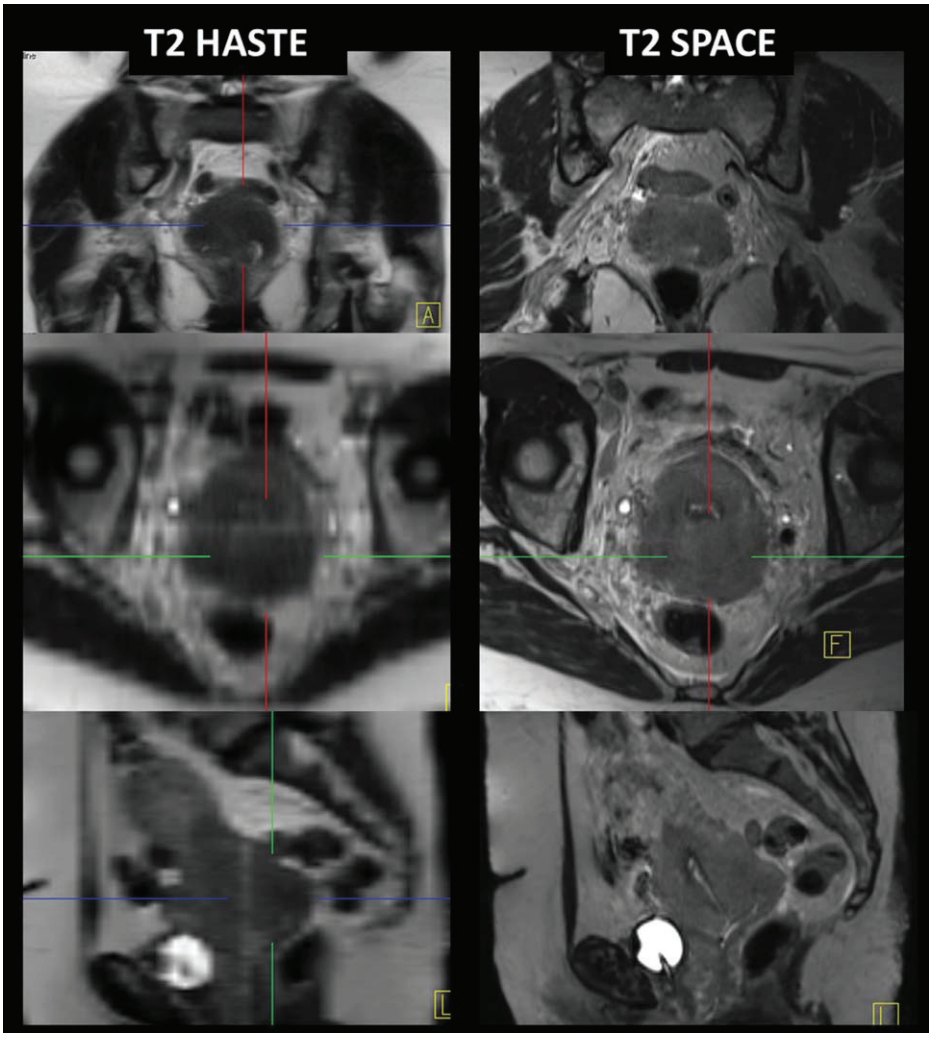

Figure 4. T2 SPACE isotropic acquisition (1.2 mm) shows no significant loss of resolution when reformatted in three other planes. Note the distortion and blurring with single-shot fast spin echo sequence acquired with non-isotropic voxels.

3D whole-body isotropic MR images would result in unacceptable spatial resolution, adding little anatomic information over that of low-dose CT, and the length of acquisition required to achieve adequate resolution would be impractical. Compromising some with regard to spatial resolution or allowing for some loss of resolution in the reconstructed images is unavoidable. While not a complete solution, acquisition in the preferred viewing plane (transverse or coronal) and slice thickness no greater than 4–5 mm may improve the quality of reconstructed images (Fig. 3, Table 2).

For localized anatomic sequences, such as brain or pelvic imaging, 3D isotropic sequences are ideal (Fig. 4) and can be reconstructed in three planes without loss of resolution. Sampling perfection with application optimized contrast using flip angle Evolution (T2 SPACE) is one possible solution for pelvic imaging. By employing a variable flip angle pulse train, constant echo amplitude can be achieved allowing for high-resolution 3D imaging with adequate contrast and SNR. The application of lower flip angles is also beneficial in avoiding SAR. By acquiring a single isotropic sequence and reconstructing images in the other planes this can also save time and obviate the need to acquire multiplanar high-resolution sequences, although this is not necessarily a straightforward tradeoff.

DEVELOPMENT OF PET/MR PROTOCOLS

Beyond the technical challenges of 3T whole-body imaging and optimizing sequences for PET/MR, protocol development must be addressed from a clinical and patient perspective. Whole-body PET/MR should be fast enough to compete with PET/CT (which takes ~20 minutes from beginning to end) and at the same time provide added clinical value over PET/CT or MRI alone. Within a few years of its clinical introduction, PET/CT is now widely accepted and has demonstrated efficacy over PET alone with regard to better attenuation correction, improved anatomic localization, and more accurate local staging of tumors (25). To demonstrate a similar improvement in diagnostic accuracy with PET/MR for whole-body cancer staging will prove challenging. The most likely gain in accuracy would be at the level of local staging (T stage) with modest improvements in anatomic localization of lymph nodes and metastases (M and N stage) over that of PET with low-dose CT. These improvements may be further reduced when comparing PET/MR to PET in conjunction with diagnostic quality contrast-enhanced CT.

As an initial step towards clinical acceptance, PET/MR protocols for whole-body staging must be fast

Table 3
Basic Whole Body Examination

PET acquisition: • 4–5 stations to cover vertex-thighs – Max transaxial FOV 59.4 cm x axial FOV 25.8 cm	Acquisition time: • Approximately 90 seconds / station[a]
MR: • 2 Point DIXON 3D VIBE – TE1/TE2 = 1.23msec/2.46 ms, TR = 3.6 ms, L-R FOV = 500 mm and A-P FOV = 300 mm. – Select extended FOV • T2 HASTE or STIR	Acquisition time: • Approximately 18–20 seconds /station, simultaneous to PET • Approximately 60–90 seconds/station, simultaneous to PET. Allow extra time for STIR
Scanner time/set up: • Allow for shim and adjustments/table translation/exam set-up. • Patient preparation (coils, positioning)	Additional time: • Approximately 45 seconds/station • Allow 15 minutes per examination
Total room time: Allowing for a 5 station examination and turnover time = 30 minutes	

[a]This is if FDG is injected for this examination. For studies done following a standard of care PET-CT utilizing same FDG dose, allow for ~4 minutes per station to account for decay.

enough to compete with PET/CT and must be tolerated by patients. Relatively short PET/MR protocols can optimize throughput, which is essential to economic viability and at the same time can improve patient comfort and compliance, reduce imaging quality degradation arising from patient motion or inability to follow instructions during image acquisition. The most basic whole-body PET/MR examination is detailed in Table 3. While using Dixon sequences for both attenuation correction and anatomic localization without additional MR sequences can certainly be done quickly enough to compete with PET/CT, this method does not fully utilize the added value of MRI. Authors have suggested several whole-body PET/MR protocols, yet no universally accepted standard of care approach exists (26–29). Eiber et al (28) have proposed a possible whole-body staging examination for head and neck cancer patients, consisting of whole-body Dixon, T2 STIR, T1 TSE before and after contrast, and T1 TSE fat-suppressed sequences, with examination scan times ranging from ~31–42 minutes (mean ~23 minutes). Martinez-Möller et al (29) suggest possible scenarios for PET/MR protocols ranging from single-station examinations for local staging information to head-to-toe examinations and also combinations of both approaches. Protocols tailored to specific disease entities with different metastatic patterns will likely be necessary. For instance, STIR images may be very helpful in identifying soft-tissue deposits, lymph nodes, and bony lesions in patients with melanoma. VIBE postcontrast images of the chest, abdomen, and pelvis can provide very good anatomic detail of solid organ metastases; however, dynamic imaging focused on the liver may be necessary for accurate staging of colorectal metastases, whereas dynamic pelvic imaging would be more appropriate for a patient with cervical cancer.

An additional consideration to development of protocols is the potential flexibility in PET acquisition time. While 90 seconds is needed for enough counts when a standard dose of FDG is given, it is possible that lower doses could be administered and imaging times per station lengthened. This approach allows more MR sequences to be obtained while decreasing the overall radiation exposure from the examination without reducing the overall counts in the PET images.

While addition of more MR sequences is tempting to improve diagnostic accuracy, overall examination time should be considered with regard to patient tolerance. MR protocols should be modified to better fit with the hybrid imaging concept and to address the specific clinical questions pertinent to individual patients. Decreasing the number of sequences by eliminating those that are not necessary for staging, shortening existing sequences, and opting for a single 3D isotropic acquisition in lieu of multiplanar high-resolution sequences are all options for decreasing examination length. Table 4, shows examples of whole-body and dedicated anatomic area PET/MR protocols. Note that the additional sequences are abbreviated versions of traditional standard of care examinations. For instance, in the proposed liver protocol, the b50 DWI sequence can substitute for a T2 fat-suppressed sequence. If hepatobiliary contrast agents are desired, such as gadoxetic acid (Eovist, Bayer Pharmaceuticals), time should be allotted for hepatobiliary phase 20-minute delayed sequences.

Specific discussion of DWI is worthwhile in the setting of PET/MR protocol development. While whole-body DWI has been suggested as an alternative to FDG-PET for detection of and treatment monitoring for neoplasms, difficulty with artifacts, consistency with image quality, and reproducibility hinder the routine implementation of this concept. Many investigators have shown a negative correlation between ADC and SUV max for solid tumors, and DWI has been suggested as a semiquantitative parameter for detecting treatment response in many tumors (30–33). Other studies have demonstrated added value of whole-body DWI in initial staging in lung cancer, bone malignancy, and lymphoma over whole-body MRI alone (34–42). However, given the delicate balance of obtaining adequate high-resolution anatomic imaging and whole-body images within a tolerable length of time, it is unclear if whole-body DWI as part of a PET/

Table 4
Possible Whole Body Plus Anatomically Focused Protocol Trees

Indication for examination	Sequences	Special considerations
Liver neoplasm	Whole body: PET 4–5 stations MR AC 2 point Dixon HASTE or STIR	Liver sequences should be breath-held DWI may be performed as free-breathing or as a navigated sequence (+/- EKG gating)
(colorectal liver metastases, hepatocellular carcinoma, cholangiocarcinoma)	Abdomen: -Transverse HASTE -In/Opposed phase (~90 sec) -DWI/ADC (~2.5 min) -+/− MRCP (~15 minutes) -Pre/postcontrast VIBE[b] (~20 sec per acquisition)	Dynamic VIBE[a]: arterial, portal venous, equilibrium, and 5-minute delay
Pelvic neoplasm	Whole body: PET 4–5 stations MR AC 2 point Dixon HASTE or STIR (~90 sec)	T2 SPACE may be reconstructed in 3 planes if acquired isotropically Glucagon may help decrease smooth muscle motion
(cervical cancer, rectal cancer, endometrial cancer)	Pelvis: -Transverse HASTE (~90 sec) -T2 SPACE (~5–10 min) -DWI/ADC (~2.5 min) -Pre/postcontrast VIBE (~20 sec per acquisition)	
Thoracic neoplasm	Whole body: PET 4–5 stations MR AC 2 point Dixon HASTE or STIR (~90 sec)	Respiratory navigated sequences or breath-held may be acquired EKG gated DWI may result in reduced artifact.
(lung cancer, mesothelioma, mediastinal tumor)	Thorax: -Cor/Tra HASTE (~90 sec) -T2 IR BH (~2.5 min) -DWI/ADC (~2.5 min) -Pre/postcontrast VIBE (~20 sec per acquisition)	

[a]Test bolus or care bolus should be used to time late arterial phase.
[b]Hepatobiliary contrast agents may be used and additional hepatobiliary phase imaging should be performed after appropriate delay.
DWI, diffusion-weighted imaging; VIBE, volumetric interpolated breath-held examination; FS, fat suppressed; Cor, coronal; Tra, transverse; BB, black blood; (ST)IR, inversion recovery. All times are listed in parentheses following sequences and are variable due to differences in patient size, sequence parameters, and potentially SAR issues. Respiratory navigation and EKG-gating will add variability to acquisition times related to frequency/periodicity of respirations and pulse rate.

MR exam would add sufficient additional information to justify its inclusion for all disease types. Dedicated DWI sequences of the area of interest are clearly beneficial and recommended as part of routine protocol, as they may add supplemental information and increase lesion conspicuity, such as the instance of colorectal liver metastases when performed in combination with hepatobiliary phase imaging (Fig. 5) (43–45).

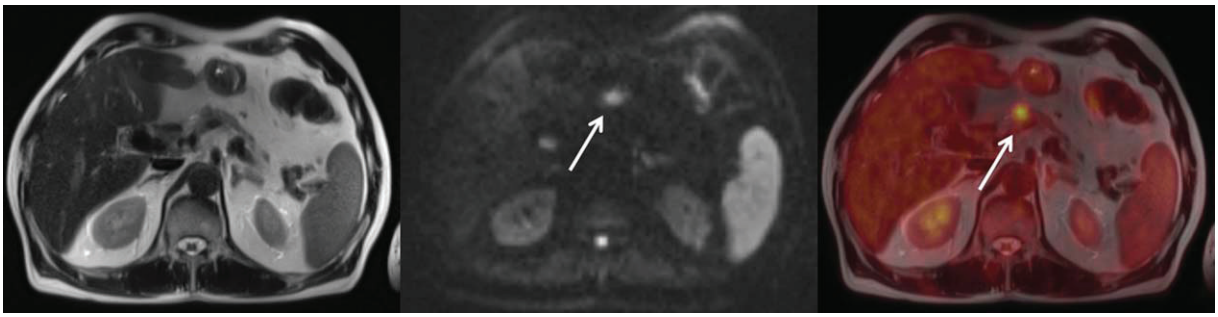

Figure 5. Added value of DWI. T2 single-shot fast spin echo, DWI (b = 500), and fused PET/HASTE images show a focus of FDG avidity at the site of pancreaticojejunostomy in this patient with recurrent pancreatic adenocarcinoma following a Whipple procedure (arrows). Note the region is relatively inconspicuous on single-shot fast spin echo image but stands out as a site of disease on DWI sequence and is confirmed on the fused image.

What constitutes a standard of care whole-body PET/MR examination is yet to be determined and will likely be influenced by local reimbursement, radiologist preference, and efficiency demands. It is also likely that protocols will be tailored to specific clinical indications and that there will not be a single PET/MR protocol that is optimal for all studies. Consideration should be given to patient comfort when developing protocols, and sensitivity to length of examination is important for optimizing compliance.

SUMMARY

PET/MR has been validated as a clinically feasible modality with similar anatomic localization and SUV measurements compared to the current standard of care PET/CT in oncologic patients. While work is ongoing to optimize MR-based attenuation correction, the current algorithm appears to be on par with PET/CT for most clinical purposes. Development of efficient, clinically relevant, and diagnostically optimal protocols will require consideration of issues related to 3T imaging, multiplanar viewing, and overall examination length. Alteration of existing MR protocols and sequences will likely be necessary in this context. Making PET/MR fast enough to compete with PET/CT yet still add additional clinical value over PET/CT will be critical for acceptance of this new hybrid modality by the medical community and for economic viability. Continued success and advancement in this field will require true collaboration between diagnostic radiology and nuclear medicine.

FINANCIAL DISCLOSURES

K.J.F.: Bracco Diagnostics, Inc: research support (for separate project). Lantheus Medical Imaging: Speaker's bureau. J.M.: Consultant and member of Speaker's Bureau for Eli Lilly/Avid. Involved in research projects sponsored by Eli Lilly/Avid. V.R.N.: None.

REFERENCES

1. Schlemmer HP, Pichler BJ, Schmand M, et al. Simultaneous MR/PET imaging of the human brain: feasibility study. Radiology 2008;248:1028–1035.
2. Schwenzer N, Stegger L, Bisdas S, et al. Simultaneous PET/MR imaging in a human brain PET/MR system in 50 patients-Current state of image quality. Eur J Radiol 2012;81:3472–3481.
3. Martinez-Moller A, Souvatzoglou M, Delso G, et al. Tissue classification as a potential approach for attenuation correction in whole body PET/MRI: evaluation with PET/CT data. J Nucl Med 2009; 50:520–526.
4. Drzezga A, Souvatzoglou M, Eiber M, et al. First clinical experience with integrated whole-body PET/MR: comparison to PET/CT in patients with oncologic diagnosis. J Nucl Med 2012;53:845–855.
5. Visvikis D, Costa DC, Croasdale I, et al. CT-based attenuation correction in the calculation of semi-quantitative indices of [18F]FDG uptake in PET. Eur J Nucl Med Mol Imaging 2003;30: 344–353.
6. Westerterp M, Pruim J, Oyen W, et al. Quantification of FDG PET studies using standardised uptake values in multi-centre trials: effects of image reconstruction, resolution and ROI definition parameters. Eur J Nucl Med Mol Imaging 2007;34:392–404.
7. Coombs BD, Szumowski J, Coshow W. Two-point Dixon technique for water-fat signal decomposition with B0 inhomogeneity correction. Magn Reson Med 1997;38:884–889.
8. Eiber M, Martinez-Moller A, Souvatzoglou M, et al. Value of a Dixon-based MR/PET attenuation correction sequence for the localization and evaluation of PET-positive lesions. Eur J Nucl Med Mol Imaging 2011;38:1691–1701.
9. Hofmann M, Bezrukov I, Mantlik F, et al. PET/MRI: quantitiative evaluation of segmentation- and atlas-based methods. J Nucl Med 2011;52:1392–1399.
10. Hofmann M, Steinke F, Scheel V, et al. MRI-based attenuation correction for PET/MRI: a novel approach combining pattern recognition and atlas registration. J Nucl Med 2008;49:1875–1883.
11. Samarin A, Burger C, Wollenweber SD, et al. PET/MR imaging of bone lesions—implications for PET quantification from imperfect attenuation correction. Eur J Nucl Med Mol Imaging 2012;39: 1154–1160.
12. Robson MD, Gatehouse PD, Bydder M, Bydder GM. Magnetic resonance: an introduction to ultrashort TE (UTE) imaging. J Comput Assist Tomogr 2003;27:825–833.
13. Keereman V, Fierens Y, Broux T, De Deene Y, Lonneux M, Vandenberghe S. MRI-based attenuation correction for PET/MRI using ultrashort echo time sequences. J Nucl Med 2010;51:812–818.
14. de Langen A, Vincent A, Velasquez L, et al. Repeatability of 18F-FDG uptake measurements in tumors: a metaanalysis. J Nucl Med 2012;53:701–708.
15. Merkle EM, Dale BM. Abdominal MRI at 3.0 T: the basics revisited. AJR Am J Roentgenol 2006;186:1524–1532.
16. Norris DG. High field human imaging. J Magn Reson Imaging 2003;15:519–529.
17. Tezlaff R, Mader I, Kuker W, et al. Hyperecho-turbo spin-echo sequences at 3T: clinical applications in neuroradiology. Am J Neuroradiol 2008;29:956–961.
18. Mawlawi O, Townsend DW. Multimodality imaging: an update on PET/CT technology. Eur J Nucl Med Mol Imaging 2009;36:15–29.
19. Alessio AM, Stearns CW, Tong S, et al. Application and evaluation of a measured spatially variant system model for PET image reconstruction. IEEE Trans Med Imaging 2010;29:938–949.
20. Daou D. Respiratory motion handling is mandatory to accomplish the high resolution PET destiny. Eur J Nucl Med Mol Imaging 2008;35:1961–1970.
21. Prince JL, McVeigh ER. Motion estimation from tagged MR image sequences. IEEE Trans Med Imaging 1992;11:238–249.
22. Ledesma-Carbayo MJ, Derbyshire JA, Sampath S, et al. Unsupervised estimation of myocardial displacement from tagged MR sequences using nonrigid registration. Magn Reson Med 2008;59: 181–189.
23. Osman NF, Prince JL. Regenerating MR tagged images using harmonic phase (HARP) methods. IEEE Trans Biomed Eng 2004;51: 1428–1433.
24. Chun SY, Reese TG, Ouyang J, et al. MRI-based nonrigid motion correction in simultaneous PET/MRI. J Nucl Med 2012;53:1–8.
25. Schoder H, Larson S, Yeung H. PET/CT in oncology: integration into clinical management of lymphoma, melanoma, and gastrointestinal malignancies. J Nucl Med 2004;45(1 Suppl):72S–81S.
26. Schwenzer N, Schmidt H, Claussen C. Whole-body MR/PET: applications in abdominal imaging. Abdom Imaging 2012;37:20–28.
27. Werner M, Schmidt H, Schwenzer N. MR/PET: a new challenge in hybrid imaging. Am J Roentgenol 2012;199:272.
28. Eiber M, Souvatzoglou M, Pickhard A., et al. Simulation of a MR-PET protocol for staging head-and-neck cancer including Dixon MR for attenuation correction. Eur J Radiol 2012;81:2658–2665.
29. Martinez-Moller A, Eiber M, Nekolla S, et al. Workflow and scan protocol considerations for integrated whole-body PET/MRI in oncology. J Nucl Med 2012;53:1415–1426.
30. Regier M, Derlin T, Schwarz D, et al. Diffusion weighted MRI and 18F-FDG PET/CT in non-small cell lung cancer (NSCLC): does the apparent diffusion coefficient (ADC) correlate with tracer uptake (SUV)? Eur J Radiol 2012;81:2913–2918.
31. Wong C, Gong N, Chu Y, et al. Correlation of measurements from diffusion weighted MR imaging and FDG PET/CT in GIST patients: ADC versus SUV. Eur J Radiol 2012;81:2122–2126.
32. Choi SH, Paeng JC, Sohn CH, et al. Correlation of 18F-FDG uptake with apparent diffusion coefficient ratio measured on standard and high b value diffusion MRI in head and neck cancer. J Nucl Med 2011;52:1056–1062.
33. Gu J, Khong PL, Wang S, Chan Q, Law W, Zhang J. Quantitative assessment of diffusion-weighted MR imaging in patients with

primary rectal cancer: correlation with FDG-PET/CT. Mol Imaging Biol 2011;13:1020–1028.
34. Takenaka D, Ohno Y, Matsumoto K, et al. Detection of bone metastases in non-cmall cell lung cancer patients: comparison of whole-body diffusion-weighted imaging (DWI), whole-body MR imaging without and with DWI, whole-body FDG-PET/CT, and bone scintigraphy. J Magn Reson Imaging 2009;30:298–308.
35. Padhani AR, Gogbashian A. Bony metastases: assessing response to therapy with whole-body diffusion MRI. Cancer Imaging 2011; 11:S129–145.
36. Yi CA, Shin KM, Lee KS. Non-small cell lung cancer staging: efficacy comparison of integrated PET/CT versus 3.0T whole-body MR imaging. Radiology 2008;248:632–642.
37. Sommer G, Wiese M, Winter L, et al. Preoperative staging of non-small-cell lung cancer: comparison of whole-body diffusion-weighted magnetic resonance imaging and (18)F-fluorodexoyglucose-positron emission tomography/computed tomography. Eur Radiol 2012;22:2859–2867.
38. Ohno Y, Koyama H, Onishi Y, et al. Non-small cell lung cancer: whole-body MR examination for M-stage assessment—utility for whole-body diffusion-weighted imaging compared with integrated FDG PET/CT. Radiology 2008;248:643–654.
39. Takenaka D, Ohno Y, Matsumoto K. Detection of bone metastases in non-small cell lung cancer patients: comparison of whole-body diffusion-weighted imaging, whole body MR imaging without and with DWI, whole-body FDG-PET/CT, and bone scintigraphy. J Magn Reson Imaging 2009;30:298–308.
40. Lin C, Luciani A, Itti E, et al. Whole-body diffusion magnetic resonance imaging in the assessment of lymphoma. Cancer Imaging 2012;12:403–408.
41. Gu J, Chan T, Zhang J. Whole-body diffusion-weighted imaging: the added value to whole body MRI at initial diagnosis of lymphoma. Am J Roentgenol 2011;197:W382–391.
42. Abdulgadhr G, Molin D, Astrom G, et al. Whole-body diffusion-weighted imaging compared with FDG-PET/CT in staging of lymphoma patients. Acta Radiol 2011;52:173–180.
43. Seo HJ, Kim MJ, Lee JD, et al. Gadoxetate disodium-enhanced magnetic resonance imaging versus contrast-enhanced 18F-fluorodeoxyglucose positron emission tomography/computed tomography for the detection of colorectal liver metastases. Invest Radiol 2011;46:548–555.
44. Zech CJ, Herrmann KA, Reiser MF, Schoenberg SO. MR imaging in patients with suspected liver metastases: value of liver-specific contrast agent Gd-EOB-DTPA. Magn Reson Med Sci 2007;6:43–52.
45. Hammerstingl R, Huppertz A, Breuer J, et al. Diagnostic efficacy of gadoxetic acid (Primovist)-enahnced MRI and spiral CT for a therapeutic strategy: comparison with intraoperative and histopathologic findings in focal lesions. Eur Radiol 2008;18:457–467.

Initial Experience of MR/PET in a Clinical Cancer Center

Sasan Partovi, M.D.[1], Mark R. Robbin, M.D.[1], Oliver C. Steinbach, Ph.D. [2], Andres Kohan, M.D. [1], Christian Rubbert, M.D. [1], Jose L. Vercher-Conejero, M.D.[1], Jeffrey A. Kolthammer, Ph.D.[3], Peter Faulhaber, M.D.[1], Raj Mohan Paspulati, M.D.[1], and Pablo R. Ros, M.D., MPH, Ph.D. [1]*

Reprinted with permission from the ISMRM Journal of Magnetic Resonance Imaging: Volume 39: 768–780 © with permission from 2014 Wiley Periodicals, Inc.

Magentic Resonance/positron emission tomography (PET) has been introduced recently for imaging of clinical patients. This hybrid imaging technology combines the inherent strengths of MRI with its high soft-tissue contrast and biological sequences with the inherent strengths of PET, enabling imaging of metabolism with a high sensitivity. In this article, we describe the initial experience of MR/PET in a clinical cancer center along with a review of the literature. For establishing MR/PET in a clinical setting, technical challenges, such as attenuation correction and organizational challenges, such as workflow and reimbursement, have to be overcome. The most promising initial results of MR/PET have been achieved in anatomical areas where high soft-tissue and contrast resolution is of benefit. Head and neck cancer and pelvic imaging are potential applications of this hybrid imaging technology. In the pediatric population, MR/PET can decrease the lifetime radiation dose. MR/PET protocols tailored to different types of malignancies need to be developed. After the initial exploration phase, large multicenter trials are warranted to determine clinical indications for this exciting hybrid imaging technology and thereby opening new horizons in molecular imaging.

Key Words: MR/PET; molecular imaging; oncologic imaging; head and neck cancer; genitourinary cancer
J. Magn. Reson. Imaging 2014;39:768–780.
© 2013 Wiley Periodicals, Inc.

Staging, re-staging, and therapy monitoring are important steps in the management of oncologic patients. All these imaging management categories consist of a determination of the local tumor extent, detection of adenopathy, and secondary spread to other organs. MRI/positron emission tomography (MR/PET) is an evolving hybrid imaging modality introduced clinically. It leverages the inherent strengths of both technologies and thereby opens new horizons in functional and molecular imaging.

MRI has a pivotal role in oncologic imaging. Historically, it was seen as an imaging modality that enabled detailed depiction of anatomical structure. It delivers high contrast resolution in soft tissues, even when applied as an unenhanced technique (1). In addition to sequences for morphological imaging, functional MRI sequences were later developed, including diffusion-weighted imaging (DWI), MR spectroscopy, and dynamic contrast enhanced (DCE) methods. In oncologic imaging, MRI has an established role for certain indications. These include but are not limited to the evaluation of pelvic malignancies such as rectal cancer, liver metastases, and renal tumor characterization. MRI as a stand-alone technique possesses certain limitations such as differentiation of benign lymph nodes versus adenopathy and its use as a whole-body approach.

PET/computed tomography (PET/CT) is a well-established modality for oncologic imaging including staging, re-staging, and treatment assessment (2,3). It opens the opportunity to depict metabolism and receptor expression on the cellular level with a high sensitivity (4,5). For anatomical correlation and attenuation correction (AC), PET/CT was introduced as a hybrid imaging modality into the clinical arena around one decade ago, advancing stand-alone PET (6,7). PET/CT can be applied in a whole-body approach and is often able to differentiate benign from malignant processes. Certainly it possesses limitations as well, such as low spatial resolution and difficulties in distinguishing malignant from inflammatory reactions.

To this end, combining PET and MRI in one integrated hybrid imaging modality was expected to have substantial scientific merit. MR/PET became commercially available first for preclinical imaging but it took until 2006 when this technology was introduced clinically as a brain-dedicated PET insert prototype for

[1]Department of Radiology, UH Seidman Cancer Center, University Hospitals Case Medical Center, Case Western Reserve University, Cleveland, Ohio, USA.
[2]Philips Healthcare, Andover, Massachusetts, USA.
[3]Department of Biomedical Engineering, Case Western Reserve University, Cleveland, Ohio, USA.
Contract grant sponsor: Philips Healthcare; Contract grant number: Ohio Third Frontier Grant TECH 11-063, Global Advanced Imaging Innovation Center.
*Address reprint requests to: P.R.R., University Hospitals Case Medical Center, Case Western Reserve University, Department of Radiology, 11100 Euclid Avenue, Cleveland, OH, 44106.
E-mail pablo.ros@uhhospitals.org
Received March 7, 2013; Accepted July 9, 2013.
DOI 10.1002/jmri.24334
View this article online at wileyonlinelibrary.com.

3 Tesla (T) (8) and 7T MRI (9). The Philips Ingenuity TF MR/PET scanner includes state-of-the-art time of flight (TOF) PET technology combined with a 3.0T MRI magnet in a sequential system (10,11). The 3.0T MRI unit opens new possibilities for sophisticated MR sequences and also increases the signal-to-noise ratio as opposed to the more routinely used 1.5 T systems (12–14). According to preliminary experiences, the image quality in MR/PET is comparable to PET/CT and fulfills oncologic diagnostic needs (15–17).

The next step for further establishing this hybrid modality is to identify clinical indications, in particular in oncologic imaging. For this, it is crucial to take advantage of the innovative opportunities of both imaging components like new PET radiotracers (18,19). Unlike the low-dose CT component, which is the minor partner in PET/CT, the full potential of the MRI can be used in MR/PET, including both its morphological and functional tools, so it becomes a hybrid imaging modality of two equals. In the hybrid imaging system PET/CT, the CT component might also be run as a full-fledged high-dose contrast enhanced diagnostic CT. By making MRI a major partner, the gap between the PET and the MRI component can be closed, leading to a true hybrid molecular imaging device, enabling correlative morphological-metabolic and -functional studies in individual patients. For oncology staging, the MR component of MR/PET focuses on the local tumor extent and depiction of metastases in anatomic regions where high soft-tissue-contrast is required such as the pelvis, liver, or brain. The PET component identifies adenopathy and distant metastases with a whole-body approach. It is key to foster collaboration between nuclear medicine and MRI experts, as well as between technologists and physicians. Specific contraindications in both imaging modalities apply to this hybrid imaging technology such as metallic implants, defibrillators, pacemakers, claustrophobia on the MR side, and pregnancy on the PET one.

TECHNOLOGY AND WORKFLOW CONSIDERATIONS IN MR/PET

Attenuation correction in PET was originally performed by acquiring a source-based transmission scan, e.g., using rotating ^{137}Cs or ^{68}Ge sources, or now a low-dose CT scan (CTAC) in PET/CT. When using low-dose CT for attenuation correction the attenuation values are transformed into coefficients at 511-keV (20,21). In contrast to CT, MRI does not provide the electron density information of the scanned object, which is the primary source of PET photon attenuation; therefore, MR images require further manipulation to derive attenuation coefficients. Several MR-based attenuation correction (MRAC) methods have been described based on anatomical atlases (22), segmentation of images obtained with specific MR sequences (23,24) or a combination thereof (25). Furthermore, MRAC images need to be acquired in a clinically reasonable timeframe especially as a significant amount of MR/PET applications are expected to require whole-body imaging and need to provide useful clinical information for whole-body disease assessment. Currently, the methods implemented on the commercial systems use MR-sequences specific to attenuation correction and also image segmentation into three (26) or four (27) different classes of attenuating media.

The accuracy of the MRAC method has been assessed in phantom studies and also in comparative studies with CTAC, and these studies reported no significant differences between the two methods (26,28). A recently published manuscript compared standardized uptake values (SUVs) in oncology using CTAC versus MRAC and also found a high correlation in certain tissues including myocardium, fat, liver, bone marrow, mediastinal blood pool, and psoas muscle (29). In initial data from our study, we applied a three-segment model that delivered robust data in a short acquisition time by acquiring a whole-body free-breathing three-dimensional (3D) T1-weighted spoiled gradient echo sequence as described in detail elsewhere (26). This three-segment model differentiates air, lung, and soft tissue as demonstrated in Figure 1. Preliminary data demonstrated that this attenuation correction technique is feasible in an oncology patient cohort (30,31).

Currently, none of the MRAC methods implemented in commercial systems take into account cortical bone, the most highly attenuating natural material in the human body, and non-bone MRAC has been shown to result in considerable underestimation of SUVs especially for areas such as spine and pelvis. As the transverse relaxation time (T2) of cortical bone is very short, the signal from bone has already decayed at the time of image acquisition in classical MR exams, which makes separation of air and bone on the acquired MR images practically not possible. To obtain a bone signal, ultra-short echo time (UTE) sequences for MR attenuation correction have been proposed (32), which sample the free induction decay (FID) very soon after the excitation of the spins, yielding signal from bone and all other tissue, and then sample again in the same sequence, when the bone signal has already decayed. Attenuation maps are subsequently derived by segmentation into air, tissue, and bone components (11,32). New triple-echo sequences combining UTE and Dixon acquisitions make it feasible to obtain information about water and fat content in conjunction with bone signal in a single sequence (33). The improvement of MRAC with clinically reasonable MR acquisition times is subject of ongoing research.

An accurate MRAC map is an important prerequisite for reliable measurements of SUVs. SUVs measured when comparing standard MRAC with a transmission-based AC approach revealed reasonable quantitative accuracy with the MRAC method (34). In a preclinical study, New Zealand white rabbits were investigated with MR/PET and PET/CT. An excellent correlation between SUVs derived from MRAC in comparison to those from CTAC was found. When analyzing the absolute SUV differences, it was shown that SUVs from MRAC maps were underestimated

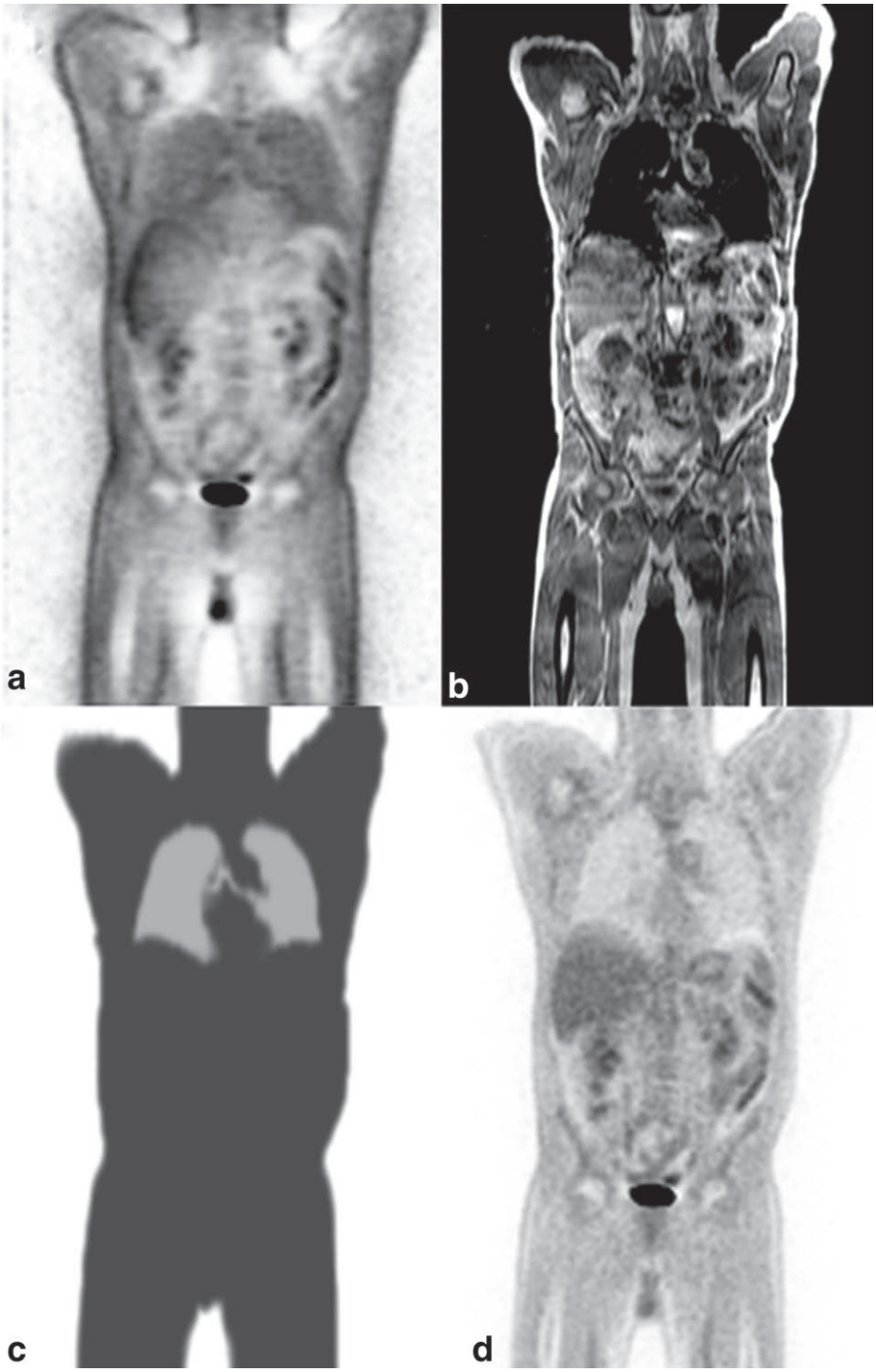

Figure 1. Representative example of MR/PET attenuation correction which was performed on a sequential MR/PET system (Philips Ingenuity TF MR/PET, Philips Healthcare, Andover, MA). Panel **a** shows the unattenuated PET. Panel **b** contains the 3D multistation T1w spoiled gradient echo of the same patient as the basis for the corresponding MR-based attenuation correction map (**c**). The three segments are comprised of outside air (white), lung (light gray), and soft tissue (gray). This map is then used in the reconstruction of a MR-attenuated PET (**d**).

compared with those from CTAC in the tissues analyzed, namely aorta, kidneys, liver, spine, and soft tissue (35). A clinical study investigated lesions with PET/CT and subsequent MR/PET using different tracers. SUVs were significantly decreased in MR/PET versus PET/CT with a strong correlation of the values between either imaging modality (36). SUVs are a surrogate marker for FDG uptake. These values actually increase with time in malignant lesions (37,38). However, these results might be explained by scatter and attenuation correction issues or by the influence of radiofrequency coils on the PET component (39,40). Another clinical study on head and neck cancer patients compared FDG-PET followed by FDG-MR/PET. The SUVmax values were significantly higher in the tumor and cerebellum in MR/PET in comparison to PET (41). The authors explained this with an FDG uptake of the tumor during time as described above (42) or differences related to MR-based attenuation correction (41). In our own study, we investigated an oncology patient population with PET/CT and subsequent MR/PET. We measured SUVs in healthy tissues

of CTAC versus MRAC maps using the three-segment model provided by the manufacturer (26). A strong correlation was observed in myocardial tissue, mediastinal blood pool, psoas muscle, fat, liver, and bone marrow. A moderate correlation was found in lung tissue and iliac muscle.

Metallic implants cause a local magnetic field heterogeneity, resulting in image distortion (43). This is a well-known limitation to MR imaging and has a direct effect on MR-based attenuation correction. The resulting MR/PET artifacts are likely to be larger in volume than the actual metallic implant, with a considerable effect on quantification. A methodology using semiautomatic inpainting has been proposed to increase accuracy (44). Single organ imaging is often performed within one (e.g., for brain) or two (e.g., for lungs) bed positions, depending on the organ size and the scanner's field of view (FOV). To study organ function (e.g., brain, heart, liver) or regional disease (e.g., tumor, carotid plaques) in detail often dynamic, gated or extended PET and/or MR acquisitions are required. MRI scans can start before or after PET depending on the workflow of the department and, in some occasions, MR scans may start during the radiotracer's uptake time (11). The sequential scanner design leverages technologies from both modalities such as TOF PET and multiple-transmission MRI to minimize the required imaging time.

For whole-body (i.e., base of the skull to mid-thighs) or total-body (i.e., head-to-toes) imaging, several bed positions are acquired and then fused during postprocessing. In modern PET scanners, the number of bed positions required are dictated by the combination of desired scan duration and the size of the scanner's axial FOV. In the current MR/PET scanners, the axial FOV ranges from 18 to 25.8 cm with overlap between adjacent of up to 50% (28,45). However, individual diagnostic MR protocols may surpass 60 min of total acquisition time. In a staging examination, both local disease and potential distant metastases need to be assessed. Hence, an MR AC/localization scan is performed first, followed by the FDG-PET acquisition and findings may indicate distant regions with putative metastasis, which will be interrogated consequently by targeted diagnostic MR contrasts (e.g., in breast cancer staging). To reduce the MRI acquisition time, several techniques have been introduced such as parallel transmission in high-field MR, which reduces the local specific absorption rate (SAR). This techniques resulted in shorter pulse repetition time and, therefore, faster acquisitions (46,47) by 31% across 77 clinically tested MR sequences (48), although acquisition time varied, depending on the pulse sequences used (49).

In January 2010, the first Philips Ingenuity TF MR/PET, a whole-body integrated MR/PET unit with sequential acquisition capability was installed (28). Later that year, the first Siemens Biograph mMR (50), a whole-body MR/PET system with simultaneous acquisition capabilities was released as well. Therefore, there are two different commercially available designs for clinical MR/PET systems: simultaneous and sequential. In the simultaneous system, the PET detector is positioned inside the MRI magnet, whereas in the sequential design, PET and MRI are positioned in tandem and connected by a sliding table top, similar to the design of PET/CT (51). Either system leads to compromises in clinical utility, flexibility, imaging capabilities, or cost compared with stand-alone, state-of-the-art PET and MRI. Standard PET and MRI when combined would interfere with each other to the point of being incompatible. Standard PET detectors made of scintillation crystals coupled to photomultiplier tubes (PMTs), do not operate in high magnetic fields. PET electronics affect MR acquisition and field homogeneity and, vice versa, MR electronics affect PET acquisition (52).

The Philips Ingenuity TF MR/PET which is in use in our department is a sequential MR/PET unit combining a state-of-the-art time-of-flight PET and a high-field MRI with parallel transmission capabilities. To avoid any interference with the MR signal of radiofrequency (RF) noise arising from PET front-end electronics, the PET system's RF-generating circuits were moved from the gantry to outside the Faraday cage. The detector power is dynamically modulated and suspends during MR acquisition. The sequential arrangement also has the benefit that no PET hardware is located within the FOV of the magnet, thereby addressing concerns about magnetic field heterogeneity (11).

OPPORTUNITIES AND CHALLENGES OF MR/PET

MR/PET as a hybrid imaging technology has the potential to significantly impact imaging, including altering patient management in some clinical indications particularly in oncology. Commercially available MR/PET units have whole-body imaging capabilities, which are necessary to perform oncological and cardiac scans. The latter is another opportunity for MR/PET to succeed given the excellent attributes of cardiac MRI and absolute quantification by PET (53). MR/PET also provides the potential to better discriminate moving structures such as the heart or bowel by applying MR-based motion correction techniques (1).

MR/PET may help increase diagnostic accuracy and help to improve TNM staging and re-staging. Due to the MR component, T staging will be superb in areas where a high soft-tissue contrast is required. According to a recently published article, N staging might be equal between PET/CT and MR/PET (54). One might, therefore, expect M staging in certain areas to benefit from the MR component as well. In summary, MR/PET might significantly improve the T and M staging, although challenges will remain to be investigated. For example, the detection of micrometastases remains limited, in particular when unselective radiotracers are used for PET imaging (55).

Cancer therapy encompasses multimodal treatment including surgery, irradiation, chemotherapy, and most recently targeted molecular therapy. MR/PET's unique combination of metabolic, functional, and high-resolution anatomical information opens a new horizon toward sophisticated therapy monitoring. To

take advantage of the full imaging capabilities of this hybrid imaging technology, it is of utmost importance to use the MRI not only as an anatomical reference technique for the PET images but also acquire dedicated functional sequences. This is a shift in paradigm in comparison to PET/CT in which the low-dose CT data are used for anatomical correlation and attenuation correction. Particularly for therapy monitoring purposes the PET and the functional MR data should be correlated with the overall goal toward a tailored therapy approach in individual patients as the future of oncology.

An important concern for MR/PET is length of scan time, as both MRI and PET require long acquisition times for a comprehensive examination. Extended scan times impact patient comfort, increase drop-out rates and decrease throughput, and thereby increase the average cost per scan. This might be addressed by moving into single-organ as opposed to whole-body imaging or acquisition over several bed positions.

The lengthy scans times, require optimization of imaging protocols to streamline workflow and the acquisition of diagnostic information. In addition to the respective design philosophies and technical concepts MR/PET as a novel hybrid imaging modality requires changes and significant innovation with respect to clinical, organizational, and technological framework conditions. Questions about how it compares with PET/CT, under which clinical scenarios either of them should be used, patient throughput, ease of workflow, building and running costs, ownership of device and staff (between different departments), reliability of the new technology, and image quality in comparison to standalone systems are points of attention.

Furthermore, to adopt successfully MR/PET, an organization has to change its logistics of disease management and patient workflow (56). One important alteration is the cross-training of MR-based and Nuclear Medicine physicians and technicians in both modalities as well as forming a strong collaboration between Nuclear and MR physicians and technicians (57). Research facilities that investigate the research capabilities of MR/PET also benefit from strong multidisciplinary research teams with the supporting infrastructure already in place, and a financial model that includes research grant attraction rather than pure reimbursement for clinical scans.

There are indications for PET and PET/CT that are reimbursed when they are medically necessary. PET scans performed using MR/PET equipment for these indications are also reimbursed to the same extent that a stand-alone PET or PET/CT. There are no approved codes for MR/PET reimbursement; therefore, there is no financial difference for a MR/PET scan compared with a stand-alone PET or PET/CT when the MR component of a MR/PET is performed for attenuation correction or to otherwise improve the diagnostic quality. If using the technology in its hybrid modality, some have recommended billing the existing PET code and an unlisted code on top of that for a fusion procedure. Other indications for PET and PET/CT are only covered if the provider complies with certain additional requirements, including registration of the study with the National Oncology PET Registry (NOPR). This registry identifies the indications that are covered without compliance with NOPR requirements and those for which NOPR provides a route to coverage (58). Patients referred for a diagnostic MRI can be reimbursed using MRI-only codes on a MR/PET system, provided the MR is of diagnostic quality and the MR/PET system has been cleared by the FDA. In this case, diagnostic MR codes can be used. Some Medicare contractors have adopted local coverage determinations (LCDs), identifying the conditions that cover a diagnostic MR when performed on a MR/PET in case a (59).

CLINICAL ONCOLOGIC APPLICATIONS

Head and Neck Cancer

Imaging techniques in head and neck cancer (H&N) play a pivotal role. Imaging helps to establish the extent of the disease with respect to tumor size, invasion of adjacent structures (surrounding soft tissue and bone), regional adenopathy, tumor recurrence and posttreatment changes, and the presence of distant metastases (60). Due to its superb soft-tissue contrast, MRI has become the most significant morphologic modality for imaging of H&N cancer in general and in particular for T staging purposes (61). MRI data are also used for radiation therapy planning (62). For detection of lymph node metastases, morphological criteria alone are not sufficient (63). The complementary metabolic information measured by whole-body PET/CT is valuable for N and M staging (64,65). Furthermore, PET/CT might help to differentiate residual or recurrent disease from therapy-induced changes (62,66,67).

The data suggest that the information from PET and MRI are significant for diagnosis, staging including restaging and treatment assessment in H&N. To this end, MR/PET seems to be a promising modality for head and neck malignancies (41,61). A recent study demonstrated the feasibility of FDG-MR/PET for initial staging of H&N without quality impairment (41). One of the first studies on integrated MR/PET of H&N demonstrated superior tumor delineation and a good correlation between the metabolic ratios measured using MR/PET and PET/CT (62). A representative instance of H&N is shown in Figure 2.

Lung Cancer

PET/CT is a well-established imaging tool in the work-up of lung cancer patients (68,69), and particularly beneficial in N and M staging (70–73). The CT component is able to detect very small nodules (74) but it is limited with regard to determining the exact tumor extent. Because of this, proper assessment of chest wall invasion or parenchymal changes induced by the tumor might be challenging when performing PET/CT. Similarly tumor characterization and the differentiation between benign lymph nodes and

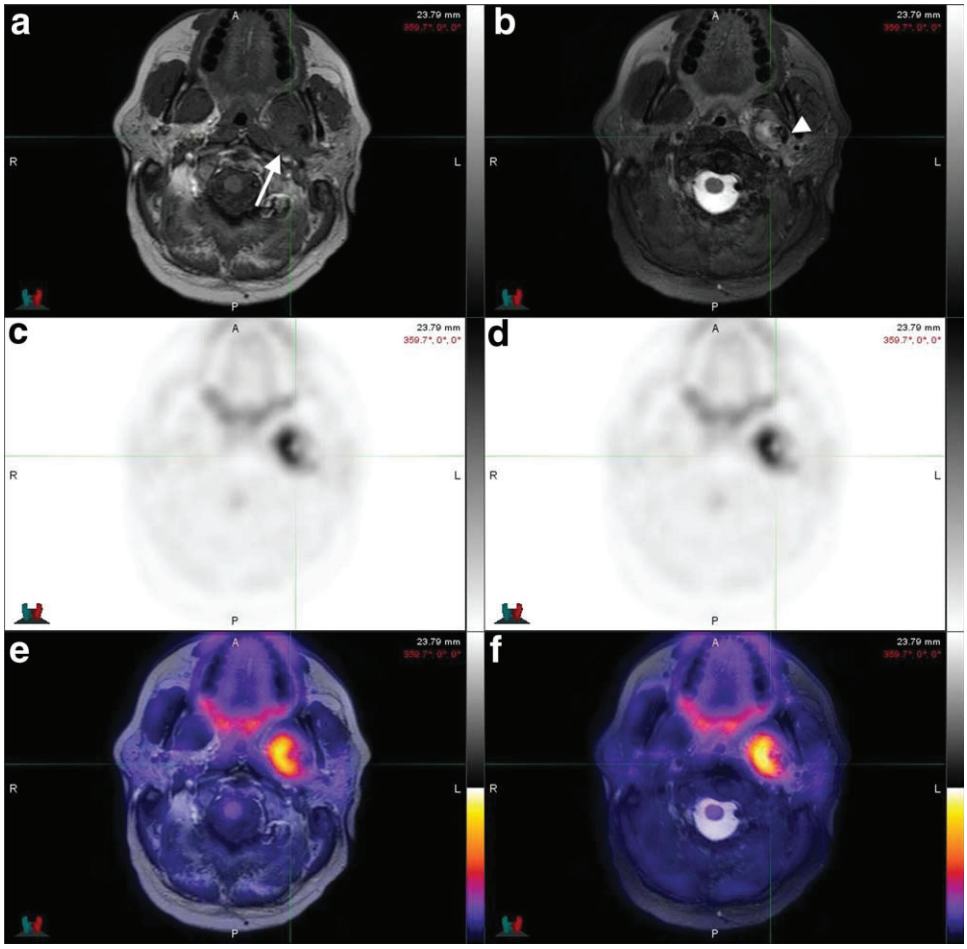

Figure 2. MR/PET of a patient with head & neck cancer which was performed on a sequential MR/PET system (Philips Ingenuity TF MR/PET, Philips Healthcare, Andover, MA). Axial T1 TSE (**a**) and axial STIR (**b**) at the level of the oropharynx show an asymmetrical enlargement of the soft tissue in the left medial pterygoid muscle (arrow). This enlargement is associated with heterogeneous tissue signal, more evident on the STIR sequence where an area of hyperintensity inside the lesion can be seen. There is also an area of signal void (arrowhead) inside the lesion that most probably represents calcium. PET images (**c,d**) show asymmetrical focal uptake in the same region of the area described previously. Symmetrical uptake is seen in the base of the tongue probably related to physiologic uptake. Fusion images (**e,f**) confirms that the uptake is from the lesion seen in the MR. Noteworthy is that the area of uptake matches almost perfectly with the area of hyperintensity described in the STIR sequence. The area described as calcium (arrowhead) shows no uptake as expected.

adenopathy based on morphologic criteria can be difficult with this hybrid imaging modality (75–77).

One of the weaker areas of MRI has traditionally been the lung. Therefore, lung cancer imaging has been conducted with CT or PET/CT. PET/CT is more accurate than MRI in detection of metastases in the lung (78,79). In particular, small lung lesions are less reliably imaged with MRI (80). Recently, progress has been made in MR lung cancer imaging through the development of advanced sequences with parallel imaging capabilities (80). Fast, T1-weighted gradient-echo sequences decreased the size threshold of lung nodules detected by MRI to 3 mm (81).

One recently published study investigated MR/PET in 10 lung cancer patients (82), demonstrating that obtained MR/PET images had high diagnostic quality. In addition, higher tumor-to-liver-ratios in comparison to PET/CT and a high correlation between the ratios in MR/PET and PET/CT were observed. TNM staging was highly concordant between MR/PET and PET/CT, with slightly different stages in only 3 of the 10 patients (82). Future studies in a larger lung cancer patient cohort using advanced lung imaging MR sequences are warranted to better define the role of MR/PET in this patient collective. In one study, PET and dynamic contrast enhanced MRI were able to identify lung cancer patients who responded to anti-angiogenic therapy (83). One possible future indication for MR/PET in this patient population is therapy assessment, taking advantage of functional MR sequences and superior anatomical resolution in MR together with the PET information.

Genitourinary Cancer

MR/PET has a bright future in areas where high soft-tissue and contrast resolution is required. One of these areas where we see a strong benefit of this evolving imaging modality is the pelvic region. MR/PET for genitourinary cancer is feasible for generating

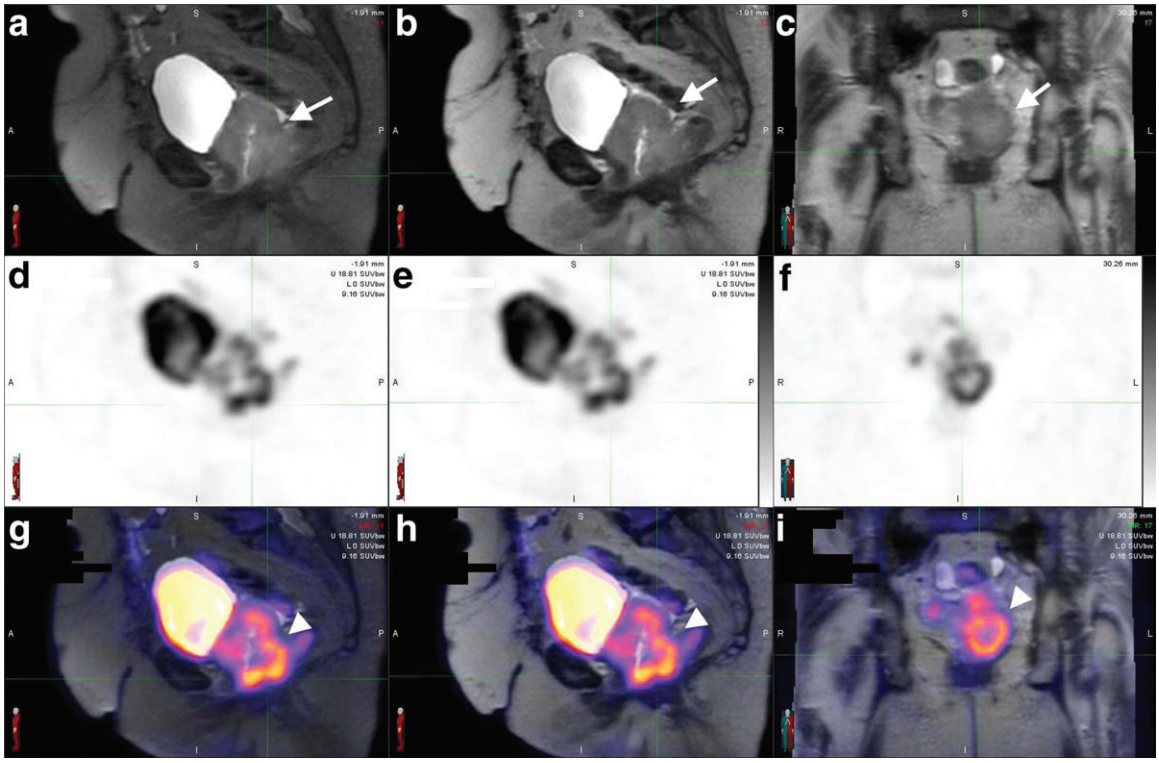

Figure 3. MR/PET of a patient with vaginal cancer which was performed on a sequential MR/PET system (Philips Ingenuity TF MR/PET, Philips Healthcare, Andover, MA). Sagittal T2 fat sat **(a)**, sagittal T2 **(b)**, and axial T2 **(c)** -weighted sequences of the pelvis. Thickening of the soft tissue of the vagina is seen (arrows) showing a low to intermediate signal. PET images **(d–f)** show an area of high FDG uptake near the bladder. Fusion images **(g–i)** show concordance between the tissue thickening and the increased FDG uptake (arrows).

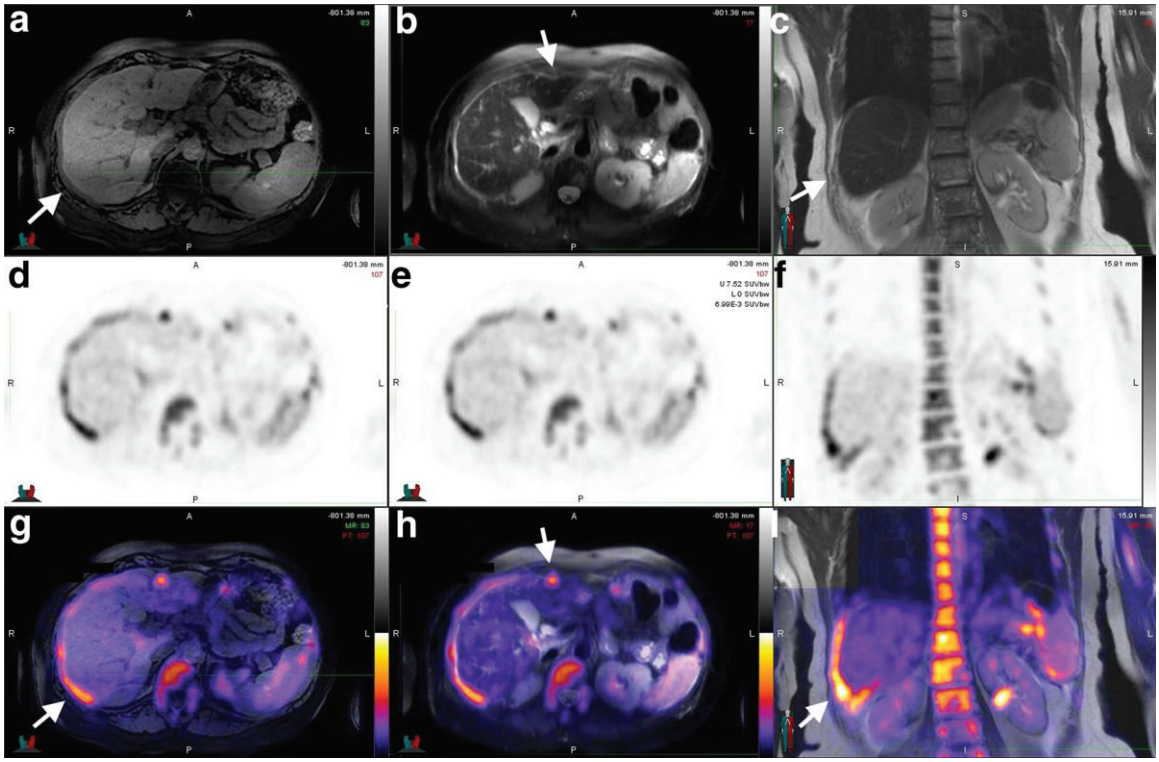

Figure 4. MR/PET of a patient with ovarian cancer which was performed on a sequential MR/PET system (Philips Ingenuity TF MR/PET, Philips Healthcare, Andover, MA). Axial T1 fat sat **(a)**, axial T2 fat sat **(b)**, and coronal T2 **(c)** MR sequences show perihepatic peritoneal thickening. PET images **(d–f)** appear to show FDG uptake following the same distribution as the lesions seen in MR. Fusion images **(g–i)** confirm the MR findings and the potentially malignant etiology of them.

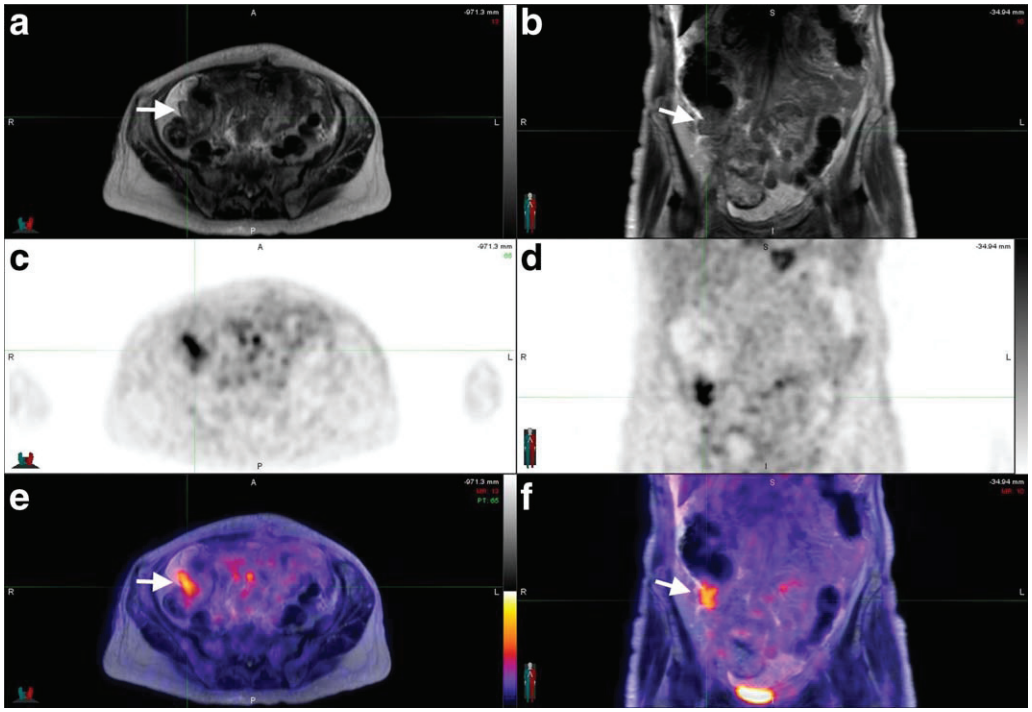

Figure 5. MR/PET of a patient with ovarian cancer which was performed on a sequential MR/PET system (Philips Ingenuity TF MR/PET, Philips Healthcare, Andover, MA). Axial and coronal T2 (**A,B**) showing free fluid and a soft-tissue lesion with an intermediate signal near the cecum. PET images (**C,D**) appear to show FDG uptake of the lesion. Fusion images (**E,F**) show the match between the lesion seen in MR and the uptake seen in the PET. [Color figure can be viewed in the online issue, which is available at wileyonlinelibrary.com.]

diagnostic-quality images, according to our experience. In Figure 3, vaginal cancer imaging with MR/PET is demonstrated. In Figures 4 and 5, we depict ovarian cancer with MR/PET. The detection of malignant lymph nodes is possible, as shown in the case of a pelvic lymph node in Figure 6. These examples

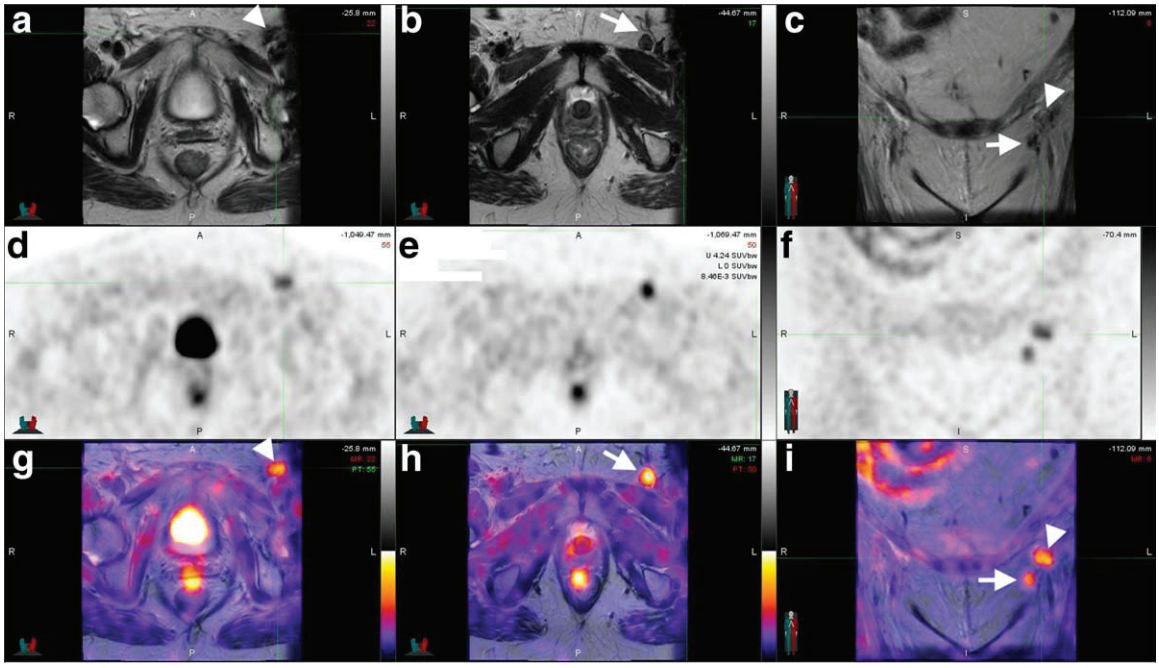

Figure 6. MR/PET of a patient with pelvic adenopathy, which was performed on a sequential MR/PET system (Philips Ingenuity TF MR/PET, Philips Healthcare, Andover, MA). Axial T2 TSE (**a,b**) and coronal T2 TSE (**c**) of the pelvis which show two hypointense lesions (arrowhead and arrow) in the left inguinal space, near the neurovascular package. PET images (**d–f**) show two areas of uptake that might be related to the previous structures. Fusion images (**g–i**) show that the lesions seen in the MRI match with the foci of uptake (arrowhead and arrow) raising concern for lymph nodes with metastasis. [Color figure can be viewed in the online issue, which is available at wileyonlinelibrary.com.]

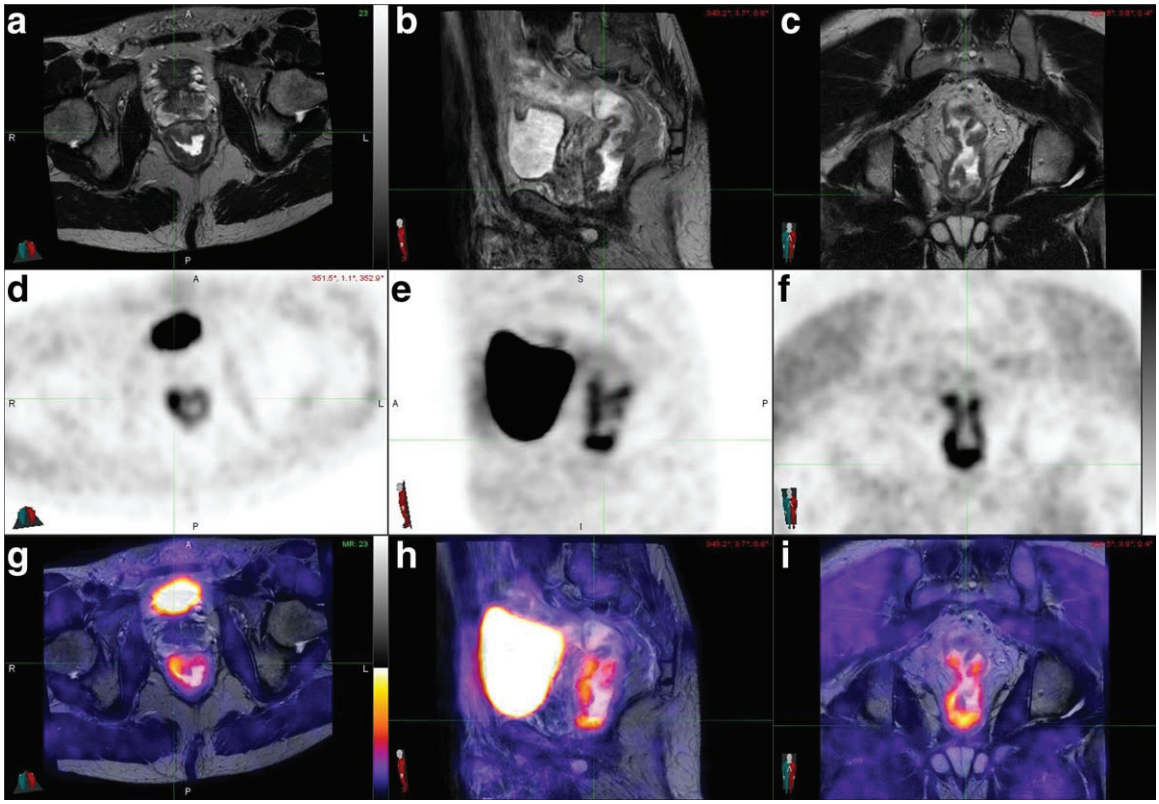

Figure 7. MR/PET of a patient with rectal cancer which was performed on a sequential MR/PET system (Philips Ingenuity TF MR/PET, Philips Healthcare, Andover, MA). Asymmetrical thickening of the rectal wall is seen in the axial **(a)**, sagittal **(b)**, and coronal **(c)** planes of the T2 TSE sequence. Associated increased FDG uptake in relationship to the finding described previously is seen in the PET acquisition **(d–f)**. Fusion images **(g–i)** help determine de malignant origin of the thickening and the absence of involved lymph nodes. [Color figure can be viewed in the online issue, which is available at wileyonlinelibrary.com.]

reveal that, even without the use of MR contrast agents, imaging of the pelvic region applying MR/PET can be conducted. Future application of MR/PET in genitourinary cancers may include dedicated protocols for radiation therapy planning. One group recently suggested using MR/PET for brachytherapy planning in cervical cancer (15). Our examples reveal that diagnosis and therapy assessment in genitourinary cancers is a potential future indication of MR/PET.

Rectal Cancer

MRI with endorectal coils is established for imaging of local tumor extent evaluation in cases where the bowel wall or mesorectum is infiltrated by the primary tumor. MRI provides an alternative to endorectal ultrasound, allowing local staging beyond the rectal wall (84). Another important indication for morphological MRI in rectal cancer is the preoperative determination of the tumor-free margin, a crucial outcome factor (85). Functional MRI is also applied in this patient population: have shown that DWI is a surrogate marker in rectal cancer for the biological behavior of the neoplasm, and lower apparent diffusion coefficient (ADC) values are associated with a more aggressive tumor phenotype (86). To provide evidence of the effect of neoadjuvant radio-chemotherapy with regard to tumor clearance of the mesorectal fascia, DWI can be combined with standard morphological MRI (87).

In a recently published study, the diagnostic accuracy for malignant lymph node detection was increased by combining PET/CT and MRI read-outs, clearly indicating the potential of MR/PET for rectal cancer N staging (88). In cases of nonlocal recurrence, whole-body MR/PET can help the tumor site and metastatic spread. Due to its high spatial resolution, we expect MR/PET to be of particular benefit for the re-staging of rectal cancer. After radio-chemotherapy or surgery alterations in the tissue, e.g., desmoplastic or fibrotic, reactions may occur. These therapy-induced reactions are sometime difficult to differentiate from residual or recurrent tumor. Morphological MRI together with DWI may increase sensitivity and specificity for the diagnosis of rectal cancer recurrence (84). To this end, MR/PET has the potential to become a valuable tool for re-staging of colorectal cancer as it is suggested in another publication and is confirmed by the experience in our MR/PET program (54,89). Furthermore, re-staging MR/PET might be of interest for increasing treatment monitoring accuracy. In particular, DWI with the derived ADC values in conjunction with the metabolic information, including SUV values obtained from the PET component, might be of significant value.

A recently published study investigated PET/CT as compared with MR/PET in an oncology patient

population including four colon cancer and two rectal cancer patients (16). Altogether 32 patients were enrolled, and the study comprised a qualitative comparison of lesion localization and count as well as a quantitative comparison of SUVs. No difference in the qualitative analysis was appreciated. A Dixon MRI sequence was beneficial for anatomical localization, revealing results comparable to the low-dose CT component of PET/CT. High correlation of both lesion and background SUVs between MR/PET and PET/CT has been found, suggesting that quantitative MR/PET will be useful for follow-up studies, including assessment of therapy response. The authors concluded that MR/PET is feasible in the clinical arena with an examination time of less than 30 minutes, and that it can be applied for lesion detection in oncologic imaging (16).

Rectal cancer images acquired with MR/PET at our institution are shown in Figure 7. Concerning rectal cancer, previous data from separate MRI and PET/CT is very promising, and we might extrapolate those expectations to envision the use of MR/PET for diagnosis, staging, re-staging, and treatment monitoring. Nevertheless, this new hybrid imaging modality needs to prove its true benefit over either standalone imaging technology.

LOW-DOSE ONCOLOGIC IMAGING IN THE PEDIATRIC POPULATION

In pediatric patients, limited exposure to radiation is of utmost importance. For follow-up, repeat imaging examinations are required and have to be conducted with low-dose protocols, whenever possible (90,91). Using MR/PET as opposed to PET/CT opens the opportunity to image this patient population with a lower radiation dose, as the MR component has no ionizing irradiation and the PET radiotracer dose is minor in comparison to CT (92,93). A successful switch from PET/CT to MR/PET was reported in a young female with aggressive fibromatosis requiring repeat follow-up studies (1). Furthermore, MR/PET as a one-stop imaging device also has the potential to obviate chest CTs, which are often included in the diagnostic work-up of pediatric solid tumors. These chest CTs are associated with a high radiation burden over time.

A first study with MR/PET for initial staging and treatment response in 15 pediatric patients has been recently published (94). The authors reported a significant reduction of radiation dose to 4.6 mSv, which is approximately 20% of the equivalent PET/CT exam. Further MR/PET was established as a comprehensive approach leading to a lower absolute number of diagnostic studies. This had a positive impact on the stress level of the children and parents, and it shortened the time frame between staging and initiating appropriate treatment (94). Whole-body DWI is a known imaging technique, also in the pediatric population (95,96). Additionally, this imaging technique proved to be useful for biopsy-site determination and treatment planning in tumors with heterogeneous FDG uptake, as demonstrated in the cases of metastatic testicular cancer and neuroblastoma (94).

The optimization of protocols for MR/PET should have the highest priority when planning to apply MR/PET in the pediatric population. The MR/PET scan time has to be decreased as low as is reasonably possible, in particular when considering that small children need to be sedated for the investigation and that older children need to be imaged in a comfortable atmosphere with low stress levels.

DISCUSSION

MR/PET is a novel, evolving, and promising hybrid imaging modality that opens new horizons in oncologic imaging and, furthermore, in other fields such as cardiovascular imaging and neurodegenerative disease. It offers a unique combination of morphological, functional, and metabolic information fostering a new dimension in molecular imaging sciences. Multiparametric MRI can be combined with new radiotracers, pursuing the imaging of cancer at very early stages and impacting on patient management.

The era of feasibility studies and preliminary qualitative comparisons between PET/CT versus MR/PET (16,17) is coming to the end, and the next phase of investigating the clinical benefits of the new technology has begun (94,97). MR/PET protocols for different types of (cancer) indications need to be developed, as dedicated MR sequences can be practically acquired only in specific regions of the body due to time constraints. Hence, the currently available MRI protocols have to be tailored to this specific hybrid modality. A uniform MR/PET protocol as it is common in PET/CT will not exist, and larger clinical trials are needed to define clear indications for this exciting technology.

Technical challenges such as attenuation correction need to be overcome for successful implementation in the clinical arena. In addition to the respective design philosophies and technical concepts, MR/PET as a novel hybrid imaging modality requires changes and significant innovation at various levels with respect to clinical, organizational, and technological framework conditions (56). Questions about how MR/PET compares with PET/CT, under which clinical scenarios either of them should be used, patient throughput, ease of workflow, building and operating costs, departmental affiliation of the device and staff, the reliability of new the technology, and image quality in comparison to stand-alone systems are all common and remaining points of consideration.

ACKNOWLEDGMENTS

The MR/PET system was funded by a State of Ohio Third Frontier Grant. Clinical MR/PET studies in the institution are funded by grants from Philips Healthcare. Oliver C. Steinbach and Jeffrey A. Kolthammer are Philips Healthcare employees.

REFERENCES

1. Werner MK, Schmidt H, Schwenzer NF. MR/PET: a new challenge in hybrid imaging. AJR Am J Roentgenol 2012;199:272–277.

2. Gambhir SS. Molecular imaging of cancer with positron emission tomography. Nat Rev Cancer 2002;2:683–693.
3. Wahl RL, Jacene H, Kasamon Y, Lodge MA. From RECIST to PERCIST: evolving considerations for PET response criteria in solid tumors. J Nucl Med 2009;50(Suppl 1):122S–150S.
4. Czernin J, Phelps ME. Positron emission tomography scanning: current and future applications. Annu Rev Med 2002;53:89–112.
5. Mussig K, Oksuz MO, Dudziak K, et al. Association of somatostatin receptor 2 immunohistochemical expression with [111In]-DTPA octreotide scintigraphy and [68Ga]-DOTATOC PET/CT in neuroendocrine tumors. Horm Metab Res 2010;42:599–606.
6. Beyer T, Czernin J. Is conflict of interest in our best interest? Eur J Nucl Med Mol Imaging 2010;37:1063–1068.
7. Townsend DW, Beyer T. A combined PET/CT scanner: the path to true image fusion. Br J Radiol 2002;75(Spec No):S24–S30.
8. Schlemmer HP, Pichler BJ, Schmand M, et al. Simultaneous MR/PET imaging of the human brain: feasibility study. Radiology 2008;248:1028–1035.
9. Judenhofer MS, Catana C, Swann BK, et al. PET/MR images acquired with a compact MR-compatible PET detector in a 7-T magnet. Radiology 2007;244:807–814.
10. Ros PR.Oncologic PET-MR imaging: counterpoint, simultaneous acquisition not needed. In: Annual Meeting of the Radiological Society of North America, Chicago, IL, 2012. (Code: SPSH50B).
11. Kalemis A, Delattre BMA, Heinzer S. Sequential whole-body PET/MR scanner: concept, clinical use, and optimisation after two years in the clinic. The manufacturer's perspective. MAGMA 2013;26:5–23.
12. Tanenbaum LN. Clinical 3T MR imaging: mastering the challenges. Magn Reson Imaging Clin N Am 2006;14:1–15.
13. Herrmann KA, Paspulati RM, Lauenstein T, Reiser MF. Benefits and challenges in bowel MR imaging at 3.0 T. Top Magn Reson Imaging 2010;21:165–175.
14. Partovi S, Schulte AC, Jacobi B, et al. Blood oxygenation level-dependent (BOLD) MRI of human skeletal muscle at 1.5 and 3 T. J Magn Reson Imaging 2012;35:1227–1232.
15. Kjær A, Loft A, Law I, et al. PET/MRI in cancer patients: first experiences and vision from Copenhagen. MAGMA 2013;26:37–47.
16. Drzezga A, Souvatzoglou M, Eiber M, et al. First clinical experience with integrated whole-body PET/MR: comparison to PET/CT in patients with oncologic diagnoses. J Nucl Med 2012;53:845–855.
17. Partovi S, Kohan AA, Gaeta MC, et al.Assessment of image quality in AC maps generated from PET/MRI vs PET/CT. In: American Roentgen Ray Society Annual Meeting, Washington, DC, 2013. (abstract 030).
18. Gulyás B, Halldin C. New PET radiopharmaceuticals beyond FDG for brain tumor imaging. Q J Nucl Med Mol Imaging 2012;56:173–190.
19. Vallabhajosula S. Positron emission tomography radiopharmaceuticals for imaging brain Beta-amyloid. Semin Nucl Med 2011;41:283–299.
20. Kinahan PE, Townsend DW, Beyer T, Sashin D. Attenuation correction for a combined 3D PET/CT scanner. Med Phys 1998;25:2046–2053.
21. Kinahan PE, Hasegawa BH, Beyer T. X-ray-based attenuation correction for positron emission tomography/computed tomography scanners. Semin Nucl Med 2003;33:166–179.
22. Schreibmann E, Nye JA, Schuster DM, Martin DR, Votaw J, Fox T. MR-based attenuation correction for hybrid PET-MR brain imaging systems using deformable image registration. Med Phys 2010;37:2101–2109.
23. Vincent K, Vandenberghe S, De Deene Y, Luypaert R, Broux T, Lemahieu I.MR-based attenuation correction for PET using an Ultrashort Echo Time (UTE) sequence. In: IEEE Nuclear Science Symposium Conference, Dresden, Germany; 2008. doi:10.1109/NSSMIC.2008.4774461.
24. Johansson A, Karlsson M, Nyholm T. CT substitute derived from MRI sequences with ultrashort echo time. Med Phys 2011;38:2708–2714.
25. Hofmann M, Steinke F, Scheel V, et al. MRI-based attenuation correction for PET/MRI: a novel approach combining pattern recognition and atlas registration. J Nucl Med 2008;49:1875–1883.
26. Schulz V, Torres-Espallardo I, Renisch S, et al. Automatic, three-segment, MR-based attenuation correction for whole-body PET/MR data. Eur J Nucl Med Mol Imaging 2011;38:138–152.
27. Martinez-Moller A, Nekolla SG. Attenuation correction for PET/MR: problems, novel approaches and practical solutions. Z Med Phys 2012;22:299–310.
28. Zaidi H, Ojha N, Morich M, et al. Design and performance evaluation of a whole-body ingenuity TF PET-MRI system. Phys Med Biol 2011;56:3091–3106.
29. Kershah S, Partovi S, Traughber BJ, et al. Comparison of standardized uptake values in normal structures between PET/CT and PET/MRI in an oncology patient population. Mol Imaging Biol 2013. [Epub ahead of print]. doi:10.1007-s11307-013-0629-8.
30. Partovi S, Lee Z, Thomas S, O'Donnell JK, Faulhaber P.Quantitative and qualitative comparison of lung cancer imaging with PET/MRI and PET/CT. In: Society of Nuclear Medicine and Molecular Imaging Mid-Winter Meeting. New Orleans, LA, 2013.
31. Partovi S, Thomas S, Traughber BJ, Ellis R, Faulhaber P. Preliminary evaluation of dedicated PET/MRI in gastrointestinal malignancy: qualitative and quantitative comparison to PET/CT. Pract Radiat Oncol 2013;3:27.
32. Keereman V, Fierens Y, Broux T, De Deene Y, Lonneux M, Vandenberghe S. MRI-based attenuation correction for PET/MRI using ultrashort echo time sequences. J Nucl Med 2010;51:812–818.
33. Berker Y, Franke J, Salomon A, et al. MRI-based attenuation correction for hybrid PET/MRI systems: a 4-class tissue segmentation technique using a combined ultrashort-echo-time/Dixon MRI sequence. J Nucl Med 2012;53:796–804.
34. Schramm G, Langner J, Hofheinz F, et al. Quantitative accuracy of attenuation correction in the Philips Ingenuity TF whole-body PET/MR system: a direct comparison with transmission-based attenuation correction. MAGMA 2013;26:115–126.
35. Bini J, Izquierdo-Garcia D, Mateo J, et al. Preclinical evaluation of MR attenuation correction versus CT attenuation correction on a sequential whole-body MR/PET scanner. Invest Radiol 2013;48:313–322.
36. Wiesmuller M, Quick HH, Navalpakkam B, et al. Comparison of lesion detection and quantitation of tracer uptake between PET from a simultaneously acquiring whole-body PET/MR hybrid scanner and PET from PET/CT. Eur J Nucl Med Mol Imaging 2013;40:12–21.
37. Matthies A, Hickeson M, Cuchiara A, Alavi A. Dual time point 18F-FDG PET for the evaluation of pulmonary nodules. J Nucl Med 2002;43:871–875.
38. Basu S, Kwee TC, Surti S, Akin EA, Yoo D, Alavi A. Fundamentals of PET and PET/CT imaging. Ann N Y Acad Sci 2011;1228:1–18.
39. Vriens D, Visser EP, de Geus-Oei LF, Oyen WJG. Methodological considerations in quantification of oncological FDG PET studies. Eur J Nucl Med Mol Imaging 2010;37:1408–1425.
40. MacDonald LR, Harrison RL, Alessio AM, Hunter WCJ, Lewellen TK, Kinahan PE. Effective count rates for PET scanners with reduced and extended axial field of view. Phys Med Biol 2011;56:3629–3643.
41. Platzek I, Beuthien-Baumann B, Schneider M, et al. PET/MRI in head and neck cancer: initial experience. Eur J Nucl Med Mol Imaging 2013;40:6–11.
42. Hustinx R, Smith RJ, Benard F, et al. Dual time point fluorine-18 fluorodeoxyglucose positron emission tomography: a potential method to differentiate malignancy from inflammation and normal tissue in the head and neck. Eur J Nucl Med 1999;26:1345–1348.
43. O'Donnell M, Edelstein WA. NMR imaging in the presence of magnetic field inhomogeneities and gradient field nonlinearities. Med Phys 1985;12:20–26.
44. Ladefoged CN, Andersen FL, Keller SH, et al. PET/MR imaging of the pelvis in the presence of endoprostheses: reducing image artifacts and increasing accuracy through inpainting. Eur J Nucl Med Mol Imaging 2013;40:594–601.
45. Delso G, Martinez-Moller A, Bundschuh RA, Nekolla SG, Ziegler SI. The effect of limited MR field of view in MR/PET attenuation correction. Med Phys 2010;37:2804–2812.
46. Zhu Y. Parallel excitation with an array of transmit coils. Magn Reson Med 2004;51:775–784.
47. Harvey PR, Zhai Z, Morich M, et al.SAR behavior during whole-body multitransmit RF shimming at 3.0T. In: Proceedings of the 17th Scientific Meeting of ISMRM, Honolulu, HI, 2009. (abstract 4786).
48. Nelles M, Konig RS, Gieseke J, et al. Dual-source parallel RF transmission for clinical MR imaging of the spine at 3.0 T:

intraindividual comparison with conventional single-source transmission. Radiology 2010;257:743–753.
49. Willinek WA, Gieseke J, Kukuk GM, et al. Dual-source parallel radiofrequency excitation body MR imaging compared with standard MR imaging at 3.0 T: initial clinical experience. Radiology 2010;256:966–975.
50. Delso G, Furst S, Jakoby B, et al. Performance measurements of the Siemens mMR integrated whole-body PET/MR scanner. J Nucl Med 2011;52:1914–1922.
51. Zaidi H, Del Guerra A. An outlook on future design of hybrid PET/MRI systems. Med Phys 2011;38:5667–5689.
52. Peng BJ, Walton JH, Cherry SR, Willig-Onwuachi J. Studies of the interactions of an MRI system with the shielding in a combined PET/MRI scanner. Phys Med Biol 2010;55:265–280.
53. Nekolla SG, Reder S, Saraste A, et al. Evaluation of the novel myocardial perfusion positron-emission tomography tracer 18F-BMS-747158–02: comparison to 13N-ammonia and validation with microspheres in a pig model. Circulation 2009;119:2333–2342.
54. Buchbender C, Heusner TA, Lauenstein TC, Bockisch A, Antoch G. Oncologic PET/MRI, Part 1. Tumors of the brain, head and neck, chest, abdomen, and pelvis. J Nucl Med 2012;53:928–938.
55. Stoeckli SJ, Steinert H, Pfaltz M, Schmid S. Is there a role for positron emission tomography with 18F-fluorodeoxyglucose in the initial staging of nodal negative oral and oropharyngeal squamous cell carcinoma. Head Neck 2002;24:345–349.
56. Kielstra P. Doctor innovation: shaking up the health system. New York: The Economist Intelligence Unit; 2009.
57. Oates ME. Integrated residency training pathways of the future: diagnostic radiology, nuclear radiology, nuclear medicine, and molecular imaging. J Am Coll Radiol 2012;9:239–244.
58. National Oncology PET Registry.National Oncology PET Registry. Available at: cancerpetregistry.org [Internet] 2013. (Accessed January 31, 2013).
59. Kaplan DA.PET/MR: how feasible is implementation? Available at: www.diagnosticimaging.com [Internet] 2012. (Accessed January 31, 2013.
60. Bezabeh T, Odlum O, Nason R, et al. Prediction of treatment response in head and neck cancer by magnetic resonance spectroscopy. AJNR Am J Neuroradiol 2005;26:2108–2113.
61. Schulthess von GK, Kuhn FP, Kaufmann P, Veit-Haibach P. Clinical positron emission tomography/magnetic resonance imaging applications. Semin Nucl Med 2013;43:3–10.
62. Boss A, Stegger L, Bisdas S, et al. Feasibility of simultaneous PET/MR imaging in the head and upper neck area. Eur Radiol 2011;21:1439–1446.
63. Loeffelbein DJ, Souvatzoglou M, Wankerl V, et al. PET-MRI fusion in head-and-neck oncology: current status and implications for hybrid PET/MRI. J Oral Maxillofac Surg 2012;70:473–483.
64. Ng SH, Yen TC, Chang JT, et al. Prospective study of [18F]fluorodeoxyglucose positron emission tomography and computed tomography and magnetic resonance imaging in oral cavity squamous cell carcinoma with palpably negative neck. J Clin Oncol 2006;24:4371–4376.
65. Hustinx R, Lucignani G. PET/CT in head and neck cancer: an update. Eur J Nucl Med Mol Imaging 2010;37:645–651.
66. Comoretto M, Balestreri L, Borsatti E, Cimitan M, Franchin G, Lise M. Detection and restaging of residual and/or recurrent nasopharyngeal carcinoma after chemotherapy and radiation therapy: comparison of MR imaging and FDG PET/CT. Radiology 2008;249:203–211.
67. Anzai Y, Carroll WR, Quint DJ, et al. Recurrence of head and neck cancer after surgery or irradiation: prospective comparison of 2-deoxy-2-[F-18]fluoro-D-glucose PET and MR imaging diagnoses. Radiology 1996;200:135–141.
68. van Tinteren H, Hoekstra OS, Smit EF, et al. Effectiveness of positron emission tomography in the preoperative assessment of patients with suspected non-small-cell lung cancer: the PLUS multicentre randomised trial. Lancet 2002;359:1388–1393.
69. Wang J, Welch K, Wang L, Kong FM. Negative predictive value of positron emission tomography and computed tomography for stage T1–2N0 non-small-cell lung cancer: a meta-analysis. Clin Lung Cancer 2012;13:81–89.
70. Turkmen C, Sonmezoglu K, Toker A, et al. The additional value of FDG PET imaging for distinguishing N0 or N1 from N2 stage in preoperative staging of non-small cell lung cancer in region where the prevalence of inflammatory lung disease is high. Clin Nucl Med 2007;32:607–612.
71. Chen W, Jian W, Li HT, et al. Whole-body diffusion-weighted imaging vs. FDG-PET for the detection of non-small-cell lung cancer. How do they measure up? Magn Reson Imaging 2010;28:613–620.
72. Lichy MP, Aschoff P, Plathow C, et al. Tumor detection by diffusion-weighted MRI and ADC-mapping--initial clinical experiences in comparison to PET-CT. Invest Radiol 2007;42:605–613.
73. Ibeas P, Cantos B, Gasent JM, Rodriguez B, Provencio M. PET-CT in the staging and treatment of non-small-cell lung cancer. Clin Transl Oncol 2011;13:368–377.
74. Petrella F, Rizzo S, Radice D, et al. Predicting prolonged air leak after standard pulmonary lobectomy: computed tomography assessment and risk factors stratification. Surgeon 2011;9:72–77.
75. Nomori H, Watanabe K, Ohtsuka T, Naruke T, Suemasu K, Uno K. Evaluation of F-18 fluorodeoxyglucose (FDG) PET scanning for pulmonary nodules less than 3 cm in diameter, with special reference to the CT images. Lung Cancer 2004;45:19–27.
76. Goo JM, Im JG, Do KH, et al. Pulmonary tuberculoma evaluated by means of FDG PET: findings in 10 cases. Radiology 2000;216:117–121.
77. Cheran SK, Nielsen ND, Patz EF Jr. False-negative findings for primary lung tumors on FDG positron emission tomography: staging and prognostic implications. AJR Am J Roentgenol 2004;182:1129–1132.
78. Antoch G, Vogt FM, Freudenberg LS, et al. Whole-body dual-modality PET/CT and whole-body MRI for tumor staging in oncology. JAMA 2003;290:3199–3206.
79. Schmidt GP, Baur-Melnyk A, Herzog P, et al. High-resolution whole-body magnetic resonance image tumor staging with the use of parallel imaging versus dual-modality positron emission tomography-computed tomography: experience on a 32-channel system. Invest Radiol 2005;40:743–753.
80. Sieren JC, Ohno Y, Koyama H, Sugimura K, McLennan G. Recent technological and application developments in computed tomography and magnetic resonance imaging for improved pulmonary nodule detection and lung cancer staging. J Magn Reson Imaging 2010;32:1353–1369.
81. Biederer J, Schoene A, Freitag S, Reuter M, Heller M. Simulated pulmonary nodules implanted in a dedicated porcine chest phantom: sensitivity of MR imaging for detection. Radiology 2003;227:475–483.
82. Schwenzer NF, Schraml C, Muller M, et al. Pulmonary lesion assessment: comparison of whole-body hybrid MR/PET and PET/CT imaging--pilot study. Radiology 2012;264:551–558.
83. de Langen AJ, van den Boogaart V, Lubberink M, et al. Monitoring response to antiangiogenic therapy in non-small cell lung cancer using imaging markers derived from PET and dynamic contrast-enhanced MRI. J Nucl Med 2011;52:48–55.
84. Lambregts DMJ, Cappendijk VC, Maas M, Beets GL, Beets-Tan RG. Value of MRI and diffusion-weighted MRI for the diagnosis of locally recurrent rectal cancer. Eur Radiol 2011;21:1250–1258.
85. Wieder HA, Rosenberg R, Lordick F, et al. Rectal cancer: MR imaging before neoadjuvant chemotherapy and radiation therapy for prediction of tumor-free circumferential resection margins and long-term survival. Radiology 2007;243:744–751.
86. Curvo-Semedo L, Lambregts DM, Maas M, Beets GL, Caseiro-Alves F, Beets-Tan RG. Diffusion-weighted MRI in rectal cancer: apparent diffusion coefficient as a potential noninvasive marker of tumor aggressiveness. J Magn Reson Imaging 2012;35:1365–1371.
87. Park MJ, Kim SH, Lee SJ, Jang KM, Rhim H. Locally advanced rectal cancer: added value of diffusion-weighted MR imaging for predicting tumor clearance of the mesorectal fascia after neoadjuvant chemotherapy and radiation therapy. Radiology 2011;260:771–780.
88. Kim DJ, Kim JH, Ryu YH, Jeon TJ, Yu JS, Chung JJ. Nodal staging of rectal cancer: high-resolution pelvic MRI versus (1)(8)F-FDGPET/CT. J Comput Assist Tomogr 2011;35:531–534.
89. Buchbender C, Heusner TA, Lauenstein TC, Bockisch A, Antoch G. Oncologic PET/MRI, Part 2. Bone tumors, soft-tissue tumors, melanoma, and lymphoma. J Nucl Med 2012;53:1244–1252.
90. Hall EJ, Brenner DJ. Cancer risks from diagnostic radiology. Br J Radiol 2008;81:362–378.

91. Chawla SC, Federman N, Zhang D, et al. Estimated cumulative radiation dose from PET/CT in children with malignancies: a 5-year retrospective review. Pediatr Radiol 2010;40:681–686.
92. Brix G, Lechel U, Glatting G, et al. Radiation exposure of patients undergoing whole-body dual-modality 18F-FDG PET/CT examinations. J Nucl Med 2005;46:608–613.
93. Pantos I, Thalassinou S, Argentos S, Kelekis NL, Panayiotakis G, Efstathopoulos EP. Adult patient radiation doses from non-cardiac CT examinations: a review of published results. Br J Radiol 2011;84:293–303.
94. Hirsch FW, Sattler B, Sorge I, et al. PET/MR in children. Initial clinical experience in paediatric oncology using an integrated PET/MR scanner. Pediatr Radiol 2013;43:860–875.
95. Takenaka D, Ohno Y, Matsumoto K, et al. Detection of bone metastases in non-small cell lung cancer patients: comparison of whole-body diffusion-weighted imaging (DWI), whole-body MR imaging without and with DWI, whole-body FDG-PET/CT, and bone scintigraphy. J Magn Reson Imaging 2009;30:298–308.
96. Kwee TC, Takahara T, Vermoolen MA, Bierings MB, Mali WP, Nievelstein RA. Whole-body diffusion-weighted imaging for staging malignant lymphoma in children. Pediatr Radiol 2010;40: 1592–1602; quiz 1720–1721.
97. Platzek I, Beuthien-Baumann B, Langner J, et al. PET/MR for therapy response evaluation in malignant lymphoma: initial experience. MAGMA 2013;26:49–55.

HOME STUDY *EDUCATIONAL SEMINARS* ORDER FORM Page 1

Back issues of SMRT educational seminars are for sale to SMRT members only!

Qty.	Vol.	CE	Home Studies Title
	1.1	3.5	Functional MRI: Capabilities and Limitations
	2.3	3.0	Directions in Advanced Cardiac Imaging
	3.1	3.0	Introduction to Spectroscopy
	3.3	3.0	A Primer on MR Pulse Sequences
	3.4	2.5	Artifacts Encountered in Abdominal MRI
	4.2	3.0	Directions in MRI of the Liver
	5.1	2.5	Atlas of Cranial Neuroanatomy
	5.3	3.0	MR Imaging of the Breast
	5.4	1.0	Diffusion-Weighted Imaging of the Brain
	6.2	3.5	Fundamental Principles of MR Imaging of the Head, Neck, and Spine
	6.3	1.5	Advances in Interventional MRI
	6.4	1.5	Diffusion-Weighted MR Imaging of the Pediatric Brain
	7.1	2.0	The Role of Neuroimaging in the Diagnosis of Alzheimer's Disease
	7.2	2.5	Cardiovascular MRI: Update I
	7.3	2.5	K-Space in the Clinic
	7.4	3.0	MR Imaging and Spectroscopy of the Prostate
	8.1	1.0	Atlas of Knee Anatomy
	8.2	2.0	Cardiovascular MRI: Update II
	8.3	2.5	Update: Safety in MR Examinations
	8.4	2.0	Parallel MR Imaging
	9.1	3.0	MRI of Breast Cancer: Update I
	9.2	2.5	MR Atlas of the Shoulder
	9.3	3.0	Exploring Magnetic Field Strengths: Challenges and Opportunities
	9.4	4.0	MRI of Breast Cancer: Update II

Qty.	Vol.	CE	Home Studies Title
	10.1	4.0	MR Imaging of Perfusion
	10.2	3.0	MR Imaging Artifacts:Appearance, Cause & Cure
	10.3	4.0	Techniques in Cardiovascular MR Imaging
	10.4	3.0	MRI of the Brain
	11.1	4.0	Update: Musculoskeletal MRI*
	11.2	2.5	Contrast Media in MRI Examinations*
	11.3	2.0	Head and Neck MRI at 3.0T
	11.4	3.0	MR Imaging of the Abdomen*
	12.1	3.0	Contrast-Enhanced Musculoskeletal MR Imaging
	12.2	3.0	Neuro MRI: Principles and Protocols*
	12.3	2.0	MR Imaging of the Spine*
	12.4	3.0	MR Imaging of the Liver*
	13.1	3.0	MR Imaging Sequences: Gradient-Recalled Echo (GRE)*
	13.2	3.5	Techniques in Cardiac MR Imaging*
	13.3	2.5	Phase Contrast MR Imaging: Techniques and Applications*
	13.4	2.0	MRI of Spinal Cord Lesions*
	14.1	3.0	Breast MRI: DCIS and Skin Lesions*
	14.2	3.5	Pediatric Magnetic Resonance Imaging*
	14.3	2.5	MR Imaging Physics Tutorial*
	14.4	2.5	Safety and Screening in MRI*
	15.1	2.0	MR of the Abdomen: Kidney*
	15.2	2.5	3D Musculoskeletal MR Imaging*
	15.3	2.5	MR Physics: Gradient Echo & Parallel Imaging*
	15.4	1	MRI Atlas of the Abdomen*

Please note: All Home Study Educational Seminars following Volume 15.4 will be available ONLINE ONLY.

*Home Study *Educational Seminars* available online at no cost to SMRT members.

HOME STUDY *EDUCATIONAL SEMINARS* ORDER FORM Page 2

Back issues of SMRT educational seminars are for sale to SMRT members only!

YOU MAY ORDER PAST ISSUES OF HOME STUDY *EDUCATIONAL SEMINARS* ONLINE:

cds.ismrm.org/protected/ehs/hsorder.htm

TO ORDER BY MAIL, PLEASE FILL OUT AND MAIL THIS FORM, INCLUDING YOUR QUANTITY AND CHOICE OF ISSUES FROM PREVIOUS PAGE

CALCULATE YOUR ORDER HERE

Total quantity ordered: _____ x US$25 each = $_____ Subtotal = US$_____

SHIPPING:

Shipping is included on orders of four volumes or less. **Shipping is charged on orders of five volumes or more.** We will contact you with the shipping cost before we process your order. No orders will be processed before you have confirmed the actual shipping cost.

PAYMENT OPTIONS & BILLING INFORMATION

PAYMENT WITHIN USA:

Personal checks, money orders, cashier's checks and company checks are acceptable. Institutional purchase orders are acceptable and will be invoiced, but payment must still be received prior to shipment.

PAYMENT FROM OUTSIDE USA:

Checks: The check must be payable "to" (NOT "through") a U.S. bank in U.S. Dollars. The check must be imprinted with the computer encoding and routing information authorized by the American Banking Association.

Traveler's Checks: Traveler's checks in U.S. dollars for the exact amount, properly counter-signed, are acceptable.

International Money Order: The money order must be in U.S. dollars and be imprinted with the computer encoding and routing information authorized by the American Banking Association. U.S. dollar International Postal Money Orders imprinted as stated above are acceptable.

Wire: Wire payments are not accepted.

SMRT Member ID# (REQUIRED)_____

Name_____

Address_____

City_____State/Province_____Postal Code/ZIP + 4_____Country_____

Phone_____Fax_____E-mail_____

❒ Credit Card: ❒ VISA ❒ MasterCard ❒ AMEX ❒ Discover

(Credit card orders may be faxed directly to SMRT: +1 510 841 2340)

Card Number: _____Expiration Date:_____Security Code:_____

Billing Address_____Billing Zip + 4/Postal Code:_____

Signature:_____

WE ARE A NETWORK OF KNOWLEDGE

SMRT – A Global Community

The Section for Magnetic Resonance Technologists (SMRT) of the International Society for Magnetic Resonance in Medicine (ISMRM) is the leading non-profit organization that provides an international forum for education, information and research in magnetic resonance for technologists and radiographers throughout the world.

The SMRT was established by technologists, clinicians and scientists of the ISMRM as a forum for technologists and radiographers to share their expertise and educational resources, with a common goal of improving healthcare for people worldwide.

As an organization, we are committed to promoting communication and the dissemination of cutting-edge MR developments. The objective of the SMRT is to advance education and training, while striving to promote a high level of knowledge and professionalism in the field of MR technology and radiography.

SMRT Member
Filip De Ridder, R.N., FSMRT
Universitair Ziekenhuis Brussel

SMRT

ISMRM
SECTION FOR MAGNETIC RESONANCE TECHNOLOGISTS

2030 ADDISON STREET
SUITE 700
BERKELEY, CALIFORNIA, 94704 USA
TEL: +1 510 841 1899
FAX: +1 510 841 2340
INFO@ISMRM.ORG/SMRT